CONTROLLING SPONTANEOUS EMISSION WITH NANOSTRUCTURES

Beheersing van spontane emissie van licht met nanostructuren

Promotiecommissie

Promotor	prof. dr. W. L. Vos
Overige leden	prof. dr. A. Lagendijk prof. dr. K.-J. Boller prof. dr. G. W. 't Hooft prof. dr. J.-J. Greffet
Paranimfen	S. Brinkers J. Hoedemaekers

The work described in this thesis is part of the research program of the 'Stichting voor Fundamenteel Onderzoek der Materie (FOM)', which is financially supported by the 'Nederlandse Organisatie voor Wetenschappelijk Onderzoek' (NWO)' and was funded by a Vici grant to prof. dr. W. L. Vos.

This work was carried out in the group *Photonic Bandgaps*, at the *Center for Nanophotonics, FOM Institute for Atomic and Molecular Physics* (AMOLF), Amsterdam, The Netherlands, and in the group *Complex Photonic Systems*(COPS), at the *Department of Science and Technology and the MESA$^+$ Institute for Nanotechnology, University of Twente*, Enschede, The Netherlands.

This thesis can be downloaded from http://www.photonicbandgaps.com.

ISBN: 978-90-365-3118-4
DOI: 10.3990/1.9789036531184

CONTROLLING SPONTANEOUS EMISSION WITH NANOSTRUCTURES

PROEFSCHRIFT

ter verkrijging van
de graad van doctor aan de Universiteit Twente,
op gezag van de rector magnificus,
prof. dr. H. Brinksma,
volgens besluit van het College voor Promoties
in het openbaar te verdedigen
op woensdag 15 december 2010 om 15.00 uur

door

Merel Daniëlle Leistikow

geboren op 9 april 1983
te Utrecht

Dit proefschrift is goedgekeurd door:

prof. dr. W. L. Vos

"We don't make mistakes here, we just have happy accidents."

Bob Ross

Contents

Chapter 1
Introduction

There are different processes that lead to the creation of light in nature. Most importantly, there is the distinction between stimulated and spontaneous emission. Stimulated emission leads to laser light, known from CD drives and laser pointers. Lasers generate light that is typically monochromatic, directional and coherent. The second main way to generate light is via the process of spontaneous emission. One important everyday example of spontaneous emission is thermal radiation. When the temperature of an object is sufficiently high, it starts emitting visible light. For instance the sun and light bulbs work this way. Spontaneous emission can also be generated by electrical excitation, known in everyday life from the yellow light emitted by street lamps. Fluorescent lamps generate their light in a two step process. First electrical current generates UV light, that is converted to visible light by special phosphors. In general, light that is generated via spontaneous emission is not directional and coherent and can have a broad spectrum, in contrast to laser light.

Although the term "spontaneous" in spontaneous emission may sound like a synonym for "random", it is possible to influence the dynamics of spontaneous emission in a controlled way. By placing an emitter inside or within a wavelength near a suitable nanostructure the spontaneous emission process can be controlled. This is the research field of nanophotonics, where the structures are on the wavelength scale of light. In this thesis several different methods are experimentally investigated to modify and control the process of spontaneous emission. In this introduction several important concepts about spontaneous emission and nanostructures are introduced and an outline of this thesis is given.

1.1. Spontaneous emission

The simplest system to show optical activity is a two-level emitter, as depicted in fig. 1.1. A two-level emitter has a ground state level and an excited state level that is higher in energy than the ground state. A two-level emitter can be excited by absorbing a photon with an energy exactly matching the energy difference between ground and excited states. This extra absorbed quantum of energy can be radiated away from the emitter by spontaneous emission. The emission is called spontaneous because there is no way to determine *a priori* the moment in time when the photon is emitted after excitation. Before the introduction of quantum optics, it seemed that this process occurred without interaction with an electric field. Although some aspects of spontaneous emission such as Einstein's coefficients can be explained classically [1], a full description of spontaneous emission needs quantisation of the light field since this process is inherently quantum mechanical in nature [2].

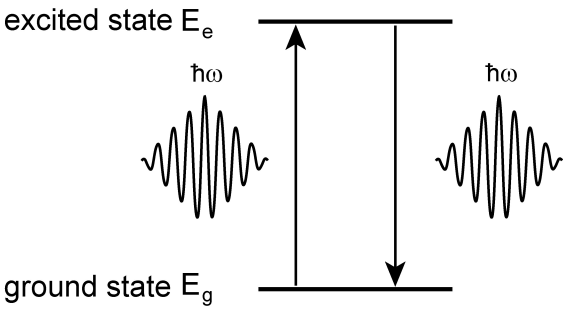

Figure 1.1.: Schematic of a two-level emitter. Light with a particular energy quantum $\hbar\omega$ is emitted.

In quantum optics, even vacuum has an energy $\frac{1}{2}\hbar\omega$ per mode. The average value for the electric field squared is non-zero causing the electric field to fluctuate around the zero mean value in time. Emitters in the excited state can interact with this electric field, and as a result make the transition to the lower energy level upon emitting a photon. Theoretically it can be derived that the decay has an exponential form when the emitter interacts with a continuum of field modes [2]. Each individual emission event remains uncertain with no way to determine *a priori* how long the emitter will stay in the excited state before emitting a photon. However, when the process is repeated many times the resulting distribution of emission decay times will show an exponential function with a characteristic decay rate γ. This decay rate for dipole transitions is determined by Fermi's Golden Rule:[3, 4]

$$\gamma(\mathbf{r}) = \frac{2\pi}{\hbar^2} \sum_{|f\rangle} |\langle f|\hat{\mathbf{d}}(\mathbf{r}) \cdot \mathbf{E}(\mathbf{r})|i\rangle|^2 \delta(E_f - E_i) \tag{1.1}$$

The decay rate γ of a dipole transition with operator $\hat{\mathbf{d}}$ and energy E_i is determined by summing over all available final states $|f\rangle$ with energy E_f. Fermi's Golden Rule can be rewritten as [5]

$$\gamma(\mathbf{r}, \mathbf{e_d}, \omega_{ab}) = \frac{\pi\omega_{ab}}{3\hbar\epsilon_0} |\langle a|\hat{\mathbf{d}}|b\rangle|^2 N_{rad}(\mathbf{r}, \mathbf{e_d}, \omega_{ab}) \tag{1.2}$$

where the expression separates into an atom part depending in the transition dipole $\langle a|\hat{\mathbf{d}}|b\rangle$ where $|a\rangle$ and $|b\rangle$ denote the emitter excited and ground state wave functions respectively and a field part given by the local radiative density of states (LDOS) N_{rad}. The LDOS is a function of position $\mathbf{r}$, dipole orientation $\mathbf{e_d}$ and frequency ω_{ab}. Although vacuum fluctuations are essentially quantum mechanical, the LDOS is a classical entity [5].

For an emitter in a homogeneous dielectric, the spontaneous emission rate is independent of position and orientation and equal to:

$$\gamma(\omega) = \frac{\pi d^2 \omega}{\hbar\epsilon_0} N_{rad}(\omega) = \frac{n d^2 \omega^3}{3\pi\hbar\epsilon_0 c^3} \tag{1.3}$$

Here the assumption is made that the emitter has the same refractive index as the medium. In more complicated situations the local field effect must be taken in to account [6].

1.2. Modifying the local density of states

Since the decay rate of an emitter is determined partly by the immediate surroundings of the emitter via the local density of states, this allows for a method to control the decay rate of the emitter. Therefore we place it in a controlled environment on the scale of the wavelength of light, entering into in the research field of nanophotonics [7]. In this section, three important nanophotonic environments are discussed: The interface, the cavity and the photonic crystal.

1.2.1. The interface

Close to an interface between two media with different refractive indices, the local density of states is modified due to interference of the emitted and reflected light [8, 9]. This modification of the LDOS has been investigated since the pioneering experiments by Drexhage in the 1960s, reviewed in [10]. The theoretically simplest situation is that of placing an emitter with a certain dipole orientation close to a perfect metal. The local density of states as a function of distance to the interface is shown in fig. 1.2. A dipole oriented parallel to the interface will cancel with its image dipole at the interface, giving LDOS = 0. For dipoles oriented perpendicular to the interface the image dipole is added to the dipole, giving a doubling of the LDOS. Further away from the interface oscillations occur that are caused by interference of the light fields with a period given by the wavelength of the light. More than a few wavelengths away from the interface these interference effects are no longer sufficiently strong to modify the LDOS, resulting in a constant value independent of dipole orientation. There is no resonance condition for this system. Therefore the LDOS is modified for all wavelengths. In reality, the LDOS will never be zero near an interface. Close to a real metal, the emitter will start coupling to surface waves called surface plasmon polaritons, that will increase the LDOS substantially [8].

1.2.2. The cavity

In a cavity confinement of light in three dimensions traps the light for a certain time inside the volume of the cavity for light that is on resonance with the resonance frequency of the cavity. For a perfect cavity, the light will be trapped indefinitely. However, in reality light will always be able to leak out through for instance mirrors that do not have 100 % reflectivity. The amount of confinement in the cavity is gauged by the quality factor Q of the cavity which is proportional to the confinement time of light inside the cavity. Q is defined as the ratio of the energy contained in the cavity and the energy leaking out within one optical cycle. A cavity has a certain frequency bandwidth $\Delta\omega$ over which it can trap light that is related to the Q factor of the cavity by $Q = \frac{\omega_0}{\Delta\omega}$ where ω_0 is the resonance frequency that is determined by the cavity size L as $\omega_0 = \frac{2\pi c}{L}$. The LDOS near

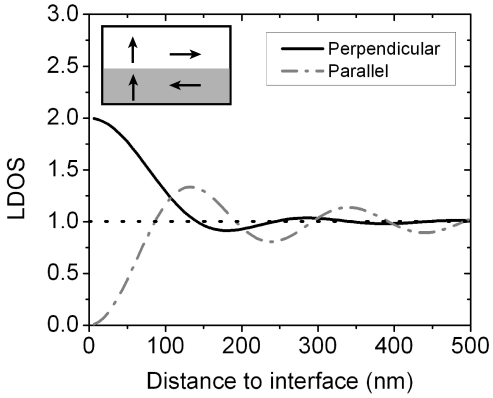

Figure 1.2.: LDOS as a function of distance to perfect metal for an emitter in n=1.5 with $\lambda = 600$ nm. The LDOS is normalised to the LDOS far away from the interface. The transition dipole is oriented perpendicular (black solid curve) or parallel (grey dash-dotted curve) to the interface. The inset shows the dipoles and their mirror image.

the resonance frequency of the cavity can be strongly increased. This effect is called the Purcell effect, named after Purcell who first realised the increased transition probability at radio frequencies [11]. In nanophotonics the increased mode density has been measured for InAs quantum dots inside tiny micropillar cavities [12]. The complementary effect of inhibition for modes with a frequency outside the cavity bandwidth has also been observed [13]. The LDOS of light on resonance with the cavity can be increased strongly. However, the effectiveness of a cavity is limited to narrow bandwidth and to a small volume. The LDOS at a frequency detuned from the cavity will be lowered, but will not reach 0.

1.2.3. Photonic crystals

Photonic crystals are a specific type of composite materials that have a modulated dielectric function with a periodicity of the order of the wavelength of light. Because of this periodicity interference effects occur in the crystal, giving rise to Bragg diffraction. Bragg diffraction is known from solid-state physics [14] and occurs when the wavelength is of the order of the distance between the lattice planes. The importance of these types of materials in the optical domain was first realised by Bykov in 1972 [15] and was brought under strong worldwide attention by the work of Yablonovitch [16] and John [17].

The Bragg condition is equal to:

$$m\lambda = 2d\cos\theta \tag{1.4}$$

where m is an integer which indicates the order of Bragg diffraction, λ is the wavelength of light, d is the distance between the lattice planes and θ is the angle of the propagating light wave with the normal to the surface. This is schematically shown in fig. 1.3 a). When the path length difference between the consecutive lattice planes is equal to a multiple of the wavelength, constructive interference occurs, giving rise to a reflection peak. If the Bragg diffraction is in the visible wavelength range this gives photonic crystals their opalescent appearance known from for instance natural opal and butterfly wings.

The dispersion of light inside periodic structures can be understood by calculating the band structure. A part of a band structure is shown in fig. 1.3 b) for propagation along the normal to the crystal planes. In a homogeneous medium the dispersion relation between frequency and the wavevector is linear with a slope equal to the speed of light divided by the refractive index c/n. For periodic media, at $k = \pi/d$ the Bragg condition is met. Here the band splits from the central frequency $\omega = \frac{2\pi}{\lambda}$ in two different branches separated by a stop gap. The upper and lower frequency of the stop gap are a consequence of the standing waves at the Bragg condition. The standing waves with the low frequency are primarily located in the high index material, while the high frequency standing wave is mostly in the low index material. Since the wavelength of the two waves is identical but the refractive index differs, the standing waves have different frequencies [18]. In a stop gap the resonance frequency is at the Bragg condition. However, contrary to a cavity here the interference is destructive.

The width of the stop gap is determined by the photonic strength $S = \frac{\Delta\omega}{\omega}$ that is a gauge for the interaction strength between light and the photonic crystal. The photonic strength is defined as the polarisability per volume of a unit cell of the crystal [19, 20]. The photonic strength depends upon a number of crystal parameters, such as refractive index contrast and the geometry of the crystal.

Bragg diffraction from a single set of crystal planes is strongly angle dependent. With increasing photonic interaction strength and increasing frequency, light can diffract from more than one set of lattice planes simultaneously, causing band repulsion [21]. If the photonic strength is sufficiently large, the edges of the stop gap hardly vary for different directions and polarisations, leading to an omni-directional stop gap, or band gap. Inside this much sought after band gap frequency range no modes are available due to complete destructive interference, meaning that the density of states is zero and the vacuum fluctuations are suppressed. This would completely inhibit the spontaneous emission of an emitter located inside such a band gap. In this thesis we present the first ever systematic study on spontaneous emission in a 3D photonic band gap.

Not any photonic crystal structure will have a band gap. Existence of a band gap is predicted for particular symmetries: The simple cubic [22], the diamond [23] and diamond-like [24] structures, the Yablonovite structure [25], the woodpile [26] and the close packed *fcc* and *hcp* structures [27]. Apart from the crystal structure, the refractive index contrast needs to be sufficiently high for the appearance of a band gap in the band structure.

Well-known colloidal crystals are grown using self assembly of dielectric spheres in an *fcc* structure and show clear stop gaps [19, 20, 28, 29]. Colloidal crystals are

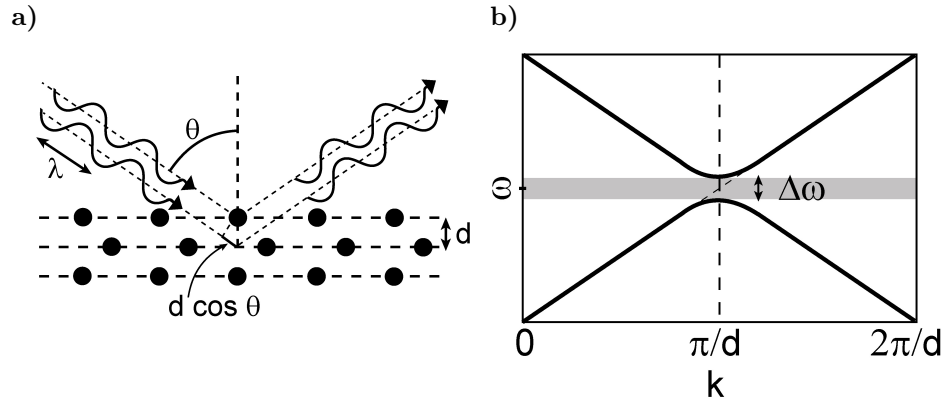

Figure 1.3.: a) Schematic of Bragg diffraction. A set of lattice planes, indicated with the dashed lines, causes constructive interference of the reflected light when the optical path length difference is a multiple of the wavelength. b) The dispersion relation along the normal to the lattice planes in a). The grey bar indicates the stop gap.

most commonly fabricated from low refractive index materials like polystyrene. These crystals do not have a band gap since their photonic strength is limited because of the low refractive index contrast [30]. Pioneering time-resolved emission experiments were performed on colloidal crystals [31]. A modification of the decay rate was found, but was probably caused by a change in the chemical environment of the emitters [32]. Recently it was shown that the decay rate can nevertheless be modified even in opal photonic crystals [33].

Inverse opals, consisting of fcc stacked air spheres with a backbone material of high refractive index material [34] can have sufficient refractive index contrast to show a band gap when the refractive index contrast is above 2.8 [27, 35]. Silicon inverse opals have been fabricated and show high reflectivity [36, 37]. Inhibition and enhancement of spontaneous emission has been shown for titania inverse opals [38]. Even though the refractive index contrast is insufficient to achieve a band gap, strong modification of the LDOS has been achieved in these structures [39].

Structures have been fabricated in silicon with simple cubic crystal structure by means of photo electrochemical etching that show high reflectivity [40, 41]. However it is hard to scale down these structures to telecom or visible wavelengths. However, these structures may be applicable to modify the blackbody radiation [42, 43] since it is possible to modify thermal radiation by nanostructures [44].

The Yablonivite structure was demonstrated in the microwave region, but is extremely hard to make in the optical domain [45].

Woodpile structures are fabricated by stacking layers of dielectric rods. Reflection and transmission measurements performed on these woodpiles show strongly photonic behavior [46–49]. However the sequential stacking process limits the

crystal size to (at most) 8 or 9 layers since it introduces alignment errors. Emission from woodpile photonic crystals has been characterised by measuring time-resolved emission from woodpiles fabricated of silicon [50]. A promising inhibition of the decay rate was seen when comparing the rate of erbium atoms inside the photonic crystal with the rate of erbium atoms implanted in silicon. However, no systematical study was performed of the effect of the crystal lattice parameters on the decay rate.

A very promising category of band gap photonic crystals is the inverse woodpile [26]. These structures promise a broad band gap with a relative width of 25 % [26, 51, 52] when fabricated of silicon. Some optical characterisation of these structures have been performed by means of reflectivity measurements [53] that show interesting results. No emission experiments have been performed as of yet. Recently, our group has developed a new CMOS compatible method to fabricate Si inverse woodpile crystals that show strong and broad reflecting peaks. In chapter 5 of this thesis we will present the first experiments to control spontaneous emission of quantum dots with these 3D inverse woodpile crystals.

1.3. When Fermi's Golden Rule does not apply

To derive Fermi's Golden Rule from first principles in quantum optics requires a number of assumptions to be made. Most notably the Markovian approximation is made that the atom-field system has no memory of previous time. There are however situations in which this assumption is not valid. Three of these very exciting physical situations will be briefly discussed in this section. Even though experiments in these regimes are not discussed in this thesis, future work might focus on this very intriguing breakdown of Fermi's Golden Rule.

1.3.1. Strong coupling

Fermi's Golden Rule applies to the interaction of one emitter with a continuous number of field modes, the bath. When the emitter can only interact with one field mode a very different outcome is found. This limit of interaction with only one mode is called the strong coupling limit (compared to the weak coupling limit for interaction with a continuous bath). The physics in such a strong coupling situation can be described by the well known Jaynes-Cummings model [2]. The quantum of energy will cycle back and forth between the excited state of the emitter and the photon in the cavity reversibly, performing vacuum Rabi oscillations at the Rabi frequency. In theory, this cycling of the quantum of energy continues indefinitely. In experiment, it depends on the cavity quality factor and mode volume whether the strong coupling regime is reached or the weak coupling Purcell effect is observed. In nanophotonics experiments, strong coupling has been achieved between nano cavities and quantum dots for photonic crystal slab cavities [54], micropillar cavities [55] and microdisks [56].

1.3.2. Fractional decay

In media with strong variations in the spectral and spatial distribution of the LDOS, a deviation from the single exponential decay is also expected. In these media the excited emitter coherently interacts with modes of low group velocity in such a way that it never fully decays but rather remains in a superposition of the excited state and the ground state, called fractional decay [57, 58]. This behavior is expected on the band edge of a photonic band gap crystal and in the frequency range near a Van Hove singularity. A Van Hove singularity is a cusp in the density of states, caused by flat bands in the band structure of the photonic crystal [59]. To the best of our knowledge fractional decay has not been observed experimentally.

1.3.3. Fast modulation of LDOS in time

So far the discussed physics holds for static environments, where the local density of states does not change with time. However, when the LDOS is modulated in time interesting new physics is expected. Fermi's Golden Rule does not apply when changes in LDOS are of the order or shorter than the decay time of the emitter. Our group has modified the LDOS in time, by optically switching photonic structures with ultrafast picosecond light pulses [60, 61]. So far the modified LDOS has been identified by measuring transient reflectivity of photonic structures. New experiments are pursued where the time-resolved emission is measured of an emitter in a dynamically changing LDOS.

1.4. Disorder

Fabricated structures will always show some unavoidable disorder. This leads to random scattering of light. In a bulk nanostructure a coherent light beam will be randomised over a length scale called the mean free path l. If the sample thickness is larger than the mean free path, multiple scattering of light occurs [62]. The light will become diffuse due to the random walk that it follows through the material. All white materials, from clouds and grains of salt to snow and beer foam, owe their white color to multiple scattering of light. When the mean free path is sufficiently short a phase transition from diffusion to localisation of light is expected [62, 63] where light is trapped due to the interference.

In a perfect photonic crystal, the mean free path would be infinite. Disorder in photonic crystals causes the light to be diffuse giving a finite mean free path. The disorder in a photonic crystal is typically unintentional due to for instance the fabrication process. Diffusion causes the interference effects in a photonic crystal to be limited to a finite part of the crystal [64]. It is expected that when the disorder is sufficiently large localisation of light will occur in a photonic crystal with a photonic band gap [17].

Strong research effort is aimed at fabricating structures with intentional strong disorder, in pursuit of localisation of light. One example of such structures are the nanowire samples discussed in chapter 7. Although extremely interesting localisation of light does not modify the local density of states. However, strong

disorder causes the local density of states to fluctuate spatially [65–67]. This spatial fluctuation has recently been observed [68].

1.5. Light sources

There are several physical emitters that can be used to mimic the behavior of the two-level system discussed in paragraph 1.1 and that show strong spontaneous emission. If one studies the decay rate of the emitter a very important property is the fluorescence quantum efficiency of the light source. In addition to the radiative decay rate γ_{rad} real emitters always show a contribution from loss processes, the non-radiative decay rate γ_{nrad}. This can be any process through which the excitation energy is lost that does not involve emission of a photon. The quantum efficiency of a light source is defined as:

$$QE = \frac{\gamma_{rad}}{\gamma_{rad} + \gamma_{nrad}} \tag{1.5}$$

For use of emitters in applications like light emitting diodes (LEDs) it is important to have a high quantum efficiency, since with high quantum efficiency more input energy is converted to light. Another important reason to use high quantum efficiency sources is based on the measurement technique. In a time-resolved experiment only the total decay rate γ_{tot} is measured, which is equal to the sum of the radiative and non-radiative decay rates $\gamma_{tot} = \gamma_{rad} + \gamma_{nrad}$. Since the LDOS only modifies the radiative decay rate, it is important for the emitter to have a high quantum efficiency if the effect of LDOS is probed with time-resolved emission. In this section two important types of emitters are discussed that will be used in experiments presented in this thesis.

The first type of emitter is the organic fluorescent molecule or organic dye [69]. These aromatic molecules fluoresce naturally, have typically a lifetime of a few nanoseconds and have high quantum efficiency near 100 % [70]. A great advantage of dye molecules is that they are all the same, contrary to metamaterials such as quantum dots. A disadvantage is that dye emitters blink and photo bleach after emitting about 10^8 photons.

The second kind of emitter that is used in this thesis are colloidal quantum dots. These are semiconductor nanocrystals with typically several nanometer diameter [71, 72]. In fig. 1.4 a) a transmission electron micrograph of a CdSe quantum dot is shown. The lattice fringes of the CdSe crystal are clearly visible. Colloidal quantum dots are typically suspended in a solvent. In a semiconductor photons can be absorbed when the energy is larger than the energy difference between the conduction and the valence band. An electron is excited to the conduction band, leaving a hole in the valence band. By the attractive Coulomb interaction, the excited electron and the hole attract each other, forming a weakly bound exciton [73, 74]. The average electron-hole distance is known as the exciton Bohr radius [75]. When the nanocrystal size is comparable or smaller than the exciton Bohr radius, the exciton is confined to the quantum dot. This causes the energy between valence and conduction band to increase and the bands gradually split into discrete levels as is schematically shown in fig. 1.4 b). This splitting results

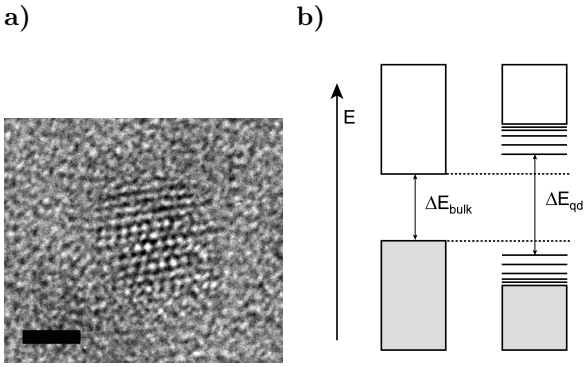

Figure 1.4.: a) A transmission electron microscope image of a CdSe quantum dot is shown. The scale bar is 2 nm. b) The band structure for bulk semiconductor and quantum dots is shown schematically.

in a narrow, atom-like emission spectrum. However, the absorption remains broadband, giving freedom to chose the excitation frequency. By changing the size of the quantum dot and selecting an appropriate semiconductor the emission energy can be tuned from the visible to the infrared. Quantum dots can have a very high quantum efficiency. Up to 98 % has been measured for CdSe quantum dots [76].

1.6. Outline of this thesis

In this thesis experiments are presented that show control of the spontaneous emission of various emitters by placing the emitters in the presence of nanostructures. By modifying the LDOS with these nanostructures the spontaneous emission decay rate is controlled.

In chapter 2 the analytically well known modification of the local density of states near a silver mirror is used to determine the quantum efficiency and size of the transition dipole moment of commonly used CdSe quantum dots as a function of emission energy. Here, knowledge of the LDOS is used as a tool to learn more about the emission properties of CdSe quantum dots, a widely used emitter not only in nanophotonics but also for biophotonic applications.

In chapter 3 the influence of the dipole orientation on ensemble measurements are presented by the time-resolved emission of Rhodamine 6G laser dye near a dielectric interface. Since the LDOS depends on the dipole orientation the decay rate of the emitter depends on the angle of its dipole with respect to the interface. Therefore, in ensemble measurements non-exponential decay is expected. Indeed non-exponential decay is observed near an interface. When the interface is removed the decay becomes exponential. For the first time the exact shape of the non-exponential decay curve is calculated *ab initio* without any adjustable parameter and shows very good agreement with the experiments.

In chapters 4 to 6 the control over spontaneous emission is demonstrated us-

ing silicon photonic band gap crystals. In chapter 4 the experimental set-up, the photonic crystals, the quantum dots and the experimental procedures are discussed. In chapter 5 strong inhibition and enhancement of the decay rate is presented for PbS quantum dots inside 3D silicon inverse woodpile crystals. These crystals have a photonic band gap overlapping with the emission frequency of the PbS quantum dots. Quantum dots emitting within the photonic band gap show strong inhibition up to a factor of 11. In chapter 6 emission measurements are presented of PbS quantum dots from 2D silicon photonic crystals with a centered rectangular structure. No modification of the decay rate is found but a strong redirection of the emission is presented, showing intriguing peaks that are linked to band edges in the band structure and may correspond to 2D Van Hove singularities.

In chapter 7 CdSe quantum dots are placed in disordered arrays of gallium phosphide nanowires that show strong multiple scattering of light. The decay rate is modified by the presence of the nanowires. The change in the most frequent decay rate is well understood by modeling the effect of a single nanowire on the decay rate of the quantum dots. No effects of multiple scattering are seen in the variation of the measured decay rates.

Chapter 8 concludes the thesis. A summary of the thesis is presented and an outlook is given on future experiments and applications.

References

[1] S. Haroche, *Systèmes fondamentaux en optique quantique/fundamental systems in quantum optics* (Elsevier Science Publishers, 1992).

[2] M. O. Scully and M. S. Zubairy, *Quantum optics* (Cambridge university press, Cambridge, 1997).

[3] E. Fermi, *Quantum theory of radiation*, Rev. Mod. Phys **4**, 87 (1932).

[4] R. Loudon, *The quantum theory of light* (Oxford university press, Oxford, 1983).

[5] R. Sprik, B. A. van Tiggelen, and A. Lagendijk, *Optical emission in periodic dielectrics*, Europhys. Lett. **35**, 265 (1996).

[6] F. J. P. Schuurmans, P. de Vries, and A. Lagendijk, *Local-field effects on spontaneous emission of impurity atoms in homogeneous dielectrics*, Phys. Lett. **264**, 472 (2000).

[7] L. Novotny and B. Hecht, *Principles of nano-optics* (Cambridge University Press, Cambridge, 2006).

[8] R. R. Chance, A. Prock, and R. Silbey, *Advances in chemical physics, volume 37* (John Wiley & Sons, 1978).

[9] W. L. Barnes, *Topical review: Fluorescence near interfaces: the role of photonic mode density*, J. Mod. Opt. **45**, 661 (1998).

[10] K. H. Drexhage, *Interaction of light with monomolecular dye layers*, Prog. Optics **12**, 165 (1974).

[11] E. M. Purcell, *Spontaneous emission probabilities at radio frequencies*, Phys. Rev. **69**, 681 (1946).

[12] J. M. Gérard, B. Sermage, B. Gayral, B. Legrand, E. Costard, and V. Thierry-Mieg, *Enhanced spontaneous emission by quantum boxes in a monolithic optical microcavity*, Phys. Rev. Lett. **81**, 1110 (1998).

[13] M. Bayer, T. L. Reinecke, F. Weidner, A. Larionov, A. McDonald, and A. Forchel, *Inhibition and enhancement of the spontaneous emission of quantum dots in structured microresonators*, Phys. Rev. Lett. **86**, 3168 (2001).

[14] N. W. Ashcroft and N. D. Mermin, *Solid state physics* (Brooks/Cole, Orlando, 1976).

[15] V. P. Bykov, *Spontaneous emission in a periodic structure*, Sov. Phys. -JETP **35**, 269 (1972).

[16] E. Yablonovitch, *Inhibited spontaneous emission in solid-state physics and electronics*, Phys. Rev. Lett. **58**, 2059 (1987).

[17] S. John, *Strong localization of photons in certain disordered dielectric superlattices*, Phys. Rev. Lett. **58**, 2486 (1987).

[18] J. D. Joannopoulos, S. G. Johnson, J. N. Winn, and R. D. Meade, *Photonic crystals: molding the flow of light* (Princeton University Press, Princeton, 2008).

[19] W. L. Vos, M. Megens, C. M. van Kats, and P. Bösecke, *Transmission and diffraction by photonic colloidal crystals*, J. Phys.: Condens. Matter **8**, 9503 (1996).

[20] W. L. Vos, R. Sprik, A. van Blaaderen, A. Imhof, A. Lagendijk, and G. H. Wegdam, *Strong effects of photonic band structures on the diffraction of*

colloidal crystals, Phys. Rev. B **53**, 16231 (1996).
[21] H. M. van Driel and W. L. Vos, *Multiple Bragg wave coupling in photonic band-gap crystals*, Phys. Rev. B **62**, 9872 (2000).
[22] H. S. Sözüer and J. W. Haus, *Photonic bands - simple-cubic lattice*, J. Opt. Soc. B **10**, 296 (1993).
[23] K. M. Ho, C. T. Chan, and C. M. Soukoulis, *Existence of a photonic gap in periodic dielectric structures*, Phys. Rev. Lett. **65**, 3152 (1990).
[24] C. T. Chan, K. M. Ho, and C. M. Soukoulis, *Photonic band-gaps in experimentally realizable periodic dielectric structures*, Europhys. Lett. **16**, 563 (1991).
[25] E. Yablonovitch, T. J. Gmitter, and K. M. Leung, *Photonic band structure: the face-centered-cubic case employing nonspherical atoms*, Phys. Rev. Lett. **67**, 2295 (1991).
[26] K. M. Ho, C. T. Chan, C. M. Soukoulis, R. Biswas, and M. Sigalas, *Photonic band-gaps on 3-dimensions: New layer-by-layer periodic structures*, Solid State Commun. **89**, 413 (1994).
[27] K. Busch and S. John, *Photonic band gap formation in certain self-organizing systems*, Phys. Rev. E **58**, 3896 (1998).
[28] V. N. Bogomolov, S. V. Gaponenko, I. N. Germanenko, A. M. Kapitonov, E. P. Petrov, N. V. Gaponenko, A. V. Prokofiev, A. N. Ponyavina, N. I. Silvanovich, and S. M. Samoilovich, *Photonic band gap phenomenon and optical properties of artificial opals*, Phys. Rev. E **55**, 7619 (1997).
[29] C. López, *Materials aspects of photonic crystals*, Adv. Mater. **15**, 1679 (2003).
[30] Z. Y. Li and Z. Q. Zhang, *Weak photonic band gap effect on the fluorescence lifetime in three-dimensional colloidal photonic crystals*, Phys. Rev. B **63**, 125106 (2001).
[31] J. Martorell and N. M. Lawandy, *Observation of inhibited spontaneous emission in a pediodic dielectric structure*, Phys. Rev. Lett. **65**, 1877 (1990).
[32] B. Y. Tong, P. K. John, Y. Zhu, Y. S. Liu, S. K. Wong, and W. R. Ware, *Fluorescence-lifetime measurements in monodispersed suspensions of polystyrene particles*, J. Opt. Soc. Am. B **10**, 356 (1993).
[33] I. S. Nikolaev, P. Lodahl, and W. L. Vos, *Fluorescence lifetime of emitters with broad homogeneous linewidths modified in opal photonic crystals*, J. Phys. Chem. C **112**, 7250 (2008).
[34] J. E. G. J. Wijnhoven and W. L. Vos, *Preparation of photonic crystals made of air spheres in titania*, Science **281**, 802 (1998).
[35] H. S. Sözüer, J. W. Haus, and R. Inguva, *Photonic bands: Convergence problems with the plane-wave method*, Phys. Rev. B **45**, 13962 (1992).
[36] A. Blanco *et al.*, *Large-scale synthesis of a silicon photonic crystal with a complete three-dimensional bandgap*, Nature **405**, 437 (2000).
[37] D. J. Norris and Y. A. Vlasov, *Chemical approaches to three-dimensional semiconductor crystals*, Adv. Mater. **13**, 409 (2001).
[38] P. Lodahl, A. F. van Driel, I. S. Nikolaev, A. Irman, K. Overgaag, D. Vanmaekelbergh, and W. L. Vos, *Controlling the dynamics of spontaneous emission from quantum dots by photonic crystals*, Nature **430**, 654 (2004).

[39] I. Nikolaev, P. Lodahl, A. van Driel, A. F. Koenderink, and W. Vos, *Strongly nonexponential time-resolved fluorescence of quantum-dot ensembles in three-dimensional photonic crystals*, Phys. Rev. B **75**, 115302 (2007).
[40] S. Matthias, F. Müller, C. Jamois, R. B. Wehrspohn, and U. Gösele, *Large-area three-dimensional structuring by electrochemical etching and lithography*, Adv. Mat. **16**, 2166 (2004).
[41] S. Matthias, F. Müller, and U. Gösele, *Simple cubic three-dimensional photonic crystals based on macroporous silicon and anisotropic post treatment*, J. Appl. Phys. **98**, 023524 (2005).
[42] M. Florescu, K. Busch, and J. P. Dowling, *Thermal radiation in photonic crystals*, Phys. Rev. B **75**, 201101 (2007).
[43] M. Laroche, R. Carminati, and J. J. Greffet, *Coherent thermal antenna using a photonic crystal slab*, Phys. Rev. Lett. **96**, 123903 (2006).
[44] J. J. Greffet, R. Carminati, K. Joulain, J. P. Mulet, S. Mainguy, and Y. Chen, *Coherent emission of light by thermal sources*, Nature **416**, 61 (2002).
[45] M. Christophersen, J. Carstensen, A. Feuerhake, and H. Föll, *Crystal orientation and electrolyte dependence for macropore nucleation and stable growth on p-type si*, Mater. Sci. Eng. B **69**, 194 (2000).
[46] S. Y. Lin, J. G. Fleming, D. L. Hetherington, B. K. Smith, R. Biswas, K. M. Ho, M. M. Sigalas, W. Zubrzycki, S. R. Kurtz, and J. Bur, *A three-dimensional photonic crystal operating at infrared wavelengths*, Nature **394**, 251 (1998).
[47] J. G. Fleming and S. Y. Lin, *Three-dimensional photonic crystal with a stop band from 1.35 to 1.95 μm*, Opt. Lett. **24**, 49 (1998).
[48] S. Noda, K. Tomoda, N. Yamamoto, and A. Chutinan, *Full three-dimensional photonic bandgap crystals at near-infrared wavelengths*, Science **289**, 604 (2001).
[49] K. Aoki, H. T. Miyazaki, H. Hirayama, K. Inoshita, T. Baba, K. Sakoda, N. Shinya, and Y. Aoyagi, *Microassembly of semiconductor threedimensional photonic crystals*, Nat. Mater. **2**, 117 (2001).
[50] M. J. A. de Dood, A. Polman, and J. G. Fleming, *Modified spontaneous emission from erbium-doped photonic layer-by-layer crystals*, Phys. Rev. B **67**, 115106 (2003).
[51] R. Hillebrand, S. Senz, W. Hergert, and U. Gösele, *Macroporous-silicon-based three-dimensional photonic crystal with a large complete band gap*, J. Appl. Phys. **94**, 2758 (2003).
[52] L. A. Woldering, A. P. Mosk, R. W. Tjerkstra, and W. L. Vos, *The influence of fabrication deviations on the photonic band gap of three-dimensional inverse woodpile nanostructures*, J. Appl. Phys. **105**, 093108 (2009).
[53] J. Schilling, J. White, A. Scherer, G. Stupian, R. Hillebrand, and U. Gösele, *Three-dimensional macroporous silicon photonic crystal with large photonic band gap*, Appl. Phys. Lett. **86**, 011101 (2005).
[54] T. Yoshie, A. Scherer, J. Hendrickson, G. Khitrova, H. M. Gibbs, G. Rupper, C. Ell, O. B. Shchekin, and D. G. Deppe, *Vacuum rabi splitting with a single quantum dot in a photonic crystal nanocavity*, Nature **432**, 200 (2004).
[55] J. P. Reithmaier, G. Sęk, A. Löffler, C. Hofmann, S. Kuhn, S. Reitzenstein,

L. V. Keldysh, V. D. Kulakovskii, T. L. Reinecke, and A. Forchel, *Strong coupling in a single quantum dot-semiconductor microcavity system*, Nature **432**, 197 (2004).

[56] E. Peter, P. Sennelart, D. Martrou, A. Lemaître, J. Hours, J. M. Gérard, and J. Bloch, *Exciton-photon strong-coupling regime for a single quantum dot embedded in a microcavity*, Phys. Rev. Lett. **95**, 067401 (2005).

[57] S. John and T. Quang, *Spontaneous emission near the edge of a photonic band gap*, Phys. Rev. A **50**, 1764 (1994).

[58] P. Kristensen, A. F. Koenderink, P. Lodahl, B. Tromborg, and J. Mørk, *Fractional decay of quantum dots in real photonic crystals*, Opt. Lett. **33**, 1557 (2008).

[59] L. V. Hove, *The occurence of singularities in the elastic frequency distribution of a crystal*, Phys. Rev. **89**, 1189 (1953).

[60] T. Euser, H. Wei, J. Kalkman, Y. Jun, A. Polman, D. Norris, and W. Vos, *Ultrafast optical switching of three-dimensional si inverse opal photonic band gap crystals*, J. Appl. Phys. **102**, 053111 (2007).

[61] P. Harding, T. Euser, Y. Nowicki-Bringuier, J. Gérard, and W. Vos, *Dynamical ultrafast all- optical switching of planar GaAs/AlAs photonic microcavities*, Appl. Phys. Lett. **91**, 111103 (2007).

[62] P. Sheng, *Introduction to wave scattering, localization and mesoscopic phenomena* (Academic Press, New York, 1995).

[63] D. Wiersma, P. Bartolini, A. Lagendijk, and R. Righini, *Localization of light in a disordered medium*, Nature **390**, 671 (1997).

[64] A. F. Koenderink, A. Lagendijk, and W. L. Vos, *Optical extinction due to intrinsic structural variations of photonic crystals*, Phys. Rev. B **72**, 153102 (2005).

[65] A. D. Mirlin, *Statistics of energy levels and eigenfunctions in disordered systems*, Phys. Rep. **326**, 259 (2000).

[66] S. E. Skipetrov and R. Maynard, *Nonuniversal correlations in multiple scattering*, Phys. Rev. B. **62**, 886 (2000).

[67] L. S. Froufe-Pérez, R. Carminati, and J. J. Sáenz, *Fluorescence decay rate statistics of a single molecule in a disordered cluster of nanoparticles*, Phys. Rev. A **76**, 013835 (2007).

[68] M. D. Birowosuto, S. E. Skipetrov, W. L. Vos, and A. P. Mosk, *Observation of spatial fluctuations of the local density of states in random media*, Phys. Rev. Lett. **105**, 013904 (2010).

[69] J. R. Lakowicz, *Principles of fluorescence spectroscopy* (Kluwer Academic, New York, 1999).

[70] R. F. Kubin and A. N. Fletcher, *Fluorescence quantum yields of some rhodamine dyes*, J. Lumin. **27**, 455 (1982).

[71] U. Woggon, *Optical properties of semiconductor quantum dots* (Springer, Berlin, 1997).

[72] A. P. Alivisatos, *Perspectives on the physical chemistry of semiconductor nanocrystals*, J. Phys. Chem. **100**, 13226 (1996).

[73] L. E. Brus, *Electron-electron and electron-hole interaction in small semiconductor crystallites: The size dependence of the lowest excited electron state*,

J. Chem. Phys **80**, 4403 (1984).

[74] A. L. Efros, M. Rosen, M. Kuno, M. Nirmal, D. J. Norris, and M. G. Bawendi, *Band-edge exciton in quantum dots of semiconductors with a degenerate valence band: Dark and bright exciton states*, Phys. Rev. B **54**, 4843 (1996).

[75] S. V. Gaponenko, *Optical properties of semiconductor nanocrystals* (Cambridge university press, Cambridge, 1998).

[76] X. Brokmann, L. Coolen, M. Dahan, and J. P. Hermier, *Measurement of radiative and nonradiative decay rates of single CdSe nanocrystals through a controlled modification of their spontaneous emission*, Phys. Rev. Lett. **93**, 107403 (2004).

Chapter 2
Optical properties of CdSe quantum dots determined by controlling the local density of states

Control over spontaneous emission is important for many applications in nanophotonics, such as efficient miniature lasers and LEDs [1, 2], efficient solar energy collection [3], and even biophotonics [4]. Increasing attention has been given to all solid state cavity quantum electrodynamics (QED) experiments [5–8]. For spontaneous emission control the oscillator strength of a light source plays a crucial role. The oscillator strength gauges the strength of the interaction of a light source with the light field. The larger the oscillator strength is, the stronger is the interaction between the source and the light field, and in cavity QED between the source and the cavity field.

As light sources in nanophotonics, quantum dots are becoming increasingly popular. Quantum dots are semiconductor nanocrystals with sizes smaller than the exciton Bohr radius. Due to their small size, quantum dots have discrete energy levels [9]. CdSe colloidal quantum dots in particular have generated enormous interest in recent years because of the tunability of their emission energy over the entire visible range with particle diameter [10]. Surprisingly no measurements have been done of the emission oscillator strength of these quantum dots, while this is highly important to interpret cavity QED experiments [11]. The oscillator strength has been investigated only qualitatively using absorption measurements [12–14]. However, the accuracy of these measurements is limited due to the strong blinking behavior of CdSe quantum dots, i.e., intermittency in the emission of photons. Moreover, the oscillator strength determined from absorption is not relevant to emission experiments since the quantum dots in the off-state do absorb while they do not contribute to the emission.

In this chapter we present quantitative measurements of the oscillator strength and quantum efficiency of colloidal CdSe quantum dots as a function of emission energy and thus dot diameter since the emission energy and diameter are uniquely related [10]. The oscillator strength of an emitter can be determined by placing it close to an interface. The emission rate is then also affected by emission which is reflected at the interface. This interference leads to a controlled modification of the local density of states (LDOS) allowing us to separate radiative and nonradiative decay rate components. This technique has been pioneered by Drexhage for dye molecules [15] and used to determine quantum efficiency of Si nanocrys-

tals [16], erbium ions [17], epitaxially grown InAs quantum dots [18] and colloidal CdSe quantum dots [19, 20]. Recently it has been found that the emission oscillator strength can also be determined with this technique [18]. Here, we place CdSe quantum dots on different distances near a silver interface to quantitatively determine the oscillator strength as a function of emission energy.

2.1. Experimental Methods

2.1.1. Sample fabrication

The planar samples with controllable LDOS consist of a glass substrate of 24 by 24 mm on which a stack of 4 different layers is made, as shown in fig. 2.1. 1) The first layer is an optically thick 500 nm layer of silver that is deposited with vapor deposition. 2) Next a layer of SiO_2 is evaporated onto the silver. The SiO_2 layer has a refractive index of 1.55 $\pm$ 0.01 at a wavelength of 600 nm as determined by ellipsometry. The thickness of the SiO_2 layer is varied to control the distance z that the quantum dots have to the silver interface. 3) On top of the SiO_2 layer, a very thin layer of polymethyl methacrylate (PMMA) is spincoated that contains the CdSe quantum dots. This layer is $\Delta z = 14 \pm 5$ nm thick, determined by profilometry. PMMA has a refractive index of 1.49 ± 0.01. 4) On top of the PMMA layer a thick $\sim 1\mu m$ layer of polyvinyl alcohol (PVA) is spincoated to avoid reflections from a PMMA/air interface. The PVA is 9.4 % by weight dissolved in a mixture of water and ethanol. Since the PMMA and quantum dots do not dissolve in water and ethanol, the PMMA layer stays intact. PVA has a refractive index of 1.50 ± 0.01. All parameters are summarized in Table 2.1.

Table 2.1.: Layer properties

Layer	Thickness (nm)	Refractive index	Fabrication method
1) Silver	500	$0.27 + 4.18i$	vapor deposition
2) SiO_2	variable z	1.55	vapor deposition
3) PMMA + QDs	14 ± 5	1.49	spincoating
4) PVA	~ 1000	1.50	spincoating

2.1.2. Quantum dots

CdSe quantum dots with a ZnS shell are purchased from Evident Technology (Fort Orange, emitting around 600 nm). We have performed transmission electron microscopy experiments to verify the quantum dot diameter. Fig. 2.2 a shows a TEM micrograph of a typical dot that has a diameter of 3.9 nm. From measurements on 98 quantum dots, we have determined the histogram of diameter distributions, see fig. 2.2 b. The quantum dots have an average diameter of D = 4.1 nm with a standard deviation of 0.5 nm. Hence, our quantum dots

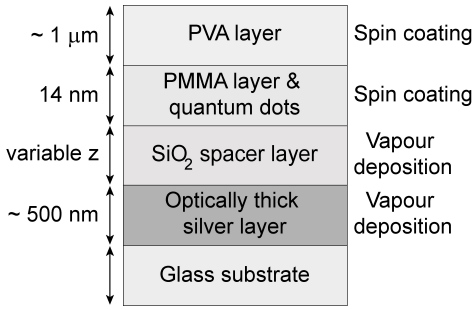

Figure 2.1.: Schematic cross-section of the sample used in the measurements. The different layers of the sample are shown together with corresponding thickness and fabrication technique.

are smaller than the exciton Bohr radius and therefore the strong confinement regime for excitons applies to our dots.

The suspension that is spincoated consists of toluene with 0.5 % by weight 495,000 molecular weight PMMA and a quantum dot concentration of 1.21 10^{-6} mol/liter. The quantum dots have an estimated density of 1 per 450 nm^2. The quantum dots are thus sufficiently dilute in the PMMA layer to exclude energy transfer and reabsorption processes between quantum dots. This was verified by measuring that the decay rate was not influenced by laser power or changes in concentration around the used concentration. The sample is contained in a nitrogen purged chamber during measurements to prevent photo oxidation of the quantum dots.

2.1.3. Optical detection

The optical set-up used in the experiments is schematically shown in fig. 2.3. Light from a pulsed frequency doubled Nd^{3+}:YAG laser (Time Bandwidth Cougar) with an emission wavelength of 532 nm, repetition rate of 8.2 MHz and pulse widths of 11 ps is used. This light is guided into an optical fiber and focused onto the sample by a lens with a focal length of 250 mm, leading to a focus with a diameter of approximately 50 μm on the sample.

The light emitted by the quantum dots is collected by a lens, collimated and focused onto the slit of a prism monochromator (Carl Leiss). The slit width is set to 400 μm giving a spectral resolution $\Delta\lambda = 6$ nm, which is narrow compared to the bandwidth of the LDOS changes. A Hamamatsu multichannel plate photomultiplier tube is used as a photon counter. With this setup it is possible to measure spectra by scanning the monochromator and to measure decay curves of emitters at particular emission frequencies by time correlated single photon counting [21]. This technique measures the time between the arrival of an emitted photon (start) and the laser pulse (stop) with ps resolution. By repeating such a measurement a histogram of the arrival times is made from which a decay rate can be determined. The time resolution of the set-up is 125 ps, given by

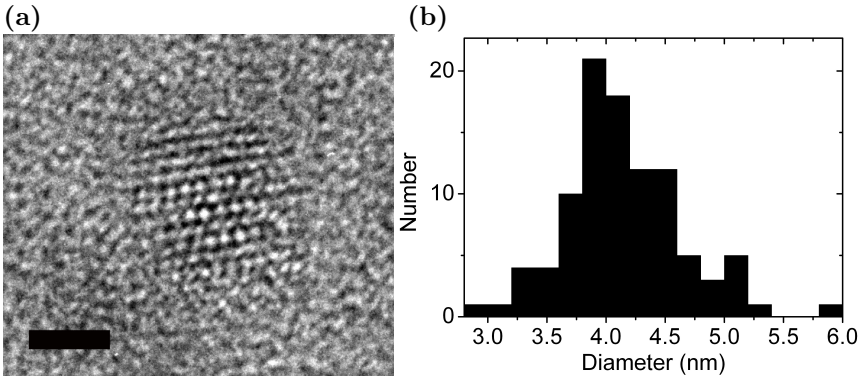

Figure 2.2.: a) Transmission electron micrograph of a CdSe quantum dot with a diameter D = 3.9 nm. The fringes from the lattice planes are clearly seen. The scale bar is 2 nm. b) The distribution in diameter found by analyzing TEM images of 98 quantum dots. The average diameter is 4.1 nm with a standard deviation of 0.5 nm.

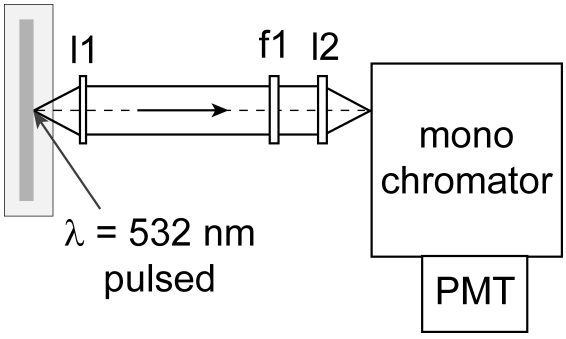

Figure 2.3.: A schematic picture of the experimental setup. Light from the laser excites the quantum dots in a layered sample inside a nitrogen purged chamber. The emitted light is collimated by a lens L1 with f=12 cm, focused by lens L2 with f=10 cm on the entrance slit of a monochromator and detected by the photomultiplier tube. A filter f1 is added to block any scattered laser light.

the full width half maximum of the total instrument response function that is shown in fig. 2.5. The instrument response function is much shorter than the decay curve of CdSe quantum dots, with a typical decay time of 16 ns in toluene. Therefore, deconvolution of the response function is not necessary to analyze the data.

2.1.4. Data interpretation

The quantum dots in the polymer layer show a nonexponential decay, probably caused by microscopic heterogeneity of the polymer [22]. Nonexponential behavior has previously been found for CdSe quantum dots in PMMA by Fisher et al. [23] even for single quantum dots. To model the decay curve the data are fitted with a distribution of decay rates as explained in ref. [24]. A function of the following form is used to model the decay curve:

$$f(t) = \int_0^\infty \sigma(\gamma_{tot}) \exp(-\gamma_{tot} t) \mathrm{d}\gamma_{\mathrm{tot}} \tag{2.1}$$

where the normalized distribution in decay rates is chosen to be lognormal

$$\sigma(\gamma) = A \exp\Big[- \Big(\frac{ln(\gamma) - ln(\gamma_{mf})}{w} \Big)^2 \Big] \tag{2.2}$$

The normalization factor A equals $A = [\gamma_{mf} w \sqrt{\pi} \exp(w^2/4)]^{-1}$. The two relevant adjustable parameters that can be extracted from the model are the most frequent decay rate γ_{mf} which is the peak of the lognormal distribution and $\Delta\gamma = 2\gamma_{mf} \sinh(w)$ which is the $\frac{1}{e}$ width of the lognormal distribution.

Decay rates presented in this paper are an average of decay rates found for at least three measurements performed on different locations on a sample with a particular SiO_2 layer thickness. The error in the decay rate is conservatively estimated to be $\pm$ 3 % which is the maximum difference found between measurements on the same sample.

2.2. Results

2.2.1. Experimental results

In fig. 2.4 the emission spectrum of CdSe quantum dots is shown for the quantum dots in toluene, in a planar sample without silver, and in a planar sample with a silver mirror. The peak energies of all three spectra are identical within experimental error. The width of the spectrum is caused by inhomogeneous broadening due to size polydispersity of quantum dots in the ensemble. The homogeneous spectral width of the individual quantum dots is much narrower [25]. By selecting a narrow emission energy window quantum dots of a particular diameter are selected. Within experimental error there is no difference between the width of the emission spectra in the different environments, indicating that there is no spectral broadening due to the polymer environment.

In fig. 2.5 decay curves are shown at the emission peak at 2.08 eV for an ensemble of quantum dots in toluene suspension and in a planar layer without

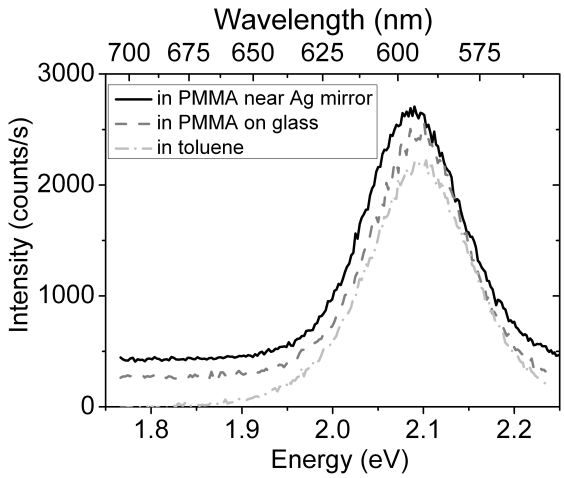

Figure 2.4.: Emission spectra of CdSe quantum dots in toluene suspension, in a planar sample without silver, and in a planar sample with a silver mirror. The spectra are offset for clarity by 200 and 400 counts/s respectively. The spectrum in PMMA near the mirror and in toluene are scaled to the spectrum in PMMA on glass by a factor of 0.75.

mirror. The quantum dots in toluene show a single exponential decay as expected, giving a decay rate $\gamma = 0.061$ ns$^{-1} \pm 0.002$. Fitting the data with a single exponential gives a value of 1.94 for the goodness of fit χ^2_{red} indicative of a reasonable fit [26].

The lognormal distribution of decay rates can be fitted to the decay curve of quantum dots inside PMMA and appears to be a good fit with $\chi^2_{red} = 1.49$. For the quantum dots inside the PMMA layer $\gamma_{mf} = 0.084$ ns$^{-1} \pm 0.002$. The decay of spontaneous emission from quantum dots in toluene suspension can also be fitted with a lognormal distribution of decay rates, giving $\chi^2_{red} = 1.71$. The distribution of decay rates in toluene is characterised by $\gamma_{mf} = 0.063$ ns$^{-1} \pm 0.002$ close to the value for the decay rate $\gamma = 0.061$ ns$^{-1} \pm 0.002$ found from a single exponential decay. In fig. 2.6 the lognormal distributions of decay rates are shown for the decay curve of quantum dots in toluene and in the polymer layer. The distribution of decay rates for quantum dots in polymer is much broader than the distribution found for quantum dots in toluene. When a curve is modeled with a single exponential decay the decay rate distribution reduces to a delta function. The decay rate at the peak of the distribution, the most frequent decay rate, characterizes the decay in the measurement best as supported by the fact that the single exponential rate γ and γ_{mf} for decay in toluene are equal within experimental error. Therefore, the most frequent decay rate will be used in our further analysis.

Measurements of decay rates for two planar samples with different SiO_2 layer thicknesses ($z = 73$ nm and $z = 166$ nm respectively for sample 1 and 2) are

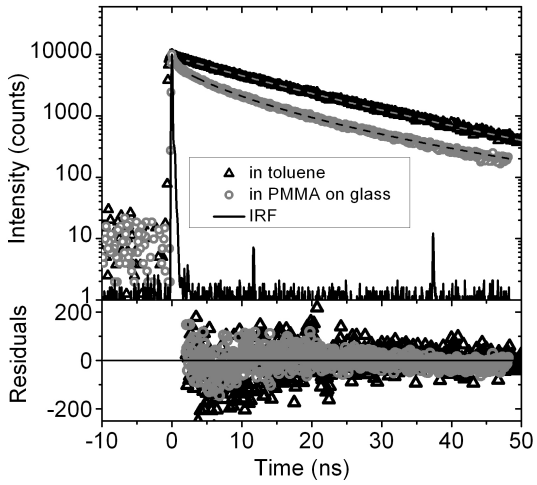

Figure 2.5.: Decay curves of quantum dots at the emission peak at 2.08 eV in PMMA on glass with a top layer of PVA (grey circles) and these quantum dots in toluene suspension (black triangles). The instrument response function (IRF) is indicated by the black line. The peaks in the IRF near 12 and 36 ns are related to the pulse picker of the laser. The decay curves are fitted with a lognormal distribution of decay rates. Residuals are shown in the bottom panel.

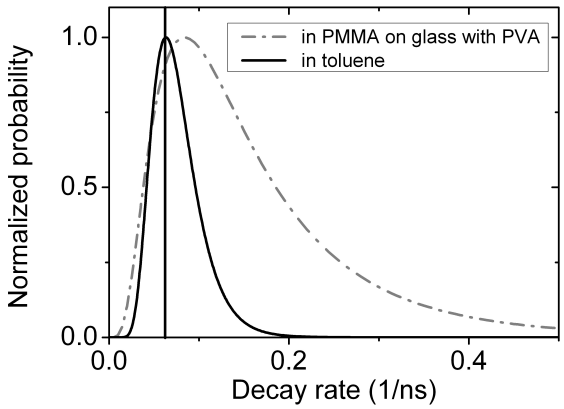

Figure 2.6.: Lognormal distribution of decay rates of quantum dots in a PMMA layer on glass with a PVA cover layer and for quantum dots in toluene resulting from fits in fig. 2.5. The black vertical line shows the delta function distribution for single exponential fit.

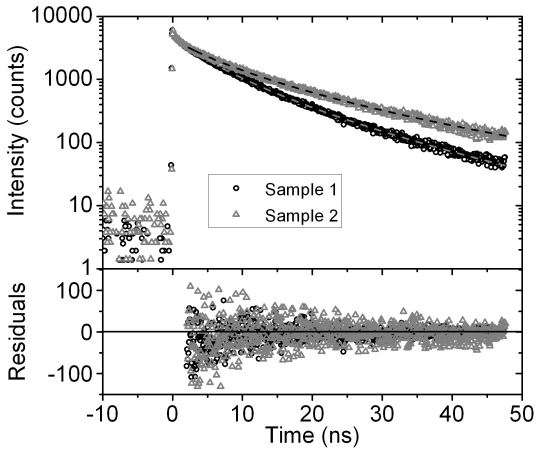

Figure 2.7.: Decay curves for quantum dots samples with different SiO_2 layer thicknesses, $z = 73$ nm and $z = 166$ nm respectively for sample 1 and 2, measured at an emission energy of 2.08 eV. The decay curves are fitted with a lognormal distribution of decay rates. Residuals are shown in the bottom panel.

shown in fig. 2.7 for quantum dots that emit at the peak emission energy of 2.08 eV. Nonexponential and significantly different decay curves are found for quantum dots that have different distances to the silver interface. The quantum dots in sample 1 clearly decay faster than those in sample 2. The experimental curves are fitted with a lognormal distribution of decay rates. The residuals shown in the bottom panel are randomly distributed around a mean value of zero, signalling a good fit. Indeed the χ^2_{red} is 0.72 and 1.44 for sample 1 and 2 respectively, close to the ideal value of 1, confirming that the decay curves are well modeled by a lognormal distribution of decay rates.

2.2.2. Model of decay rates

Results for the most frequent decay rate for different distances to the interface are presented in fig. 2.8 for two different emission energies. The most frequent decay rate decreases with increasing distance to the silver mirror. The measured decay rate γ_{tot} is a sum of radiative γ_{rad} and nonradiative γ_{nrad} decay rate, $\gamma_{tot} = \gamma_{rad} + \gamma_{nrad}$. From Fermi's golden rule the radiative decay rate is proportional to the projected LDOS $\rho(\omega, z)$. Therefore, the total decay rate can be expressed as

$$\gamma_{tot}(\omega, z) = \gamma_{nrad}(\omega) + \gamma^{hom}_{rad}(\omega)\frac{\rho(\omega, z)}{\rho_{hom}(\omega)} \tag{2.3}$$

Here, $\rho_{hom}(\omega)$ is the LDOS in a homogeneous medium. The LDOS near an interface has been calculated using a theory developed by Chance, Prock and Silbey [27]. As a model an interface between two semi infinite media has been used, with $n_1 = 0.27 + 4.18i$ (Ag layer) [28] and $n_2 = 1.52$ (SiO2, PMMA and PVA). The LDOS is calculated for transition dipoles oriented parallel or perpendicular to the interface, since our measurements are performed on an ensemble of quantum dots that are randomly oriented with respect to the interface. This situation differs from self-assembled dots that are strongly oriented [18]. A decay measurement $f(t)$ for an ensemble of emitters can be described by the following expression [29, 30]:

$$f(t) = \frac{I_0}{2\pi} \int_0^{2\pi} \mathrm{d}\phi \int_0^{\pi/2} \mathrm{d}\theta \mathrm{A}(\theta,\phi)\ \gamma(\theta,\phi)\ \mathrm{e}^{-\gamma(\theta,\phi)\mathrm{t}}\ \sin\theta \tag{2.4}$$

The term $A(\theta,\phi)$ accounts for angle dependence of absorption, emission and detection. CdSe quantum dots do not have angle dependent absorption [31]. Moreover, CdSe quantum dots are known to have a 2D transition dipole described by a "dark axis" along the c-axis of the nanocrystal and a "bright plane" perpendicular to this axis in which the transition dipole can be oriented [31, 32]. Since the quantum dots have a 2D dipole, the emission is less directional than if it were a 1D dipole. Because the angle dependence of the emission and detection plays a small role, the factor $A(\theta,\phi)$ can be safely taken to be independent of θ and ϕ. Near an interface, the decay rate γ is no longer dependent on ϕ and is given by $\gamma(\theta) = \gamma_\parallel \cos(\theta)^2 + \frac{(\gamma_\parallel+\gamma_\perp)}{2} \sin(\theta)^2$ where θ is the angle between the dark axis of the quantum dot and the normal to the interface as defined in fig. 2.9. Therefore, carrying out the integral over ϕ results in

$$f(t) = I_0 \int_0^{\pi/2} \left(\gamma_\parallel \cos^2\theta + \frac{(\gamma_\parallel+\gamma_\perp)}{2} \sin^2\theta\right)\ e^{-(\gamma_\parallel \cos^2\theta + \frac{(\gamma_\parallel+\gamma_\perp)}{2} \sin^2\theta)\ t}\ \sin\theta\ \mathrm{d}\theta \tag{2.5}$$

If $\gamma_\parallel = \gamma_\perp$ the decay curve shows a single exponential decay. When $\gamma_\parallel$ and $\gamma_\perp$ have different values a multi-exponential decay is found. In our experiment, $\gamma_\parallel$ and $\gamma_\perp$ only differ by about at most 10 %. If $f(t)$ is calculated for an intensity range of 3 decades relevant to our experiment, a single exponential decay is found to a very high precision with a decay rate given by $\gamma_{tot} = \frac{1}{3}\gamma_\perp + \frac{2}{3}\gamma_\parallel$. This isotropic decay rate is also used for experiments with atoms near an interface, where the atom have a rotating transition dipole moment [33].

2.2.3. Discussion

The lines in fig. 2.8 show the calculated isotropic decay rate versus distance to the interface. The calculations are in very good agreement with the data.

By calculating the LDOS for each distance, the distance axis in fig. 2.8 can be converted to an LDOS axis. In fig. 2.10 the results are shown for two different emission frequencies together with a linear fit. Very good agreement between experiments and theory is observed as expected from Fermi's golden rule. For an

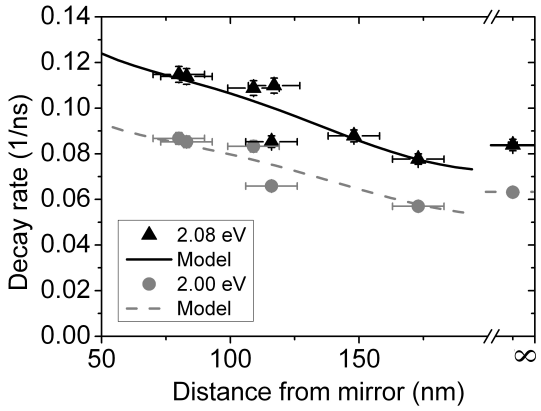

Figure 2.8.: Most frequent decay rate γ_{mf} versus distance to the interface for an emission energy of 2.08 eV (grey circles) and 2.00 eV (black triangles). The lines show calculations of the decay rate using the model developed by Chance, Prock and Silbey [27].

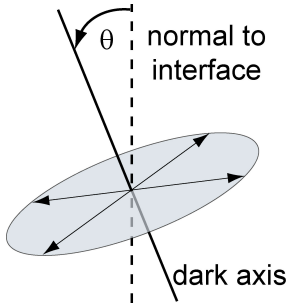

Figure 2.9.: The angle θ is the angle between the dark axis of the CdSe quantum dot and the normal to the interface

emission energy of 2.08 eV $\gamma_{nrad} = 0.017 \pm 0.006$ ns^{-1} and $\gamma_{rad}^{hom} = 0.065 \pm 0.005$ ns^{-1} giving a quantum efficiency of 80 ± 5 %.

In fig. 2.11 a) the homogeneous radiative decay rate γ_{rad}^{hom} is shown as a function of the emission energy. The homogeneous radiative decay rate is observed to first increase and then decrease with emission frequency. The radiative decay rate found by Brokmann *et al.* [19] corresponds very well to our data. It should be noted that we derive the homogeneous radiative decay from the most frequent decay rate of the distribution. Since our data agree very well with the decay rate found using a single exponential model and a much shorter integration time [19], this corroborates our choice for the most frequent decay rate as the parameter that describes the decay curves best. Our results also validate the choice for the isotropic decay rate model assumed by Brokmann *et al.*

Previously Van Driel *et al.* reported that the total decay rate (which is the sum of radiative and nonradiative decay rate) of CdSe colloidal quantum dots increase with emission energy [34] in agreement with our measurements. A theory was developed for the radiative decay rate as a function of frequency. For an ideal two level exciton, the radiative decay rate should be proportional to frequency. If a multilevel model of the exciton is considered this increase will be supra-linear. In reference [34] the model for the excitonic multilevel emitter shows agreement with the total decay rate data for CdSe quantum dots and excellent agreement for CdTe dots. The assumption was also made that the total decay rate is equal to the radiative decay rate. However, this is not valid, as can be seen in fig. 2.11 a). Results for the multilevel exciton model for radiative decay rate are plotted in fig. 2.11 a). The model does not match the data, indicating that the multilevel exciton model is not a correct description for CdSe quantum dots. The results of a tight binding calculation [35] has values 75 % lower than in the experiment, which thus also do not describe CdSe quantum dots. Califano *et al.* [36] calculated the room temperature radiative decay rate via a pseudopotential calculation. A good agreement between this calculation and our data is seen, both qualitatively and quantitatively.

The quantum efficiency for different emission energies is shown in fig. 2.11 b). The quantum efficiency is found to be between 66 % and 89 % depending on emission energy. These values are significantly higher then the value stated by the supplier Evident, 30-50 %. This latter value was determined by comparing the emission intensity to an emitter with known quantum efficiency [26]. This method leads to an underestimation of the quantum efficiency because it depends on absorption of light: CdSe quantum dots show strong blinking behavior [23] and quantum dots that are in the off-state do absorb light, but do not emit. These quantum dots are probed with an absorption measurement, while there is no contribution to the emission. This causes an underestimation of the quantum efficiency in absorption measurements.

On the right axis in fig. 2.11 b) the nonradiative decay rate is plotted. The nonradiative decay rate increases with emission energy or equivalently decreases with quantum dot size. This is probably due to the fact that for smaller quantum dots the surface is relatively more important: Since the surface is a source of nonradiative decay, this decay rate is increased for smaller quantum dots. An

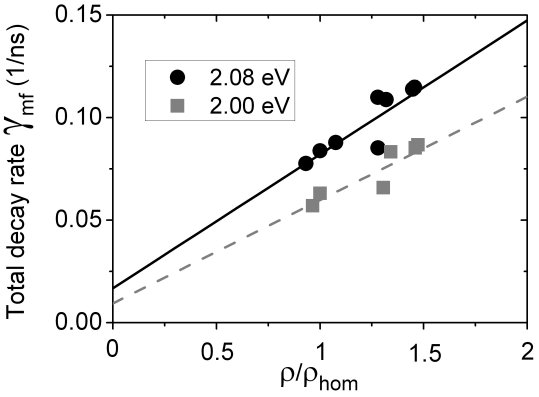

Figure 2.10.: The decay rate versus the normalised isotropic LDOS for two different emission energies. Data are fitted with a linear function as expected from Fermi's golden rule.

increased nonradiative decay rate for smaller quantum dots agrees with previous results for CdSe quantum dots [37] as well as for epitaxially grown InAs quantum dots [18]. The nonradiative decay rate found by Brokmann *et al.* [19] for a different batch of quantum dots is lower than our results. The difference could very well be caused by a difference in the ZnS capping layer since this drastically changes the nonradiative decay.

The emission oscillator strength f_{osc} of the transition can be calculated from the homogeneous radiative decay rate via [39]

$$f_{osc}(\omega) = \frac{6 m_e \epsilon_0 \pi c^3}{q^2 n \omega^2} \gamma_{rad}^{hom}(\omega) \tag{2.6}$$

where m_e is the electron mass, ϵ_0 is the vacuum permittivity, c is the speed of light, q is the electron charge and n is the refractive index of the surrounding material. For an emission energy of 2.08 eV $f_{osc} = 0.69 \pm 0.04$. This is, to our knowledge, the first experimental determination of the oscillator strength of colloidal quantum dots that is determined by measuring the photoluminescent emission from quantum dots. Previous qualitative experiments to determine the relation between oscillator strength and size of quantum dots used the absorption spectrum of the quantum dots [12–14]. The absorption oscillator strength is not necessarily equal to the emission oscillator strength since our measurement is only sensitive to quantum dots that emit light and are in the on-state, while absorption measurements probe all quantum dots of the strongly blinking ensemble, including dots that are in the off-state.

In fig. 2.11 c) the experimentally found oscillator strength is shown for different emission energies. The oscillator strength is only weakly dependent on energy: at first showing a slight increase which is followed by a slight decrease with increasing emission energy. Indeed for quantum dots in the strong confinement regime the oscillator strength is expected to be only weakly dependent on emission energy

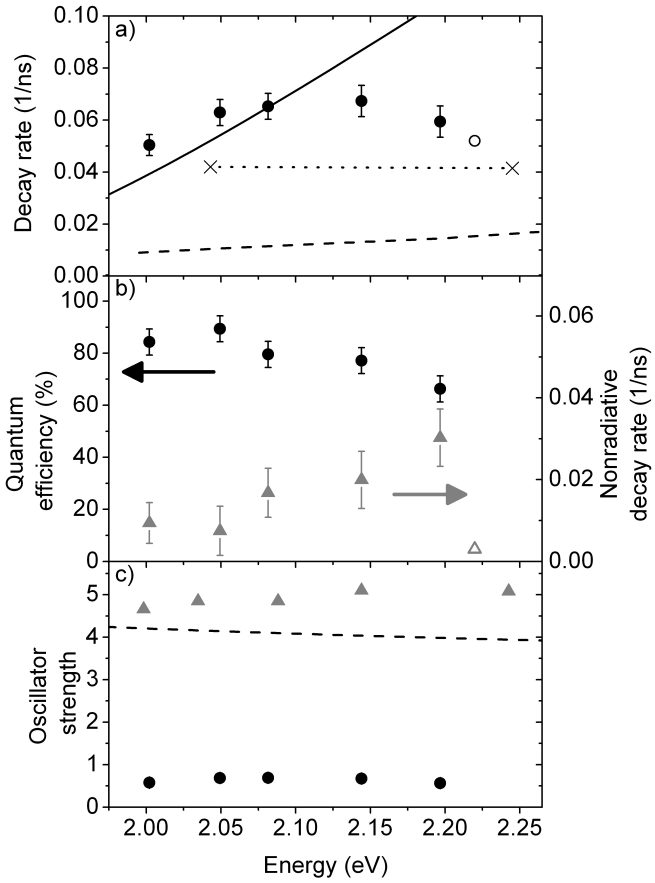

Figure 2.11.: a) Radiative decay rate (filled circles), determined from the linear fit in fig. 2.10 shown versus emission energies. One data point by Brokmann *et al.* [19] is plotted with the open circle. A model for a multilevel exciton from [34] is shown with a solid line. The dashed line is a tight binding calculation of radiative decay rate [35]. The crosses connected with the dotted line are the results from pseudopotential calculations [36]. b) Quantum efficiency (circles) and nonradiative decay rate (filled triangles) versus emission energies. The open triangle is the result for nonradiative decay from Ref. [19]. c) Oscillator strength for different emission energies (circles) together with a model describing a strongly confined quantum dot (equation 2.7, dashed line), and results from tight binding calculations (triangles) [38].

since in this regime, the wavefunctions of electron and hole overlap completely independent of quantum dot size [9, 40]. To verify whether this overlap between electron and hole is indeed unity, the wavefunctions for electron and hole were calculated using a finite-element method for a simple effective-mass quantum dot model. The overlap was calculated for a spherical CdSe quantum dot core with a 2 nm ZnS shell. As expected, the overlap deviated from unity by only 10^{-4} for core radii ranging from 2 to 4 nanometer.

In the strong confinement limit the oscillator strength is given by [40]

$$f_{osc} = \frac{3}{4}\frac{a_B^{*3}}{R^3}\frac{\omega_{bulk}}{\omega_{dot}} f_{bulk} \frac{\frac{4}{3}\pi R^3}{\frac{1}{2}\frac{\sqrt{3}}{2}a^2 c} = \frac{4}{\sqrt{3}}\pi\frac{a_B^{*3}}{a^2 c}\frac{\omega_{bulk}}{\omega_{dot}} f_{bulk} \tag{2.7}$$

where f_{osc} is the oscillator strength of the quantum dot, f_{bulk} is the oscillator strength in bulk per chemical CdSe unit, a_B^* is the exciton Bohr radius, R is the radius of the quantum dot, ω_{bulk} is the bulk emission frequency, ω_{dot} is the emission frequency of the quantum dot and a and c are the hexagonal lattice constants of CdSe (wurtzite structure). For $a_B^* = 5.4$ nm, $a = 0.4302$ nm, $c = 0.7014$ nm, $f_{bulk} = 5\ 10^{-4}$ per chemical CdSe unit [13] and $\omega_{bulk} = 2.79\ 10^{15}$ rad/s the expected curve is shown in fig. 2.11 c). The calculated values are surprisingly a factor of 5 larger than the experimentally found values. The oscillator strength has also been calculated by Ramaniah and Nair [38] by a tight binding approach and was found to be 4.9 for spherical CdSe quantum dots with a radius of 2.07 nm. Interestingly, if the oscillator strength is calculated from the radiative decay rate found by the tight binding approach [35] from fig. 2.11 a) oscillator strengths a factor of four lower than our experimental values are found, opposite to Ref. [38]. The cause of the differences between strong confinement (eq. 2.7), tight binding calculations and our data is not known. However, qualitatively in all cases a weak dependence on emission energy is found that slightly decreases for higher emission energy, in agreement with our results.

Results from absorption measurements [12, 13] also find that the oscillator strength is independent of radius. Leatherdale *et al.* [14] find a different behavior, seeing a linear relation between oscillator strength per volume and radius instead of a cubic dependence.

Remarkably, for such a widely studied quantum dot as CdSe, theoretical understanding of the emission behavior is limited. Only the pseudopotential calculations show quantitative agreement with our experiments while tight binding results show either under- or overestimation. Therefore, a fundamental study is warranted to interpret the large variations among the theoretical predictions.

2.2.4. Relative width of the distribution

In this chapter results are presented of the effect of modified LDOS on the most frequent decay rate. This most frequent decay rate is found by fitting a lognormal distribution of decay rates to the experimental decay curves. The other independent fitting parameter in this fit is the relative width of the lognormal distribution. In this section results for the relative width are presented.

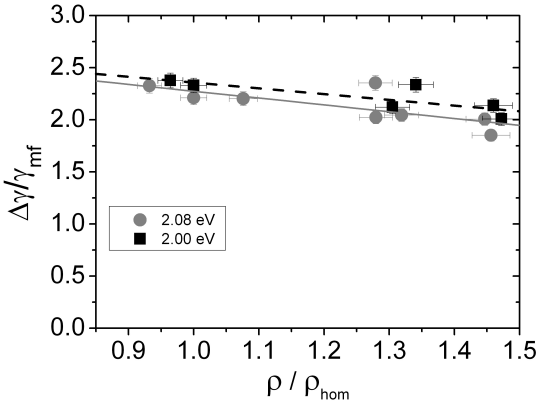

Figure 2.12.: Relative width of the lognormal distribution versus LDOS for emission energies of 2.08 and 2.00 eV. The lines are linear fits of the data.

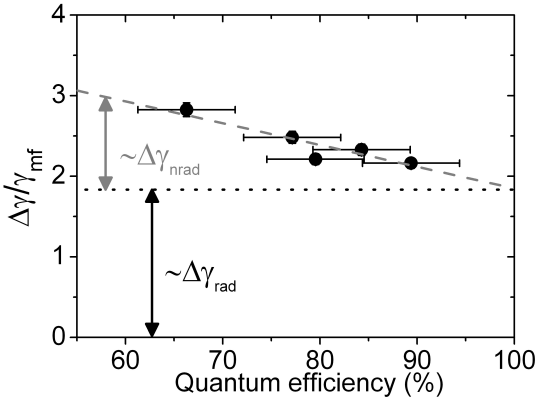

Figure 2.13.: Measurements of relative width for a homogeneous system (LDOS=1) plotted versus the extracted quantum efficiency (see fig. 2.11 b) together with a linear fit.

In fig. 2.12 the relative width, defined as $\frac{\Delta\gamma}{\gamma_{mf}}$, is plotted versus normalised local density of states for emission energies of 2.08 and 2.00 eV. For increasing LDOS the relative width decreases linearly. Increasing the LDOS effectively increases the quantum efficiency because the radiative decay rate is increased while the nonradiative decay rate is constant. For increasing quantum efficiency the distribution in decay rates gets narrower, giving a strong indication that the width of the distribution is determined by the nonradiative decay rate, which confirms the proposition by Fisher *et al.* [23].

In fig. 2.13 the relative width measured in the homogeneous environment with LDOS = 1 is plotted versus the extracted quantum efficiency for each emission

energy. The same trend is found: For increasing quantum efficiency the relative width of the distribution decreases linearly. When the quantum efficiency is 100 %, the decay rate is purely radiative. If the width in the distribution of decay rates is only caused by the nonradiative rate, the width should be zero at 100 % efficiency. This is not the case, indicating that there is a distribution in radiative decay rate as well. Vallée *et al.* [22] have also found distributions of decay rates for single dye in polymer and attribute this to local density variations in the surrounding polymer matrix causing a distribution in radiative decay rate. In conclusion, our data shows that there is both a distribution in nonradiative and radiative decay rate that cause the distribution in total decay rate.

2.3. Conclusions

In conclusion, we have separately determined the radiative and nonradiative decay of CdSe quantum dots by modifying the LDOS in a controlled way and measuring the total decay rate. This allows us to quantitatively determine the oscillator strength and quantum efficiency versus emission frequency. The nonradiative decay rate increases with emission energy corresponding to a decrease in quantum efficiency. The radiative decay rate first increases and then decreases with energy. This leads to the conclusion that the increase in total decay rate with energy measured previously is due to an increasing nonradiative component. The emission oscillator strength as a function of emission energy is determined with unprecedented accuracy since for the first time this quantity is determined directly from emission experiments. The oscillator strength is weakly size dependent, which is expected in the strong confinement regime. The oscillator strength is found to be on the order of 0.7. Previous calculations of the radiative decay rate by pseudopotential method agree well with our results, whereas the results from tight binding differ considerably. The limited oscillator strength makes the CdSe colloidal quantum dots less suited for cavity QED experiments. On the other hand, the quantitative determination of the oscillator strength paves the way for an *ab initio* understanding of spontaneous emission control [7].

References

[1] E. Yablonovitch, *Inhibited spontaneous emission in solid-state physics and electronics*, Phys. Rev. Lett. **58**, 2059 (1987).

[2] H.-G. Park, S.-H. Kim, S.-H. Kwon, Y.-G. Ju, J.-K. Yang, J.-H. Baek, S.-B. Kim, and Y.-H. Lee, *Electrically driven single-cell photonic crystal laser*, Science **305**, 1444 (2004).

[3] M. Grätzel, *Photoelectrochemical cells*, Nature **414**, 338 (2001).

[4] C. Blum, A. P. Mosk, I. S. Nikolaev, V. Subramaniam, and W. L. Vos, *Color control of natural fluorescent proteins by photonic crystals*, Small **4**, 492 (2008).

[5] T. Yoshie, A. Scherer, J. Hendrickson, G. Khitrova, H. M. Gibbs, G. Rupper, C. Ell, O. B. Schekin, and D. G. Deppe, , Nature **432**, 200 (2004).

[6] J. P. Reithmaier, G. Sek, A. Loffler, C. Hofmann, S. Kuhn, S. Reitzenstein, L. V. Keldysh, V. D. Kulakovskii, T. L. Reinecke, and A. Forchel, *Strong coupling in a single quantum dotsemiconductor microcavity system*, Nature **432**, 197 (2004).

[7] P. Lodahl, A. F. van Driel, I. S. Nikolaev, A. Irman, K. Overgaag, D. Vanmaekelbergh, and W. L. Vos, *Controlling the dynamics of spontaneous emission from quantum dots by photonic crystals*, Nature **430**, 654 (2004).

[8] E. Peter, P. Senellart, D. Martrou, A. Lemaître, J. Hours, J. M. Gérard, and J. Bloch, *Exciton-photon strong-coupling regime for a single quantum dot embedded in a microcavity*, Phys. Rev. Lett. **95**, 067401 (2005).

[9] L. E. Brus, *Electron-electron and electron-hole interactions in small semiconductor crystallites: the size dependence of the lowest excited electronic state*, J. Chem. Phys **80**, 4403 (1984).

[10] A. L. Efros, M. Rosen, M. Kuno, M. Nirmal, and M. Bawendi, *Band-edge exciton in quantum dots of semiconductors with a degenerate valence band: dark and bright exciton states*, Phys. Rev. B. **54**, 4843 (1996).

[11] N. Le Thomas, U. Woggon, O. Schöps, M. V. Artemyev, M. Kazes, and U. Banin, *Cavity qed with semiconductor nanocrystals*, Nano Lett. **6**, 557 (2006).

[12] O. Schmelz, A. Mews, T. Basche, A. Herrmann, and K. Müllen, *Supramolecular complexes from cdse nanocrystals and organic fluorophors*, Langmuir **17**, 2861 (2001).

[13] A. Striolo, J. Ward, J. M. Prausnitz, W. J. Parak, D. Zanchet, D. Gerion, D. Milliron, and A. P. Alivisatos, *Molecular weight, osmotic second virial coefficient, and extinction coefficient of colloidal cdse nanocrystals*, J. Phys. Chem. B. **106**, 5500 (2002).

[14] C. A. Leatherdale, W. K. Woo, F. V. Mikulec, and M. G. Bawendi, *On the absorption cross section of cdse nanocrystal quantum dots*, J. Phys. Chem. B. **106**, 7619 (2002).

[15] K. H. Drexhage, *Influence of a dielectric interface on fluorescence decay time*, J. Lumin. **1-2**, 693 (1970).

[16] R. J. Walters, J. Kalkman, A. Polman, H. A. Atwater, and M. J. A. de Dood, *Photoluminescence quantum efficiency of dense silicon nanocrystal ensem-*

bles in sio2, Phys. Rev. B. **73**, 132302 (2006).

[17] E. Snoeks, A. Lagendijk, and A. Polman, *Measuring and modifying the spontaneous emission rate of erbium near an interface*, Phys. Rev. Lett. **74**, 2459 (1995).

[18] J. Johansen, I. S. Nikolaev, T. Lund-Hansen, P. T. Kristensen, J. M. Hvam, W. L. Vos, and P. Lodahl, *Size dependence of the wavefunction of self-assembled inas quantum dots from time-resolved optical measurements*, Phys. Rev. B. **77**, 073303 (2008).

[19] X. Brokmann, L. Coolen, M. Dahan, and J. P. Hermier, *Measurement of radiative and nonradiative decay rates of single cdse nanocrystals through a controlled modification of their spontaneous emission*, Phys. Rev. Lett. **93**, 107403 (2004).

[20] J. Y. Zhang, X. Y. Wang, and M. Xiao, *Modification of spontaneous emission from CdSe/CdS quantum dots in the presence of a semiconductor interface*, Optics Lett. **27**, 1253 (2002).

[21] D. V. O'Connor and D. Philips, *Time correlated single photon counting* (Academic Press, 1984).

[22] R. A. L. Vallée, N. Tomczak, L. Kuipers, G. J. Vancso, and N. F. van Hulst, *Single molecule lifetime fluctuations reveal segmental dynamics in polymers*, Phys. Rev. Lett. **91**, 038301 (2003).

[23] B. R. Fisher, H. Eisler, N. E. Stott, and M. G. Bawendi, *Emission intensity dependence and single-exponential behavior in single colloidal quantum dot fluorescence lifetimes*, J. Phys. Chem. B. **108**, 143 (2004).

[24] A. F. van Driel, I. S. Nikolaev, P. Vergeer, P. Lodahl, D. Vanmaekelbergh, and W. L. Vos, *Statistical analysis of time-resolved emission from ensembles of semiconductor quantum dots: Interpretation of exponential decay models*, Phys. Rev. B. **75**, 035329 (2007).

[25] S. A. Empedocles, D. J. Norris, and M. G. Bawendi, *Photoluminescence spectroscopy of single cdse nanocrystallite quantum dots*, Phys. Rev. Lett. **77**, 3873 (1996).

[26] J. R. Lakowicz, *Principles of fluorescence spectroscopy* (Kluwer Academic, 1999).

[27] R. R. Chance, A. Prock, and R. Silbey, *Advances in chemical physics, volume 37* (John Wiley & Sons, 1978).

[28] D. R. Lide (editor-in chief), *Crc handbook of chemistry and physics, 88th edition 2007-2008* (CRC Press, 2007).

[29] N. Danz, J. Heber, A. Bräuer, and R. Kowarschik, *Fluorescence lifetimes of molecular dye ensembles near interfaces*, Phys. Rev. A **66**, 063809 (2002).

[30] A. F. Koenderink, M. Kafesaki, C. M. Soukoulis, and V. Sandoghdar, *Spontaneous emission rates of dipoles in photonic crystal membranes*, J. Opt. Soc. Am. B. **23**, 1196 (2006).

[31] S. A. Empedocles, R. Neuhauser, and M. G. Bawendi, *Three-dimensional orientation measurements of symmetric single chromophores using polarization microscopy*, **399**, 126 (1999).

[32] A. L. Efros, *Luminescence polarization of cdse microcrystals*, Phys. Rev. B. **46**, 7448 (1992).

[33] W. L. Barnes, *Topical review: Fluorescence near interfaces: the role of photonic mode density*, J. Mod. Opt. **45**, 661 (1998).

[34] A. F. van Driel, G. Allan, C. Delerue, P. Lodahl, W. L. Vos, and D. Vanmaekelbergh, *Frequency-dependent spontaneous emission rate from cdse and cdte nanocrystals: Influence of dark states*, Phys. Rev. Lett. **95**, 236804 (2005).

[35] A. F. van Driel, *Light sources in semiconductor photonic materials*, Ph.D. thesis, University of Utrecht, 2006.

[36] M. Califano, A. Franceschetti, and A. Zunger, *Lifetime and polarization of the radiative decay of excitons, biexcitons, and trions in cdse nanocrystal quantum dots*, Phys. Rev. B. **75**, 115401 (2007).

[37] X. Fan, M. C. Lonergan, Y. Zhang, and H. Wang, *Enhanced spontaneous emission from semiconductor nanocrustals embedded in whispering gallery optical microcavities*, Phys. Rev. B. **64**, 115310 (2001).

[38] L. M. Ramaniah and S. V. Nair, *Optical absorption in semiconductor quantum dots: A tight-binding approach*, Phys. Rev. B. **47**, 7132 (1993).

[39] A. E. Siegman, *Lasers* (University Science Books, 1986).

[40] Y. Kayanuma, *Quantum-size effects of interacting electrons and holes in semiconductor microcrystals with spherical shape*, Phys. Rev. B. **38**, 9797 (1988).

Chapter 3
Non exponential decay of ensembles of emitters near an interface

From Fermi's golden rule it is known that the radiative decay rate is proportional to the local density of states (LDOS), see *e.g.* [1]. This LDOS is a function of position $\mathbf{r}$, frequency ω and dipole orientation $\mathbf{e_d}$. The effect of position (see e.g. chapter 2 and references therein) and frequency (chapter 5 and references) has often been studied. The experimental study on the effect of dipole orientation on the emission properties has only received attention recently, especially with the possibility of detecting light from a single emitter. A recent theoretical study has emphasised that the orientational dependence is fully characterised by the (extreme) rates along three perpendicular main axes, namely the minimum and the maximum rates and an intermediate rate [2].

Previously, ensembles of emitters were studied, starting with the pioneering experiments by Drexhage of emitters near an interface, reviewed in [3]. In the first experiments the decay was modeled with a single exponential with the isotropic decay rate, the decay rate averaged over all directions [4, 5]. However, if the emitter has a fixed transition dipole moment it is only sensitive to the LDOS projected on that particular orientation. In experiments on single emitters in an inhomogeneous environment a single exponential decay is found with a decay rate that depends on the dipole orientation [6, 7]. If one studies an ensemble of fixed emitters in a inhomogeneous environment, every different orientation of the transition dipole moment has a different decay rate leading to a multi-exponential decay curve [8, 9]. The degree of non-exponentiality depends on the difference between the extreme decay rates for different orientations of the transition dipole moment. While non-exponential decay is usually avoided in experiments, it has recently been realised that a careful analysis of such behavior yields new insight in the variation of the decay rates of the ensemble of emitters [10–12]. Even a relatively simple geometry close to an interface can have almost a factor of 3 difference between the extreme decay rates for differently oriented dipoles. However, up to now only single exponential decay curves were measured from ensembles near such interfaces [8, 13–15], due to limitations in the experimental set-up or sample preparation. Thus, the extreme rates of the ensemble remain obscured.

In this chapter, we present measurements of emission of ensembles of emitters near an interface, where a factor of 2.6 difference in LDOS for different dipole orientations is present. The non-exponential decay is clearly observed. The decay

curve agrees very well with the theoretically calculated decay curve. By using a Monte Carlo approach, it is shown that the distribution of the decay rates is purely caused by the dipole orientation, allowing an *ab initio* determination of the distribution of decay rates.

3.1. Experimental Methods

3.1.1. Sample fabrication

The samples consist of a glass substrate of 24 by 24 mm on which a layer of polyvinyl alcohol (PVA) with Rhodamine 6G (R6G) laser dye is spincoated. This layer is 21 nm thick as measured with profilometry with a 5 nm accuracy. On top of the PVA layer a 600 nm layer of polystyrene (PS) is added for a reference measurement to obtain a system with homogeneous decay rate without nearby interfaces.

The local density of states (LDOS) near an interface can be calculated by a method developed by Chance, Prock and Silbey [4] for a dipole oriented parallel or perpendicular to the interface. The theoretical curve for LDOS near an interface can be seen in fig. 3.1. The LDOS is normalised to vacuum. Rhodamine 6G has almost 100 % quantum efficiency [16], meaning that the measured total decay rate is almost equal to the radiative decay rate, so that the measured decay rate is proportional to the LDOS shown in figure 3.1. The grey bar in fig. 3.1 indicates the sample thickness used in our experiments. For a dipole moment oriented parallel to the interface the LDOS is 1.46, for a dipole oriented perpendicularly it is 0.56, giving a factor of 2.6 difference in LDOS between the extremes for differently oriented dipoles. The thickness of the layer causes a variation in LDOS for equally oriented dipoles but this spread is much smaller than the difference between the LDOS for different dipole orientations. For parallel dipoles the variation due to the layer thickness is $\pm$ 3 %, for the perpendicular dipoles this is $\pm$ 23 %.

3.1.2. Optical detection

The optical set-up used in the experiments is schematically shown in figure 3.2. Light from a diode laser (Picoquant) with an emission wavelength of 447 nm, repetition rate of 20 MHz and pulse widths of 78 ps is used to excite the dye. This light is guided into an optical fiber and focused onto the sample by an objective with NA = 0.05, leading to a focus with a diameter of approximately 10 μm on the sample.

The light emitted by the R6G dye is collected by a lens, collimated and focused onto the slit of a prism monochromator (Carl Leiss). The slit width is set to 1000 μm giving a spectral resolution $\Delta\lambda = 6$ nm. All decay measurements presented here are measured at a free space wavelength $\lambda = 563$ nm. A Hamamatsu photomultiplier tube is used as a photon counter. With this setup it is possible to measure spectra by scanning the monochromator and to measure decay curves of emitters at particular emission frequencies by time correlated single photon counting. This technique measures the time between the arrival of an emitted

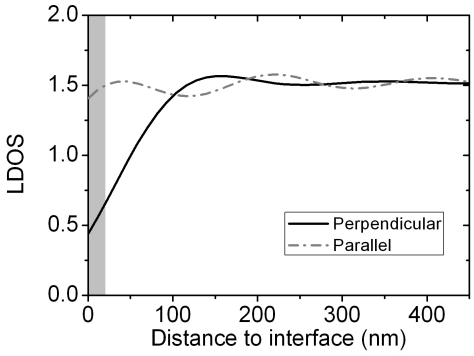

Figure 3.1.: Calculation of local density of states near an n=1 (air) to n=1.52 (polymer) interface for parallel and perpendicularly oriented dipoles (grey dash-dotted and black solid line respectively). The LDOS is normalised to the LDOS in vacuum.

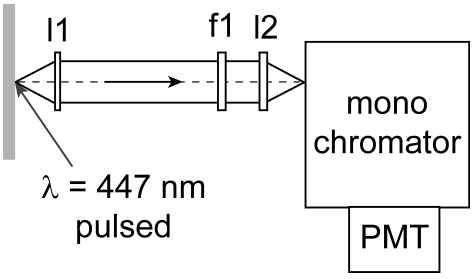

Figure 3.2.: A schematic picture of the experimental setup. Light from the laser excites the Rhodamine 6G in the sample. The emitted light is collimated by a lens l1 with f=12 cm, focused by lens l2 with f=10 cm on the entrance slit of a monochromator and detected by the photomultiplier tube. A filter f1 serves to block scattered laser light.

photon (start) and the laser pulse (stop) with ps resolution [17, 18]. By repeating this measurement a histogram of the arrival times is made from which a decay rate can be determined. The time resolution of the set-up is 125 ps, given by the full width half maximum of the total instrument response function (IRF).

3.2. Calculating the distribution of decay rates of ensembles

The fluorescence decay curve of an ensemble of emitters near an interface can be calculated analytically. In a decay measurement the decay of the excited state level is measured by observing the number of emitted photons as a function of time. A decay measurement $f(t)$ for an ensemble of emitters with 100 % quantum efficiency can be described by the following expression [8, 9]:

$$f(t) = \frac{I_0}{2\pi} \int_0^{2\pi} \mathrm{d}\phi \int_0^{\pi/2} \mathrm{d}\theta \mathrm{A}(\theta,\phi)\ \gamma(\theta,\phi)\ \mathrm{e}^{-\gamma(\theta,\phi)\mathrm{t}}\ \sin\theta \tag{3.1}$$

The term $A(\theta,\phi)$ accounts for angle dependence of absorption, emission and detection where θ and ϕ is the angle with respect to the interface and the azimuthal angle respectively. This experimental term is neglected for now. In section 3.3 experimental evidence is presented that validates our choice to neglect this prefactor.

In general, the decay rate of a dipole with a random orientation in the x-y-z space is equal to

$$\gamma = \gamma_{max}\ x^2 + \gamma_{med}\ y^2 + \gamma_{min}\ z^2 \tag{3.2}$$

where the x-y-z coordinates are chosen to match the directions of the main axes in the system [2]. The x-y-z coordinates lie on a sphere $x^2 + y^2 + z^2 = 1$ because they are the components of the dipole orientation vector $\mathbf{e_d}$. The x, y and z coordinates are conveniently transformed to a spherical coordinate system. For an emitter in our experiment closer than 100 nm to the interface $\gamma_{max} = \gamma_{med} = \gamma_{\parallel}$ and $\gamma_{min} = \gamma_{\perp}$. For emission near an interface equation 3.1 can be simplified to

$$f(t) = I_0 \int_0^{\pi/2} \mathrm{d}\theta\ (\gamma_{\parallel} \sin^2\theta + \gamma_{\perp} \cos^2\theta)\ \mathrm{e}^{-(\gamma_{\parallel} \sin^2\theta + \gamma_{\perp} \cos^2\theta)\mathrm{t}}\ \sin\theta \tag{3.3}$$

To calculate the distribution of decay rates that is expected in the experiment a Monte Carlo method was used. Monte Carlo methods are a class of computational algorithms that rely on repeated random sampling to compute results [19]. Since we have a large number of emitters with a randomly oriented dipole moment, we calculate for a certain number of emitters N the decay rate, where the orientation of the dipole moment for each emitter is generated randomly. The sum of exponentials of these decay rates weighed with the decay rate gives the overall decay curve of the ensemble. If a sufficient number of emitters is chosen, the results converge to the analytical decay curve $f(t)$ presented in equation 3.3.

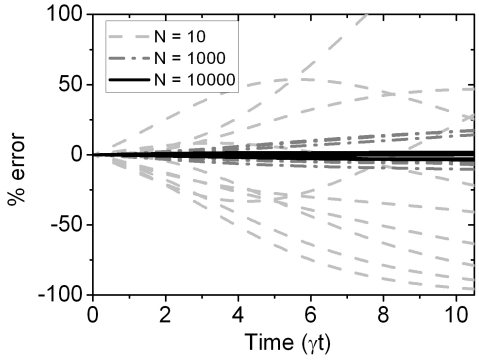

Figure 3.3.: The error in % is shown of the Monte Carlo simulation compared to the analytical decay curve. Shown are 10 realisations of ensembles consisting of $N = 10$, 1000 and 10000 respectively for the light grey dashed, the grey dash-dotted and the black solid lines. The time axis is normalised to the decay rate in a homogeneous medium.

In fig. 3.3 the error in % is shown of the Monte Carlo simulation compared to the analytical decay curve for an ensemble of $N = 10$, 1000 of 10000 emitters. The time axis is normalised to the decay rate in a homogeneous medium γ. The values for $\gamma_{\parallel}$ and $\gamma_{\perp}$ are chosen identical to the experimental situation. For each number of emitters N, 10 realisations are calculated to show the typical variation in calculated decay curve. For $N = 10000$ emitters at $\gamma t = 11$ ns there is a 5 % variation in the calculated decay curve, compared to 14 % for 1000 emitters and as much as 85 % for 10 emitters. Distributions are calculated with the Monte Carlo method for 10000 individual emitters in this chapter.

3.3. Results

In fig. 3.4 results are presented of time resolved emission from R6G from a 21 nm thick layer of PVA on a glass substrate and from the homogeneous reference system with an added layer of PS. Measurements were performed on the same sample, before and after depositing the thick PS layer. In fig. 3.4 a) the experimentally measured decay curves are shown. Time resolved emission from dye in the homogeneous medium shows a single exponential decay with a decay rate $\gamma_{hom} = 0.35$ ns^{-1}. When the R6G molecules are close to an interface, the decay curve becomes non-exponential. The vertical dashed line indicates the intersection of the two measurements. In fig. 3.4 b) the calculated decay curves are shown. In a homogeneous medium, a single exponential is expected with $\gamma = 0.35$ ns^{-1} in good agreement with previous experiments [16]. The decay curve for an ensemble of dye molecules close to an interface is calculated with equation 3.3. The curve is seen to be clearly non-exponential. Again the vertical dashed line indicates the intersection of the two calculations. The intersection occurs at the

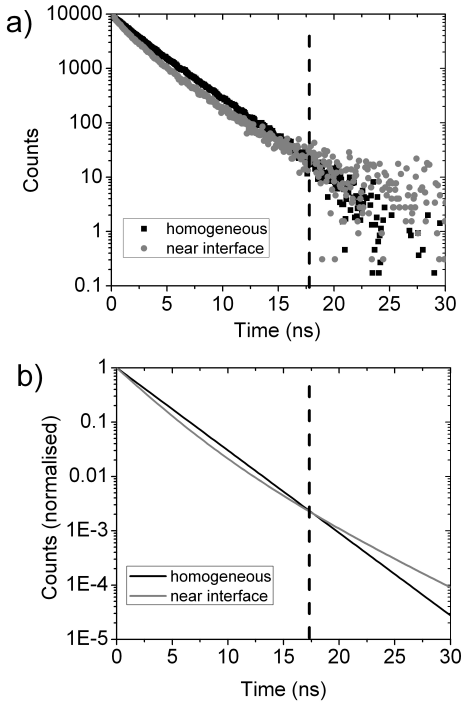

Figure 3.4.: a) The measured decay curves for R6G in a homogeneous medium and and 10 nm from an $n = 1.52/n = 1$ interface (black and grey data respectively). b) The calculated decay curves for an ensemble of emitters in the experimental configuration. The vertical dashed lines indicate the intersection of the exponential and non-exponential curves.

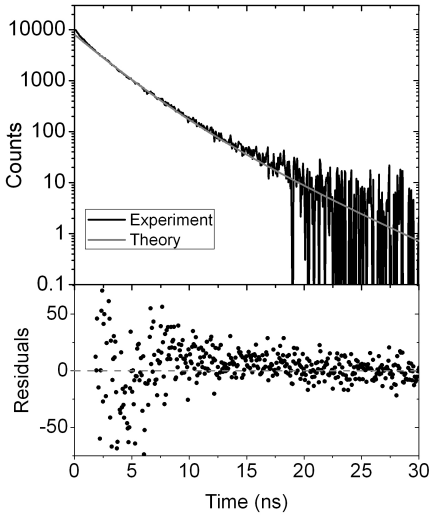

Figure 3.5.: In the top panel the experimental and analytically calculated decay curves are shown that are measured at 10 nm to the interface. In the bottom panel the residuals are shown, calculated as $I_{exp} - I_{theory}$.

same time delay as in the experiment. The agreement between experiment and theory is very good especially considering that there are no free parameters in the calculation.

In fig. 3.5 both the experimental and calculated decay curves are shown for dye near the interface. The agreement between the experimental and theoretical curve is very good since the residuals are centered around zero, as shown in the bottom panel. At t $<$ 2.5 ns the agreement is not as good, because our experimental curve is convoluted with the instrument response function for these short timescales while this is not the case for the theoretical curve.

In fig. 3.6 the distribution of decay rates is shown that we have calculated for our sample geometry. The distribution is highly asymmetrical. It is strongly peaked at the value for the parallel decay rate, since in three dimensions, there are two orthogonal directions that have a parallel dipole orientation, while there is only one direction for the perpendicular orientation. While considerable success has recently been achieved with parametrised decay rate distributions [10–12] the shape of the distribution is quite different from any functional form (lognormal, gammafunction) considered so far. This shows that the ability to know the distribution *a priori* is even more powerful than parametrising.

To verify that the angle dependence of the detection of the decay curve, the term $A(\theta, \phi)$ in eq. 3.1, can be neglected, we have performed measurements of the decay curve for different angles with respect to the normal to the interface,

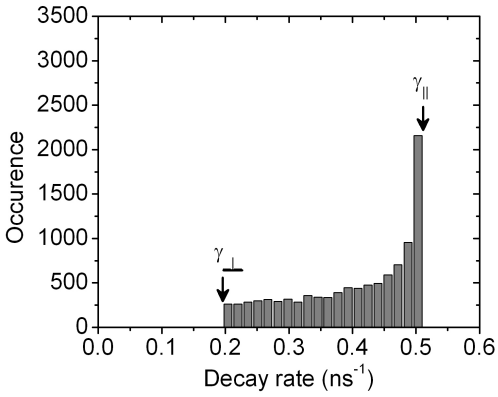

Figure 3.6.: The distribution of decay rates calculated with the Monte Carlo method is shown. The parallel and perpendicular decay rates are indicated.

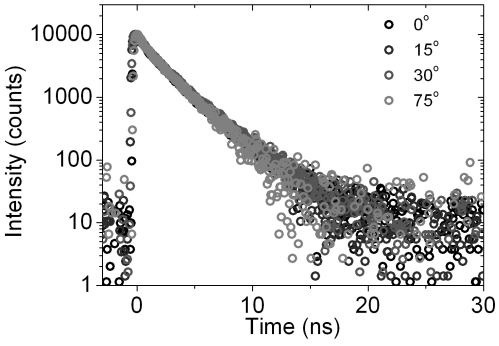

Figure 3.7.: Decay curves that are measured for different detection angles with respect to the normal to the interface.

see fig. 3.7. No significant difference in the decay curve is found for external angles ranging from 0 to 75°. Even though the radiation pattern of an emitter close to an interface is strongly dependent on orientation of the dipole [20], in our experiments no effect of this distribution on the decay curve is found. This confirms our choice to neglect the detection angle dependence.

3.4. Conclusions

We have measured time resolved emission from an ensemble of R6G dye molecules near an interface. Depending on dipole orientation a difference of a factor of 2.6 in the local density of states was expected. A clear non-exponential decay is observed from this ensemble of emitters. The ensemble decay curve shows single exponential decay when a layer is added to remove optical interface effects. A theoretical decay curve only taking into account the dipole orientation agrees very well with the experimental decay curve. This result allows us to, for the first time, model *ab initio* the decay rate distribution analytically in stead of assuming a certain shape of the distribution like a lognormal or gamma distribution [10, 12].

References

[1] L. Novotny and B. Hecht, *Principles of nano-optics* (Cambridge University Press, Cambridge, 2006).

[2] W. L. Vos, A. F. Koenderink, and I. S. Nikolaev, *Orientation-dependent spontaneous emission rates of a two-level quantum emitter in any nanophotonic environment*, Phys. Rev. A **80**, 053802 (2009).

[3] K. H. Drexhage, *Interaction of light with monomolecular dye layers*, Prog. Optics **12**, 165 (1974).

[4] R. R. Chance, A. Prock, and R. Silbey, *Molecular fluorescence and energy transfer near interfaces* (1978).

[5] W. Barnes, *Topical review: Fluorescence near interfaces: the role of photonic mode density*, Rev. Mod. Opt. **45**, 661 (1998).

[6] M. Kreiter, M. Prummer, B. Hecht, and U. P. Wild, *Orientation dependence of fluorescence lifetimes near an interface*, J. Chem. Phys. **117**, 9430 (2002).

[7] X. Brokmann, L. Coolen, M. Dahan, and J. P. Hermier, *Measurement of radiative and nonradiative decay rates of single CdSe nanocrystals through a controlled modification of their spontaneous emission*, Phys. Rev. Lett. **93**, 107403 (2004).

[8] N. Danz, J. Heber, A. Bräuer, and R. Kowarschik, *Fluorescence lifetimes of molecular dye ensembles near interfaces*, Phys. Rev. A **66**, 063809 (2002).

[9] A. F. Koenderink, M. Kafesaki, C. M. Soukoulis, and V. Sandoghdar, *Spontaneous emission rates of dipoles in photonic crystal membranes*, J. Opt. Soc. Am. B. **23**, 1196 (2006).

[10] A. F. van Driel, I. S. Nikolaev, P. Vergeer, P. Lodahl, D. Vanmaekelbergh, and W. L. Vos, *Statistical analysis of time-resolved emission from ensembles of semiconductor quantum dots: Interpretation of exponential decay models*, Phys. Rev. B. **75**, 035329 (2007).

[11] I. Nikolaev, P. Lodahl, A. van Driel, A. F. Koenderink, and W. Vos, *Strongly nonexponential time-resolved fluorescence of quantum-dot ensembles in three-dimensional photonic crystals*, Phys. Rev. B **75**, 115302 (2007).

[12] R. A. L. Vallée, N. Tomczak, L. Kuipers, G. J. Vancso, and N. F. van Hulst, *Single molecule lifetime fluctuations reveal segmental dynamics in polymers*, Phys. Rev. Lett. **91**, 38301 (2003).

[13] E. Snoeks, A. Lagendijk, and A. Polman, *Measuring and modifying the spontaneous emission rate of erbium near an interface*, Phys. Rev. Lett. **74**, 2459 (1995).

[14] A. Pomozzi, M. K. Park, and M. Kreiter, *Ensemble measurement of the orientation-dependent variations in chromophore lifetimes near a dielectric interface*, Phys. Rev. B **79**, 165435 (2009).

[15] M. D. Leistikow, J. Johansen, A. J. Kettelarij, P. Lodahl, and W. L. Vos, *Size-dependent oscillator strength and quantum efficiency of CdSe quantum dots controlled via the local density of states*, Phys. Rev. B **79**, 045301 (2009).

[16] J. R. Lakowicz, *Principles of fluorescence spectroscopy* (1999).

[17] V. O. O'Connor and D. Philips, *Time correlated single photon counting* (1984).

[18] I. S. Nikolaev, *Spontaneous-emission rates of quantum dots and dyes controlled with photonic crystals*, Ph.D. thesis, University of Twente, 2006.

[19] S. E. Koonin, *Computational physics* (Addison-Wesley Publishing Company, Inc., Redwood city, California, 1986).

[20] W. Lukosz, *Light emission by magnetic and electric dipoles close to a plane dielectric interface. III. radiation patterns of dipoles with arbitrary orientation*, J. Opt. Soc. Am. **69**, 1495 (1979).

Chapter 4
Measuring emission from silicon photonic crystals

The seminal paper of Yablonovitch in 1987 [1] inspired a quest for photonic crystals with a band gap, a frequency range for which no modes exist. Excited emitters placed inside a photonic crystal with their emission frequency in this band gap will not be able to radiatively decay spontaneously because there are no vacuum fluctuations allowed in the photonic band gap, giving ultimate control over spontaneous emission.

The relative frequency width of the dominant stop gap, a gap in the band structure for one particular direction is an experimentally accessible gauge of the photonic interaction strength between light and the crystal. The relative width is determined by crystal parameters, including crystal symmetry, the effective refractive index and refractive index contrast [2–4]. When stop gaps for different directions overlap in frequency a band gap is formed. In general, the higher the refractive index contrast, the stronger the interaction of light with the photonic crystal leading to wider frequency ranges for photonic band gaps. For this reason, silicon has long been a material of choice to fabricate photonic crystals, since it has a high refractive index of about 3.5. Another big advantage of using silicon is that there is a huge amount of technology already developed, since computer chips are mainly created from silicon wafers. Silicon photonic crystals fabricated from wafers could therefore potentially also offer a easy integration into existing circuitry. However, fabricating periodic structures with wavelength-sized features in silicon is no easy task, see, e.g., [5].

A first candidate for a silicon band gap photonic crystal is the inverse opal, consisting of fcc stacked air spheres with a backbone material of high refractive index material [6]. These inverse opals can have a band gap in case of sufficient refractive index contrast above 2.8 [7, 8]. Silicon inverse opals are fabricated and show high reflectivity [9, 10]. This type of crystal can in theory reach a relative width of 12 % when the backbone is carefully tailored [11]. However, the band gap in fcc structures is very sensitive to fabrication errors [12]. Crystals with simple cubic symmetry can also form a band gap. This band gap can have a maximum relative width of 13 % using silicon [13]. However, again this broad band gap is very sensitive to fabrication errors, similar to fcc structures. Structures have been fabricated in silicon with simple cubic crystal structure by means of photo electrochemical etching. The crystals show high reflectivity in the infrared [14, 15]. However it is hard to scale down these structures to telecom wavelengths.

Diamond-like photonic crystals offer a more substantial band gap compared

to the previously mentioned structures, and can reach this gap with less refractive index contrast. Another benefit is that for these structures the band gap is in the range of first order Bragg diffraction, only needing scattering from the nearest neighbors in the reciprocal lattice, making it less sensitive to structural disorder. One type of crystal has been proposed by Yablonovitch *et al.* [16] and demonstrated in the microwave region, but is extremely hard to make in the optical domain [17]. Woodpile photonic crystals were introduced in reference [18]. These structures are fabricated by stacking layers of dielectric rods which limits the structure to (at most) 8 or 9 layers. Reflection and transmission measurements performed on these woodpiles show strongly photonic behavior [19–22]. However the stacking process introduces alignment errors since it consists of many fabrication steps that limits the crystal size. Inverse woodpile structures were also introduced by Ho *et al.* [18]. These consist of two identical pore sets etched in a high refractive index medium. The advantage of inverse woodpiles over woodpiles is that the filling fraction can be optimised, since the pores can overlap. Another advantage is that these inverse woodpiles can be fabricated with only two etching steps. These structures promise a broad first order band gap with a relative width of 25 % [18, 23, 24] when fabricated of silicon.

For the first time, these silicon inverse woodpile photonic crystals have been used for emission measurements, by infiltrating the crystals with PbS quantum dots. In chapter 5 and chapter 6 of this thesis these emission experiments are discussed. Therefore in this chapter, the inverse woodpile photonic crystals, the quantum dots and experimental setup used will be described, including alignment and modeling procedures.

4.1. Sample fabrication and optical characterization

To create an inverse woodpile structure we have devised a CMOS compatible method to etch two orthogonal sets of pores [5, 25–27]. First, a centered rectangular array of air cylinders is etched in silicon by means of reactive ion etching (RIE). The lattice spacing in one direction is $\sqrt{2}$ times the spacing in the other direction $a = \sqrt{2}c$. A drawing of this lattice is shown in fig. 4.1 a). With this RIE step, a two dimensional (2D) photonic crystal is formed. To realize the refractive index modulation in the third dimension, the 2D crystal is cleaved. Perpendicular to the existing first set of pores a second set of pores is made. This is done by first defining a mask of the same centered rectangular lattice by focussed ion beam (FIB) milling. The inverse of this mask is etched using an identical RIE step, creating a three dimensional (3D) photonic crystal. A schematic representation of the 3D structure is shown in fig. 4.1 b).

In fig. 4.2 a scanning electron microscope (SEM) picture of a typical sample is shown. The pores that are etched in the first direction have a depth of approximately 6 μm. The size of the 3D crystal is limited by this depth of the first set of pores and by the field of view of the FIB that is used to create the mask for the second set of pores. The 3D crystal dimensions are approximately 6 by 8 by 6 μm. Alignment of the second set of pores with respect to the first set is crucial to get a broad band gap [24]. By visual inspection of the SEM picture this

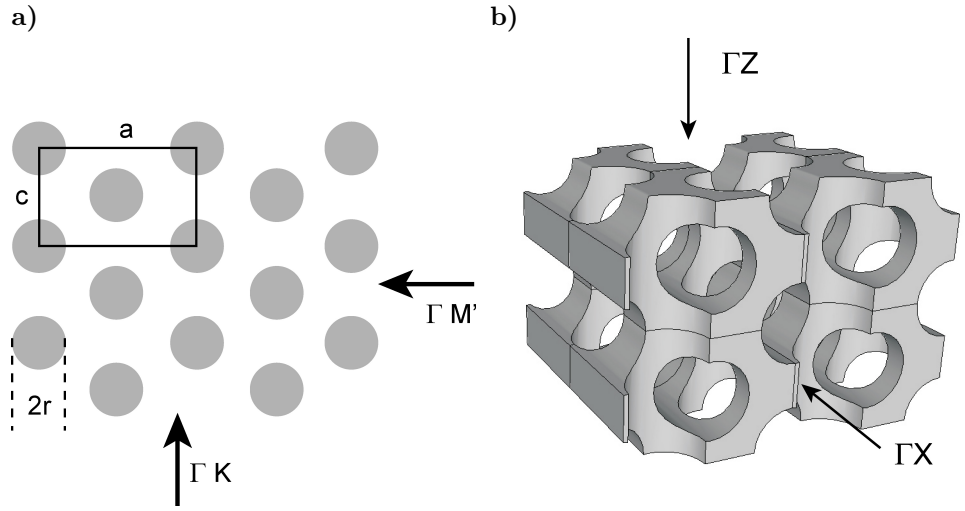

Figure 4.1.: a) Schematic of the 2D crystal. The two directions parallel to the a and c axes, respectively ΓM' and ΓK, are indicated. b) A part of the 3D crystal structure. Lines indicate edges of the unit cell. Two directions along the first and second etch direction are indicated by ΓZ and ΓX respectively. Illustration courtesy of Simon Huisman.

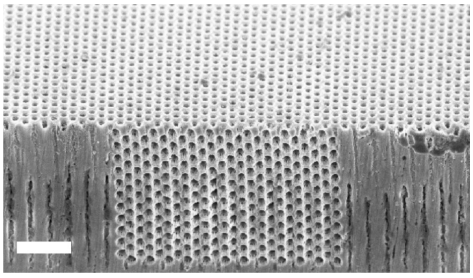

Figure 4.2.: Scanning electron micrograph of a part of the structure. The top of the picture shows the pores in the first etch direction. The second set of etched pores are shown in the center. The scale bar is 2 μm. Image made by J. M. van den Broek.

alignment can be estimated so that emission experiments are performed only on well aligned crystals. The tapering of the pores has been studied. This tapering is $< 0.1°$ for the first etch direction and is approximately $1°$ for the pores in the second etch direction. A tapering of $1°$ is known from calculations to narrow the photonic band gap frequency range [24]. However, in reflectivity measurements broad stop bands are observed, showing strong peaks in the presence of some tapering.

The optical quality and photonic strength of the fabricated silicon structures

have been investigated by measuring reflectivity of the crystals. The results of typical reflectivity measurements for a 3D and a 2D photonic structure are shown in fig. 4.3. The crystals are investigated from two different directions for two orthogonal polarisations. A more thorough analysis of the reflectivity data is beyond the scope of this thesis and can be found elsewhere [28, 29].

For a 3D structure a reflectivity measurement is shown in fig. 4.3 a). The structure is probed along the first etch direction (ΓZ) and the second etch direction (ΓX) with a polarisation either parallel or perpendicular to the pores. Clear peaks in reflectivity are seen, with a height of approximately 60 % and a relative width of 20 % for the 3D structure, indicating that the structures are of very high optical quality. Most importantly the reflectivity peaks overlap for all directions and polarisations measured. This frequency region is indicated with the grey bar. This overlap of the reflectivity peaks is a clear indication of a photonic band gap.

Reflectivity results for a 2D structure are shown in fig. 4.3 b). Here two different directions in-plane are probed, indicated by ΓM' and ΓK. The polarisation is either TE oriented (perpendicular to the pores) of TM oriented (parallel to the pores). Very broad high reflectivity features are seen in the reflectivity measurement. The observed peaks agree well with expected stop gaps from band structure calculations. For TE polarised light the peaks in the ΓM' and ΓK directions overlap, indicative of the TE 2D band gap expected from calculations. The reflectivity for the 2D crystals is in general higher than the reflectivity of the 3D structures, probably because of a better surface quality of the measured structures.

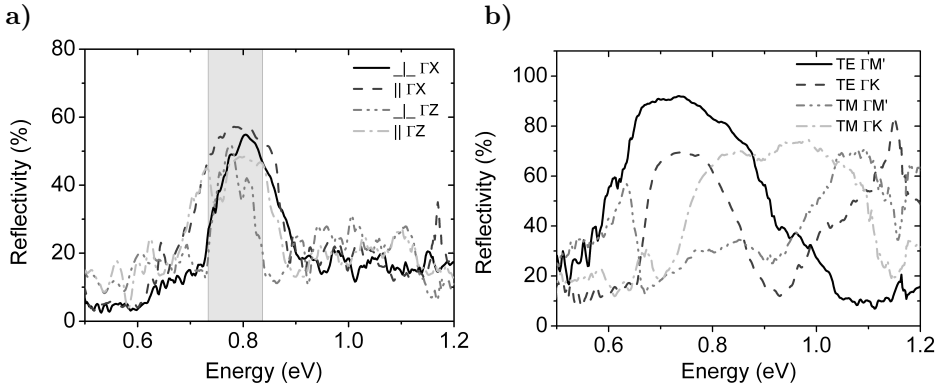

Figure 4.3.: a) Reflectivity spectrum of a 3D photonic crystal, measured along two different directions and polarisations. b) The reflectivity spectrum of a 2D photonic crystal, measured along two different in-plane directions with two different polarisations.

4.2. Quantum dots

Because silicon absorbs light with an energy larger than the electronic band gap of about 1.12 eV (1100 nm), it is not possible to use visible emitting quantum dots or molecules to probe the density of states inside the photonic crystal. Therefore PbS quantum dots suspended in toluene are used that are purchased from Evident. These quantum dots emit around 0.85 eV (1460 nm). An emission spectrum is shown in fig. 4.4 a. The broad emission spectrum is mostly caused by inhomogeneous broadening due to size polydispersity (see appendix A). It is estimated by Evident that these quantum dots have a quantum efficiency of 30-50 %.

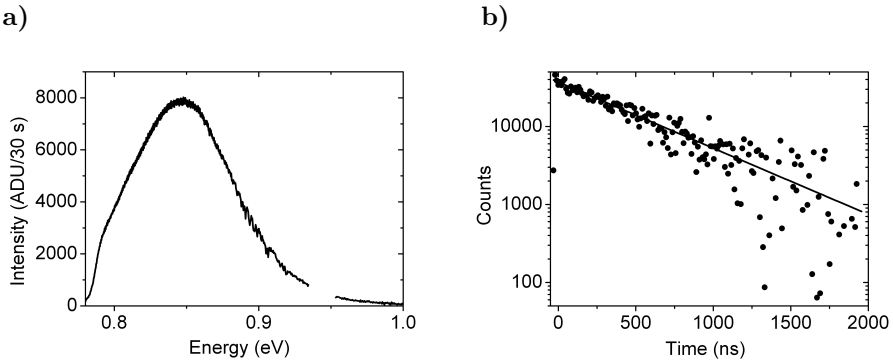

Figure 4.4.: a) The emission spectrum of an ensemble of PbS-1500 quantum dots. The steep edge at low energy is caused by the cut-off of the detector. The lack of data points around 0.94 is caused by dead pixels of the detector. b) The decay curve measured at 0.85 eV together with a single exponential fit.

PbS quantum dots in suspension show single exponential decay. These quantum dots have a typical decay rate of 1.9 μs^{-1} in toluene. A decay curve of PbS quantum dots emitting at 0.85 eV is shown in fig. 4.4 b, together with a single exponential fit. The goodness of fit χ^2_{red} is 1.03 close to 1 thus indicating a good fit. All measurements shown in this thesis on PbS quantum dots are performed at room temperature.

4.3. Experimental set-up

A schematic of the experimental setup is shown in fig. 4.5. Light pulses with a pulse width of 11 ps from a pulsed frequency doubled Nd^{3+}:YAG laser (Time Bandwidth Cougar) at $\lambda = 532$ nm with a repetition rate of 409 kHz are used to excite the quantum dots. The light is focused with an NA=0.12 4X objective (o2), which will be called the excitation objective. The laser power is kept sufficiently low so that the quantum dot excitation stays in the linear regime, where emitted power is proportional to excitation power. Emitted light is collected at

an angle of 90 degrees to the excitation path where a second objective (o1) is placed with NA=0.7 100x with a relatively long working distance of 6 mm. This objective is used to collect quantum dot emission signal and will be called the detection objective. The detection objective is mounted on an x-y-z piezo stage for alignment purposes. Laser light can also be sent through the detection objective by flipping down the flip mirror (fm), via a dichroic mirror (dm) that reflects light with wavelengths below 670 nm. The sample is placed on a x-y translation stage to locate regions of interest on the sample. The image of the sample can be viewed on the CCD camera to facilitate alignment. More details of this set-up can be found in reference [30].

Light emitted by the quantum dots is collected via the detection objective, passes through a 1100 nm long pass filter (f1) to filter out stray laser light, is dispersed by a grating and is imaged onto a liquid nitrogen cooled InGaAs array diode. The array is sensitive from 1000 to 1650 nm to measure emission spectra. Alternatively, the time-resolved emission is detected with a Hamamatsu NIR photomultiplier tube (PMT). The selected emission energy range that is detected by the PMT is set by a slit width, and is chosen to be approximately 3 meV. The PMT is connected to a Picoquant PicoHarp 300 timing card. By measuring the time difference between the laser pulse signal generated by a diode in the laser and the detection pulse of the PMT, we obtain a histogram of the decay: a decay curve [31]. This method is also called time correlated single photon counting (TCSPC). An optional polariser (p1) can be added to the detection path to select either TE or TM polarised emission light.

The time-resolved data needs to be processed before it can be used. Most importantly the background must be removed. Since we are performing experiments in the near infrared spectral region, the background contribution is substantial. Even with the peltier-cooled PMT approximately $3 \cdot 10^5$ dark counts per second are recorded. The number of signal counts is typically 1 % of the repetition frequency, or $4 \cdot 10^3$ signal counts per second. Since the signal counts are correlated with the laser start signal, they can be separated from the background that is uncorrelated and adds a constant background level. This constant background level is determined by averaging the data in the 6.4 ns time interval before the laser pulse.

4.4. Sample holder

The sample consists of a small bar of silicon of approximately 500 μm by 500 μm by about 2 cm in which pores are etched at certain locations. To hold this sample a custom holder is made out of stainless steel and polychlorotrifluoroethylene (a type of teflon that is more rigid than normal teflon) that clamps the sample while leaving the etched areas free for probing with the optical setup. Photographs of this sample holder are shown in fig. 4.6.

This entire sample holder including sample is placed in a Hellma fluorescence cell, fixed to the wall of the cell from the outside with magnets and immersed with quantum dots in suspension. The concentration is $2 \cdot 10^{-6}$ M PbS in toluene, leading to an estimated $1.2 \cdot 10^6$ quantum dots in the focus if the focal

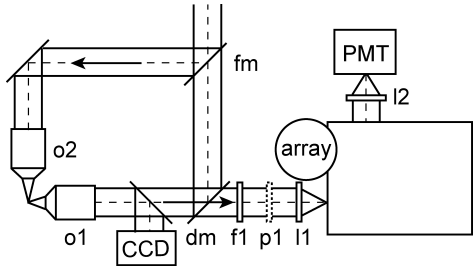

Figure 4.5.: Schematic of the experimental setup to measure near infrared emission. The excitation light is guided with a flip mirror (fm) to the excitation objective (o2) to be focused on the sample. Emitted light is detected with the emission objective (o1), passed through a dichroic mirror (dm), a filter to block stray laser light (f1), an optional polariser (p1) and focused with a lens (l1) through the slit of a grating spectrometer. The light is detected either with an InGaAs diode array to measure the spectrum or sent to the PMT via a lens (l2).

volume is 10x10x10 μm in suspension. By leaving the quantum dots suspended in toluene, the photo physical properties remain stable for months, much longer than the one day stability when dried [32]. Even when kept in nitrogen gas atmosphere to prevent photo oxidation the optical properties of dried quantum dots are unstable. Since sample fabrication of the Si structures is a complex procedure involving many fabrication steps, this one day time limit for optical measurements would be prohibitive.

There are, however, two disadvantages to immersion in suspension. One disadvantage of placing the entire structure in toluene is that the refractive index contrast of the photonic crystal is decreased, since toluene has a refractive index n of 1.5 compared to n=1 in air. Fortunately, however, even with lowered refractive index contrast the crystal scatters light sufficiently strongly to show a 3D band gap in band structure calculations. The relative width of the gap is decreased from 25 % for Si-air to 8.5 % for Si-toluene, which is still larger than the relative gap width of silicon inverse opals (see chapter 5). The other disadvantage is that emitted light does not only originate from quantum dots in the photonic crystal but also from the direct surrounding of the crystal. Aligning the photonic crystal and excitation focus with respect to the detection focus is crucial for successful measurements. In the next paragraph the alignment procedure is discussed.

4.5. Aligning of photonic crystals

A schematic of how the sample is placed in the setup is shown in fig. 4.7. The detection focus can be positioned on a 2D or 3D part of the structure, using the translation stage and the piezo actuators with an accuracy of 10 nm [30]. The detection focus objective is attached to an x-y-z manual translation stage with an accuracy of 10 μm. When the detection focus is placed in suspension, the

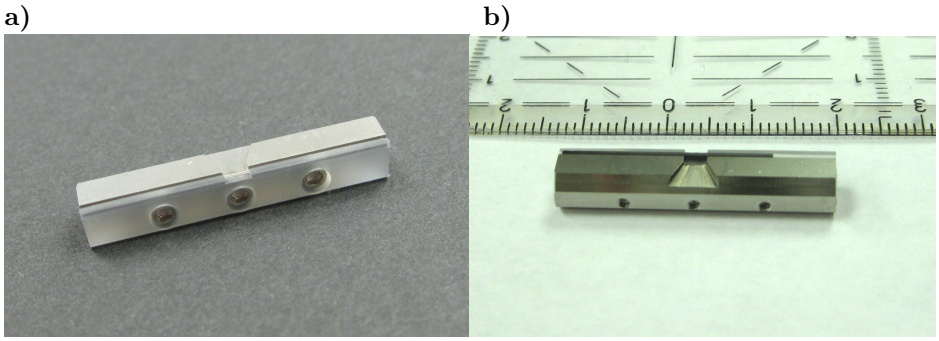

Figure 4.6.: The sample holder that was designed for these types of samples. In a) the empty holder is shown, in b) a piece of silicon is inserted.

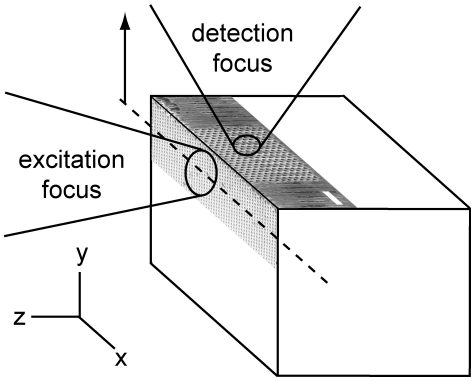

Figure 4.7.: A schematic drawing of how the sample is positioned in the setup. The excitation focus is scanned in the y direction indicated by the arrow.

location of the excitation focus is optimized by maximizing the detected signal from the quantum dots. When positioned over the silicon structure the height of the detection focus is optimized by scanning the height of the detection focus along the y direction indicated by the arrow in fig. 4.7. In this way the edge of the structure is determined precisely.

Such a scan along the y direction is shown in fig. 4.8. Here the peak intensity at 0.842 eV (1475 nm) is plotted versus the translation of the excitation focus. The black squares correspond to the situation as shown in fig. 4.7 in which a photonic crystal is placed in the detection focus. A clear transition to lower intensity is seen. The gray circles indicate the same scan, but now performed with the detection focus on the bare silicon wafer next to the crystal. A similar transition

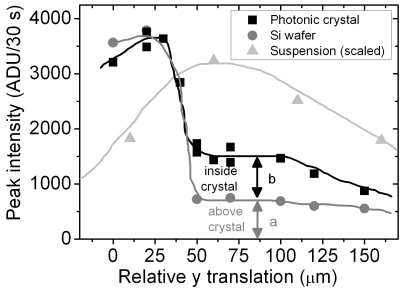

Figure 4.8.: Scanning the excitation focus in height for three different situations: On a photonic structure (black squares), in silicon wafer (gray circles) and in suspension (light gray triangles). Lines are guides to the eye. The intensity measured in suspension is scaled down by a factor $\frac{1}{3}$ for comparison.

is seen. However, the intensity is about half of the intensity when focusing on the photonic crystal. We conclude from this graph that when measuring on the photonic crystal approximately half of the intensity is emitted by quantum dots inside the photonic crystal while the other half of the intensity originates from outside the structure. For reference a similar scan is shown in suspension when no silicon structure is present (light gray triangles). No sharp transition in intensity is visible.

By performing such a y-scan before measuring spectra and decay curves, the ratio of light coming from the structure is determined. A typical set of emission spectra for different y-positions is shown in fig. 4.9. Here the ratio of the emission spectrum measured on the photonic crystal and the spectrum when focused on silicon is shown. This particular crystal structure shows narrow features in the emission spectrum (details can be found in chapter 6). It can clearly be seen that first the spectrum is similar to the spectrum above silicon (y = 0) but when the excitation focus is moved onto the photonic structure (y = 40 μm) the ratio increases and clear peaks appear above 0.85 eV. The ratio decreases again slightly and peaks get less pronounced when the excitation focus is moved further.

Fig. 4.10 shows a spectrum from this same photonic crystal with features in gray. The black line shows the emission spectrum from the same structure but excited through the detection objective. Peaks in the emission spectrum are now no longer visible, because a much larger part of the total spectral intensity is emitted by quantum dots outside the photonic crystal structure. We have tried to use a confocal pinhole to exclude this out-of-focus light of the surrounding quantum dots. However, adding a pinhole reduces the measured intensity drastically and does not show more clearly visible peaks. This is probably due to extra abberations introduced by the thick glass wall of the fluorescence cell.

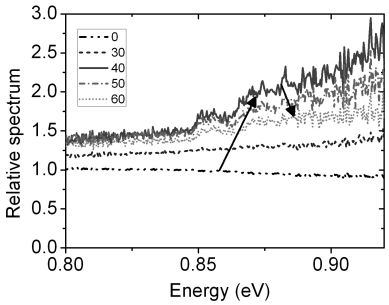

Figure 4.9.: The relative spectrum is shown of the emission spectra measured on the photonic crystal and the spectrum above silicon. The y-location is indicated in the legend. When scanning the excitation focus on to the structure, clear peaks appear in the emission spectrum.

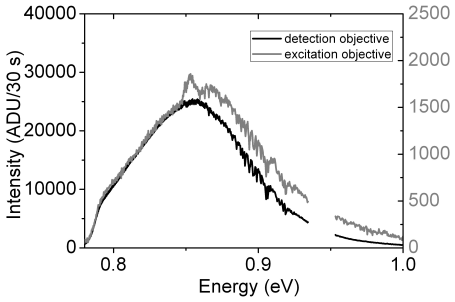

Figure 4.10.: Two emission spectra from quantum dots in a 2D photonic crystal are shown. When exciting through the detection objective, no features are visible, while clearly peaks are seen when exciting through the excitation objective.

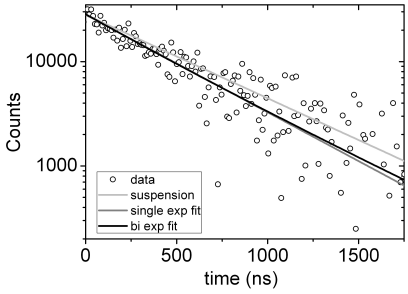

Figure 4.11.: The decay curve of quantum dots measured in a photonic crystal is shown. The lines are decay in suspension (light grey), a single exponential fit to the data (grey line) and a bi-exponential fit (black line). In this case a=1, b=0.77 and I_0=16103.

4.6. Modeling of time resolved measurements

Since we know from the y-scan of the excitation focus that part of the light originates from quantum dots in suspension and part of the light originates from the photonic crystal, a double exponential model is a logical choice. Therefore, the decay curves are modeled using a double exponential model with two independent adjustable parameters:

$$f(t) = I_0(a\exp(-\gamma_{susp}t) + b\exp(-\gamma_{crystal}t)) \tag{4.1}$$

The first term of the intensity originates from outside the structure and has a decay rate given by the rate in suspension γ_{susp} that is independently determined by measuring on a suspension of quantum dots. The second term of the intensity of the light originates from the photonic crystal and has a decay rate $\gamma_{crystal}$ that we want to retrieve. The value of a and b are determined independently by performing a y-scan of the detection focus as described in paragraph 4.5, by comparing the intensity when measuring emission from the structure or on bare silicon, see for instance fig. 4.9. The only unknown parameters that remain are $\gamma_{crystal}$ and I_0.

In fig. 4.11 an example of a measured decay curve is shown. The black line shows the fit performed with the double exponential model eq. 4.1. This model gives a goodness of fit χ^2_{red} of 1.025 indicating a good agreement between data and model. We find a photonic crystal decay rate $\gamma_{crystal}$=2.76 μs^{-1}. The data can also be modeled with a single exponential decay (grey line), giving a χ^2_{red} of 1.027 and a decay rate γ=2.16 μs^{-1} is found. On the basis of the value of χ^2_{red} or the residuals (not shown) there is no preference for one model over the other. However, since we know from measurements that part of the light originates from outside the crystal structure and part from within, it is much more reasonable to fit with a double exponential model than a single exponential model. Note that the number of free parameters remains the same, namely 2.

For reference, the decay in suspension is shown in fig. 4.11 by the light grey line with a decay rate γ=1.85 μs^{-1}. Clearly the decay measured and the suspension fit do not match, also indicated by the higher χ^2_{red} which is 1.282. Thus the decay rate found when measuring emission from quantum dots in a photonic crystal is significantly different from the decay rate in suspension.

4.7. Calculating band structures and DOS with MPB

The freely available program MIT Photonic Bands (MPB) [33, 34] was used to calculate band structures and the density of states (DOS) inside photonic crystals. This program computes definite-frequency eigen states of Maxwell's equations in periodic dielectric structures for arbitrary wave vectors, using a plane wave basis.

We performed calculations on a grid of size 70 x 100 x 70 using ϵ = 12.1 for silicon, ϵ = 1 for air and ϵ = 2.25 for toluene. A band structure is shown for a 3D crystal in fig. 4.12 a). The corresponding first Brillouin zone is shown in fig. 4.12 b). For the band structure 72 wave vector points are used, taking about 3 hours to calculate.

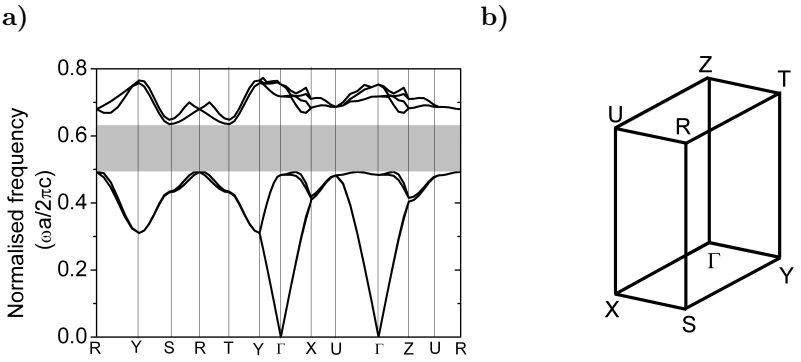

Figure 4.12.: In a) a band structure is shown of a 3D structure for r/a=0.24 made from silicon (ϵ=12.1) in air (ϵ=1). The band gap is indicated with the grey bar. In b) irreducible part of the first Brillouin zone is shown of the 3D structure. Letters mark points of high symmetry on the lattice.

Since we measure on an ensemble of quantum dots, we have to average the local density of states over all these positions and dipole orientations. Since the quantum dots are moving freely in suspension, a random distribution of dipole moments is expected. Because of this reason we use the unit cell averaged local density of states, which is called simply the radiative density of states (DOS). As an extra advantage, this quantity is far more easily calculated than the local density of states since it only involves solving the eigen values of the Maxwell equations while for the local density of states the eigen functions also need to be computed. A better model for the measured ensemble averaging would be to calculate the LDOS for all positions only in the pores of the crystal

for different dipole orientations since the DOS also takes into account locations in the silicon, where no quantum dots are present. However, this is computationally too extensive and will take at least several months to calculate, see, *e.g.* [35].

The DOS is calculated using a random selection of 2000 wave vector points in the first Brillouin zone of the lattice. For a 2D photonic crystal, the density of states is calculated in 3 dimensions. The length of the third direction in which the crystal is not periodic can be set arbitrarily, and is chosen such that it corresponds to the 3D first Brillouin zone for convenience. All plots of the density of states in this thesis are scaled to the density of states in a vacuum such that in vacuum for normalised frequency 1 the DOS is unity. A frequency spacing of 0.005 is used when calculating the histogram of the DOS.

To verify the correctness of the DOS calculation, our results are compared to the analytically known DOS in free space and calculations performed by Hillebrand *et al.* [23] for inverse woodpiles structures. In fig. 4.13 a) the DOS is shown for a vacuum by calculating the DOS for an empty crystal, where the refractive index contrast is 0. The DOS is clearly seen to follow the quadratic behavior expected for a homogeneous medium. In fig. 4.13 b) a comparison is shown between our calculations and data from reference [23]. Our calculation reproduces their result well, validating our calculations.

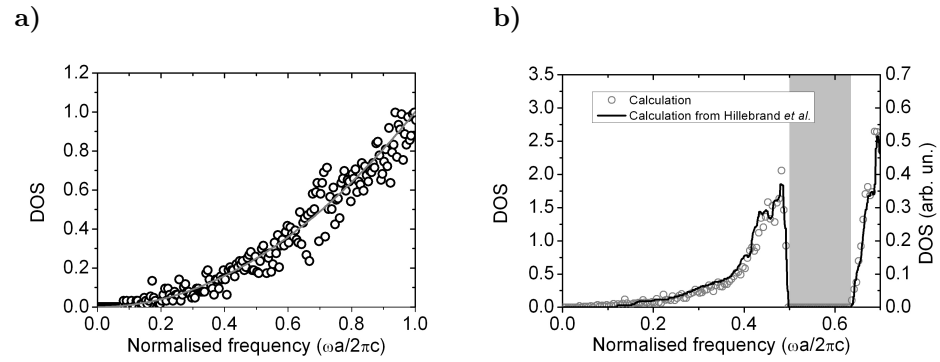

Figure 4.13.: In a) the calculated DOS is shown for vacuum. The line shows the analytical quadratic function. In b) a comparison is shown of our DOS results in units of ω^2/π^2c^3 per volume with calculations performed by Hillebrand *et al.* [23]. The agreement is very good.

References

[1] E. Yablonovitch, *Inhibited spontaneous emission in solid-state physics and electronics*, Phys. Rev. Lett. **58**, 2059 (1987).

[2] W. L. Vos, M. Megens, C. M. van Kats, and P. Bösecke, *Transmission and diffraction by photonic colloidal crystals*, J. Phys.: Condens. Matter **8**, 9503 (1996).

[3] W. L. Vos, R. Sprik, A. van Blaaderen, A. Imhof, A. Lagendijk, and G. H. Wegdam, *Strong effects of photonic band structures on the diffraction of colloidal crystals*, Phys. Rev. B **53**, 16231 (1996).

[4] W. L. Vos, H. M. van Driel, M. Megens, A. F. Koenderink, and A. Imhof, in *Proceedings of the NATO ASI photonic crystals and light localization in the 21st century*, edited by C. M. Soukoulis (Kluwer, Dordrecht, 2001).

[5] L. A. Woldering, *Fabrication of photonic crystals and nanocavities*, Ph.D. thesis, PhD thesis, University of Twente, 2008.

[6] J. E. G. J. Wijnhoven and W. L. Vos, *Preparation of photonic crystals made of air spheres in titania*, Science **281**, 802 (1998).

[7] H. S. Sözüer, J. W. Haus, and R. Inguva, *Photonic bands: Convergence probles with the plane-wave method*, Phys. Rev. B **45**, 13962 (1992).

[8] K. Busch and S. John, *Photonic band gap formation in certain self-organizing systems*, Phys. Rev. E **58**, 3896 (1998).

[9] A. Blanco *et al.*, *Large-scale synthesis of a silicon photonic crystal with a complete three-dimensional bandgap*, Nature **405**, 437 (2000).

[10] D. J. Norris and Y. A. Vlasov, *Chemical approaches to three-dimensional semiconductor crystals*, Adv. Mater. **13**, 409 (2001).

[11] A. F. Koenderink, *Emission and transport of light in photonic crystals*, Ph.D. thesis, University of Amsterdam, 2003.

[12] Z. Y. Li and Z. Q. Zhang, *Fragility of photonic band gaps in inverse-opal photonic crystals*, Phys. Rev. B **62**, 1516 (2000).

[13] M. Maldovan and E. L. Thomas, *Photonic crystals: six connected dielectric networks with simple cubic symmetry*, J. Opt. Soc. Am. B **22**, 466 (2005).

[14] S. Matthias, F. Müller, C. Jamois, R. B. Wehrspohn, and U. Gösele, *Large-area three-dimensional structuring by electrochemical etching and lithography*, Adv. Mat. **16**, 2166 (2004).

[15] S. Matthias, F. Müller, and U. Gösele, *Simple cubic three-dimensional photonic crystals based on macroporous silicon and anisotropic posttreatment*, J. Appl. Phys. **98**, 023524 (2005).

[16] E. Yablonovitch, T. J. Gmitter, and K. M. Leung, *Photonic band structure: the face-centered-cubic case employing nonspherical atoms*, Phys. Rev. Lett. **67**, 2295 (1991).

[17] M. Christophersen, J. Carstensen, A. Feuerhake, and H. Föll, *Crystal orientation and electrolyte dependence for macropore nucleation and stable growth on p-type si*, Mater. Sci. Eng. B **69**, 194 (2000).

[18] K. M. Ho, C. T. Chan, C. M. Soukoulis, R. Biswas, and M. Sigalas, *Photonic band gaps in three dimensions: new layer-by-layer periodic structures*, Solid State Comm. **89**, 413 (1994).

[19] S. Y. Lin, J. G. Fleming, D. L. Hetherington, B. K. Smith, R. Biswas, K. M. Ho, M. M. Sigalas, W. Zubrzycki, S. R. Kurtz, and J. Bur, *A three-dimensional photonic crystal operating at infrared wavelengths*, Nature **394**, 251 (1998).

[20] J. G. Fleming and S. Y. Lin, *Three-dimensional photonic crystal with a stop band from 1.35 to 1.95 μm*, Opt. Lett. **24**, 49 (1998).

[21] S. Noda, K. Tomoda, N. Yamamoto, and A. Chutinan, *Full three-dimensional photonic bandgap crystals at near-infrared wavelengths*, Science **289**, 604 (2001).

[22] K. Aoki, H. T. Miyazaki, H. Hirayama, K. Inoshita, T. Baba, K. Sakoda, N. Shinya, and Y. Aoyagi, *Microassembly of semiconductor threedimensional photonic crystals*, Nat. Mater. **2**, 117 (2001).

[23] R. Hillebrand, S. Senz, W. Hergert, and U. Gösele, *Macroporous-silicon-based three-dimensional photonic crystal with a large complete band gap*, J. Appl. Phys. **94**, 2758 (2003).

[24] L. A. Woldering, A. P. Mosk, R. W. Tjerkstra, and W. L. Vos, *The influence of fabrication deviations on the photonic band gap of three-dimensional inverse woodpile nanostructures*, J. Appl. Phys. **105**, 093108 (2009).

[25] L. A. Woldering, R. W. Tjerkstra, H. V. Jansen, I. D. Setija, and W. L. Vos, *Periodic arrays of deep nanopores made in silicon with reactive ion etching and deep UV lithography*, Nanotechnology **19**, 145304 (2008).

[26] R. W. Tjerkstra, L. A. Woldering, J. M. van den Broek, F. Roozeboom, I. D. Setija, and W. L. Vos1, *A method to pattern masks in two inclined planes for three-dimensional nano- and microfabrication*, Submitted (2010).

[27] J. M. van den Broek, L. A. Woldering, R. W. Tjerkstra, F. B. Segerink, I. D. Setija, and W. L. Vos, *Inverse woodpile photonic band gap crystals with a diamond-like structure made from single crystalline silicon*, In preparation (2010).

[28] S. R. Huisman, R. Nair, L. A. Woldering, A. P. Mosk, and W. L. Vos, *Signature of a photonic band gap for three dimensional silicon inverse woodpile photonic crystals*, In preparation (2010).

[29] S. R. Huisman, *Observing the forbidden zone for light*, Master's thesis, University of Twente, 2010.

[30] B. H. Husken, *Spontaneous emission of near-infrared quantum dots controlled with photonic crystals*, Ph.D. thesis, University of Twente, 2009.

[31] J. R. Lakowicz, *Principles of fluorescence spectroscopy* (Kluwer Academic, New York, 1999).

[32] M. D. Leistikow, J. Johansen, A. J. Kettelarij, P. Lodahl, and W. L. Vos, *Size-dependent oscillator strength and quantum efficiency of CdSe quantum dots controlled via the local density of states*, Phys. Rev. B **79**, 045301 (2009).

[33] Web page of the MIT Photonic-Bands Package: http://ab-initio.mit.edu/mpb/.

[34] S. G. Johnson and J. D. Joannopoulos, *Block-iterative frequency-domain methods for maxwell's equations in a planewave basis*, Opt. Express **8**, 173 (2001).

[35] I. S. Nikolaev, W. L. Vos, and A. F. Koenderink, *Accurate calculation of the*

local density of optical states in inverse-opal photonic crystals, J. Opt. Soc. Am. B **26**, 987 (2009).

Chapter 5
Controlling the emission of PbS quantum dots with 3D silicon photonic crystals

Photonic crystals are periodic structures that strongly modify the dispersion of light. As was first realised by Bykov [1] and Yablonovitch [2] there may be a frequency range for which no modes exist in these photonic crystals, in analogy with the band gap of semiconductors in solid state physics. As a fundamental consequence, an excited atom will forever remain in its excited state since it can not decay by emitting a photon. Since these seminal papers many experiments have been performed and published that have claimed to see band gaps. At first, attention was focused on measuring the reflectivity (or transmission) of photonic crystals. However it was later realised that other effects, like odd-symmetry modes, grating modes and slow modes could lead to strong reflection peaks that are not at all related to the modified density of states in the photonic crystal, see *e.g.* [3–5]. Much experimental effort became focused on measuring emission from photonic crystals to study the existence of a band gap. Both experiments measuring the intensity and measuring the decay were pursued.

In literature very often a trough in the spectrum of an emitter has been linked to a photonic band gap or inhibition [6–10]. However, these structures are often made with low contrast media which do not show a band gap or strong LDOS modification but a stop gap in a certain direction making the inhibition of spontaneous emission for these structures very unlikely. In contrast, the local density of states is an angle integrated property, and is not necessarily modified when there is either a Bragg condition for one direction or a strong reflection peak [11]. By measuring the angle integrated intensity a clear minimum is observed that obeys the Bragg law, showing inhibition of the spontaneous emission [12, 13].

Since Fermi's Golden Rule relates the local density of states directly to the radiative decay rate, measuring this quantity seems the easiest route to show a band gap or pseudo gap in the LDOS. Pioneering experiments were performed on colloidal crystals that have a low refractive index contrast [14]. A modification of the decay rate was found, but was probably caused by a change in the chemical environment of the emitters [15]. It is therefore very important to keep the chemical environment of the emitters constant to ensure that only the radiative decay rate is changed. Finding a good reference is crucial to a successful demonstration of emission control. As explained in ref. [16], one suitable reference system is a photonic crystal in the long wavelength limit where the LDOS has a known ω^2 frequency dependence. In 2004 Lodahl *et al.* [17] were the first to show a

significant effect on the decay rate while keeping the chemical environment constant. Later it was realised that in two dimensional photonic crystal membranes the emission rate can also be modified substantially as shown in experiments [18–21] and calculations [22]. The 2D slab measurements benefit from the fact that quantum dots are used with a fixed dipole orientation that is always in the plane of the membrane. The LDOS for this dipole can be very low, while the LDOS for a dipole that is oriented perpendicular to this plane is hardly modified [22]. None of these structure show a 3D photonic band gap, a frequency range where there are no modes at all for any arbitrary dipole orientation.

In this chapter experiments will be discussed on emission of PbS quantum dots inside 3D silicon inverse woodpile photonic crystals that are expected to have a broad band gap. It will be shown that both the decay rate and emission spectra of the emitters is strongly modified by the photonic crystal and show good agreement with the calculated density of states for these structures.

5.1. Samples

For our measurements 3D silicon inverse woodpile crystals are used. Details on fabrication of these samples can be found in chapter 4. The lattice parameter a of all the structures is fixed by the mask used for the first etch direction. For all structures discussed here $a = 693$ nm. By changing the diameter of the pores, a different filling fraction of silicon is obtained, giving a different band structure and DOS. Diameters of 2r = 271, 290, 340 and 361 nm are used. These diameters are determined with SEM, and have an accuracy of about 5 %.

In fig. 5.1 a) a calculated band structure is shown for a 3D inverse woodpile crystal with a pore diameter of 340 nm filled with toluene (the liquid in which the quantum dots are suspended). Clearly a band gap is present, indicated by the grey bar. In b) the corresponding DOS calculation is shown. For lower frequency the DOS follows the quadratic relation of a homogeneous medium. Since at a frequency of 0.35 the frequency gets into the photonic regime the DOS starts to deviate from the quadratic case.

When increasing the diameter of the pores, the center frequency and the relative width of the band gap shift up, because the volume fraction of silicon is decreased. This shift is shown in fig. 5.2. Here the lower and upper edge of the band gap is plotted versus the normalised radius r/a. The dashed area indicates the region of parameter space that is in the band gap. On the right axis the relative width of the band gap is plotted in grey. The band gap is widest - 8 % relative bandwidth - at approximately $r/a = 0.22$.

All measurements on 3D photonic crystals were performed in the Γ X direction parallel to the second set of etched pores (see fig. 4.1 b)).

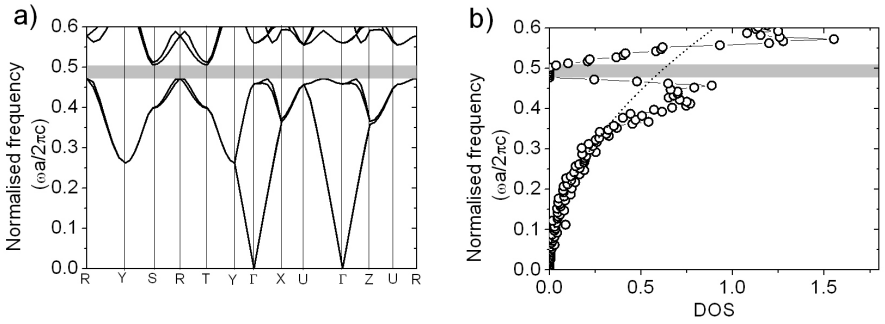

Figure 5.1.: a) The first 8 bands of a band structure of a 3D inverse woodpile photonic crystal structure are shown for a pore diameter of 340 nm, giving r/a=0.245. This structure consists of silicon (ϵ=12.1) and the pores are filled with toluene (ϵ=2.25). The band gap is indicated with the grey bar. b) The density of states per volume in units of ω^2/π^2c^3 for the same structure. The dotted line is a quadratic fit in the low frequency limit, where the crystal acts as a homogeneous medium. The DOS is calculated with 2000 k points.

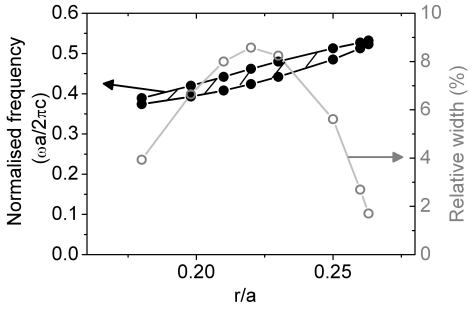

Figure 5.2.: The frequency position of the band gap as a function of the normalised radius of the pores is shown in black. On the right axis the relative width of the band gap is plotted in grey.

5.2. Role of quantum efficiency and local density of states

The decay rate that is measured in experiments is the total decay rate γ_{tot} which consists of a radiative and a non-radiative part:

$$\gamma_{tot} = \gamma_{rad} + \gamma_{nrad} \tag{5.1}$$

In the radiative process the emitter returns to the ground state through emission of a photon. The emitter can also return to the ground state non-radiatively, for example by generating phonons. The quantum efficiency (QE) of an emitter, given by

$$\eta = \frac{\gamma_{rad}}{\gamma_{tot}} \tag{5.2}$$

gives the fraction of excitation energy that is transferred to spontaneous emission. Depending on the value of the QE the (local) density of states will have a different effect on the emission [13, 16].

If the QE is 100 % all the absorbed energy is converted into light and $\gamma_{tot} = \gamma_{rad}$. Since the local density of states only affects the radiative decay rate (see chapter 1), modification of the measured total decay rate will be proportional to the LDOS change. However, the intensity emitted by the emitters is not dependent on the LDOS but only proportional to the pump intensity, since each pump photon is converted to an emitted photon.

If the QE is very low $\gamma_{tot} \approx \gamma_{nrad}$. In this situation modifying the density of states hardly affects the measured total decay rate. However, the modification of DOS can now be seen in the emitted intensity, since this is proportional to γ_{rad}.

The PbS quantum dots that are used in our experiments have an estimated quantum efficiency of 30 - 50 %. This quantum efficiency is determined by comparing the emitted intensity of quantum dots to a dye with known efficiency (IR125 in DMSO) [23]. However, this way of determining the quantum efficiency is known to underestimate the value of the quantum efficiency for blinking emitters [24].

In cases where the quantum efficiency is neither unity nor very low, both the intensity and the decay rate can be modified by the LDOS. To complicate matters further, for emitters in an environment with inhomogeneous LDOS, the quantum efficiency also depends on frequency, position and dipole orientation, since the radiative decay rate is modified by the LDOS. In appendix B a more thorough analysis can be found of the effect of local density of states on the emitted intensity. Even for quantum efficiencies as high as 90 % the intensity can be modified substantially.

In the following sections results of measurements of decay rate and emitted intensity of PbS quantum dots inside 3D inverse woodpile photonic crystals will be discussed respectively.

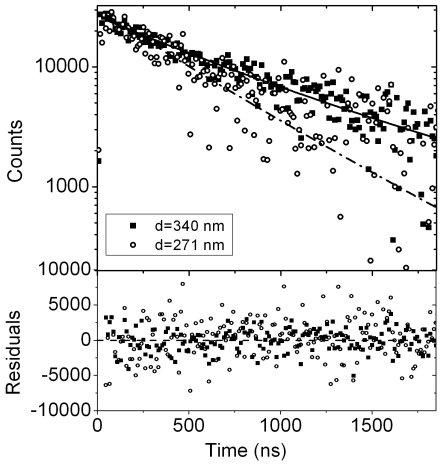

Figure 5.3.: Two decay traces measured at 0.850 eV are shown, that are measured in two different photonic crystals with a pore diameter of 340 nm (closed squares) and 271 nm (open circles). Bi-exponential fits are indicated by the curve (black solid for 340 nm and dash-dotted for 271 nm). In the lower panel the residuals are seen to be random indicative of good fits.

5.3. Measured decay rates compared to DOS

The decay rate has been measured for three different emission energies: 0.828 eV (1500 nm), 0.850 eV (1460 nm) and 0.893 eV (1390 nm) with a spectral width of 0.003 eV. In fig. 5.3 two decay curves are shown. Both decay curves are measured at 0.850 eV. There is a clear difference between the curve measured from the d = 340 nm structure compared to the measurement from the d = 271 nm photonic crystal. This difference confirms that the emission by excited quantum dots is clearly controlled by the inverse woodpile crystals. The curves indicate the fits that were used to extract the decay rate. For the fitting procedure of the time resolved measurements see paragraph 4.6. A decay rate of 3.1 and 0.88 μs^{-1} is found respectively for quantum dots inside the photonic crystal. Therefore these two crystals results are enhanced and inhibited compared to the quantum dots in suspension. In the bottom panel the residuals are plotted. Both residuals are centered around 0 indicating a good fit, as also confirmed by the goodness of fit χ^2_{red} that is 1.01 and 0.93 close to unity.

In fig. 5.4 a) to d) both the measured decay rate (filled symbols) and the DOS (open symbols connected with a guide to the eye) are shown for four different diameters of the pores in silicon. Different squares indicate different measure-

ments that have been performed on the same crystal and location on the crystal, but on different days. Therefore, variation of the data gives a measure for the reproducibility of the measurement.

Different emission energies correspond to a different radii of the quantum dots. Decay properties of quantum dots are usually dependent on the size of the quantum dot [24–26]. However, the PbS quantum dots used here have within error margin the same total decay rate of 1.81 μs^{-1} in suspension, as shown in table 5.1. Moreover, since the chemical environment in the photonic crystal is equal to that in suspension, we expect that the quantum dots in the photonic crystals will have the same non-radiative component of the decay rate.

Table 5.1.: Quantum dot total decay rates in suspension

Emission energy (eV)	Decay rate (μs^{-1})	error (μs^{-1})
0.828	1.80	0.04
0.850	1.85	0.09
0.893	1.79	0.06

For all four samples a qualitative or even a quantitative agreement between the measured total decay rate and the DOS is found. In fig. 5.4 a) the quantum dot emission is higher in frequency than the band gap. No features are seen in the decay rate or DOS. In fig. 5.4 b) an enhancement of the decay rate with more than a factor of 2 is found when increasing the frequency, corresponding well to the DOS. Most strikingly, in fig. 5.4 c) for the d = 340 nm sample a clear inhibition of the decay can be seen when the emitters in the band gap are probed in going from below the band gap to within the gap. A minimum decay rate of 0.16 μs^{-1} or a corresponding to a lifetime of 6.25 μs is found. The decay rate in the band gap is a factor of 11 lower than the decay rate in suspension. For fig. 5.4 d) also a clear inhibition of the decay rate is seen for emitters emitting inside the band gap, in good agreement with a density of states for d = 351 nm. Again a factor of 11 reduction in the decay rate is found compared to suspension. Since the diameter of the pores is measured with a 5 % accuracy by SEM the DOS calculations are performed with a diameter 3 % smaller than d = 361 nm.

5.4. Measured emission spectra compared to DOS

For real emitters with a quantum efficiency smaller than 1 it is expected that the emitted intensity in the form of emission spectra contains information on the (L)DOS, see appendix B for more details. Therefore, in fig. 5.5 two spectra are shown: one measured when the focus is on the photonic crystal (I_{PhC}) and one when the focus is an the silicon wafer (I_{Si}). See paragraph 4.5 for more details. These spectra are used to determine the relative emission spectrum I_{rel}, given by:

$$I_{rel} = \frac{I_{PhC} - I_{Si}}{I_{Si}} \tag{5.3}$$

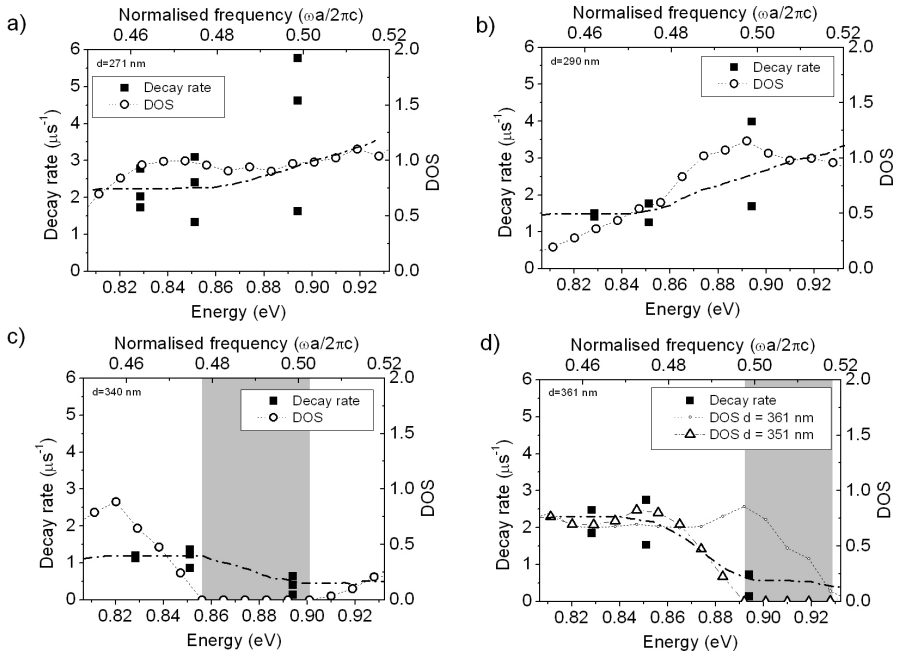

Figure 5.4.: Panel a) to d) show the measured decay rate (filled squares) and DOS (open circles) for photonic crystals with pore diameters of 271 nm, 290 nm, 340 nm and 361 nm respectively. The dash-dotted curves are guides to the eye for our experimental results.

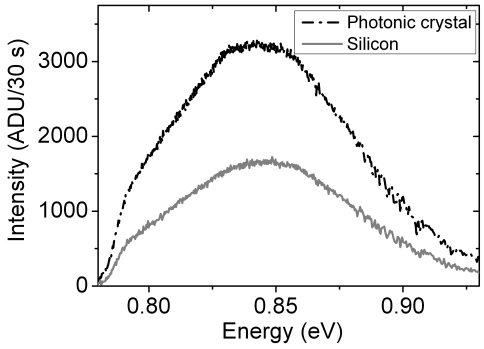

Figure 5.5.: The emission spectrum of PbS quantum dots measured when the focus is on the photonic crystal with a pore diameter of 340 nm (grey dash-dotted line) and on silicon wafer (black solid line). The sharp edge at low energy is caused by the cut-off of the detector.

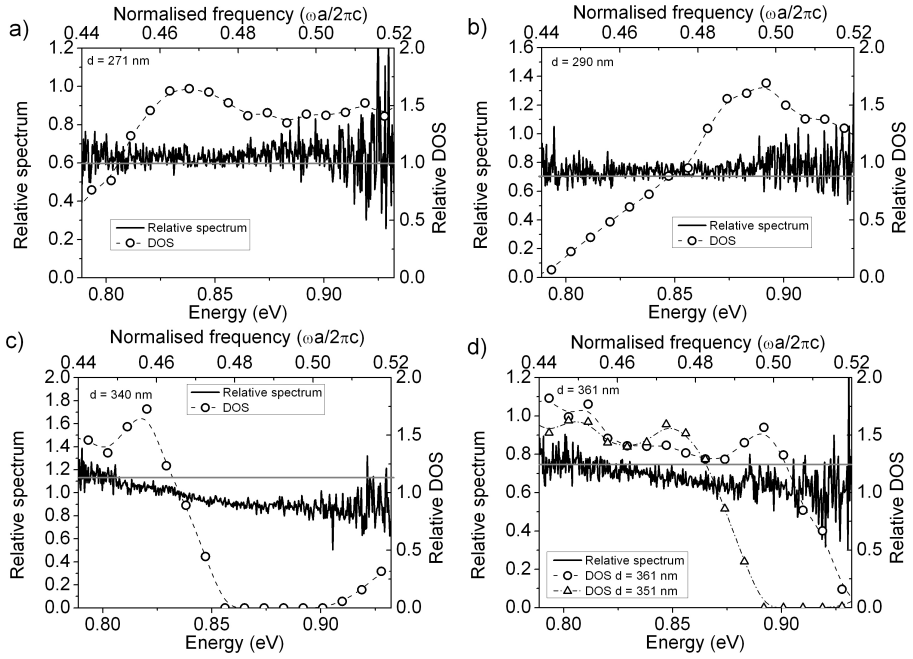

Figure 5.6.: Panel a) to d) show the emission spectrum from the emitters in the photonic crystal divided by the reference spectrum measured above silicon wafer for four different samples. Respectively, diameters are 271, 290, 340 and 361 nm. The calculated relative DOS is also shown. The dashed line is a guide to the eye.

In fig. 5.6 a) to d) the relative emission spectrum is plotted. A relative spectrum in an environment without DOS modification remains constant. Changes in the spectrum show up as deviations from this constant, illustrated by a line in fig. 5.6 for comparison. As can clearly be seen in fig. 5.6 c) and d) part of the spectrum is inhibited. To a lesser extent in figure b) the higher frequency part is enhanced. In stead of the density of states the relative DOS is now plotted with the open symbols. The relative DOS is the DOS divided by ω^2, since we are looking at intensity ratios, the ω^2 must be divided out [27]. The relative DOS agrees well with the data. Especially in the range where the band gap is expected for d = 340 nm and d = 351 nm.

5.5. Measured decay rates compared to emission spectra

In fig. 5.7 both the measured total decay rate (open circles) and the relative emission spectrum (black line) are plotted for the four different samples. The trend of both data sets is qualitatively the same: When there is no change in the

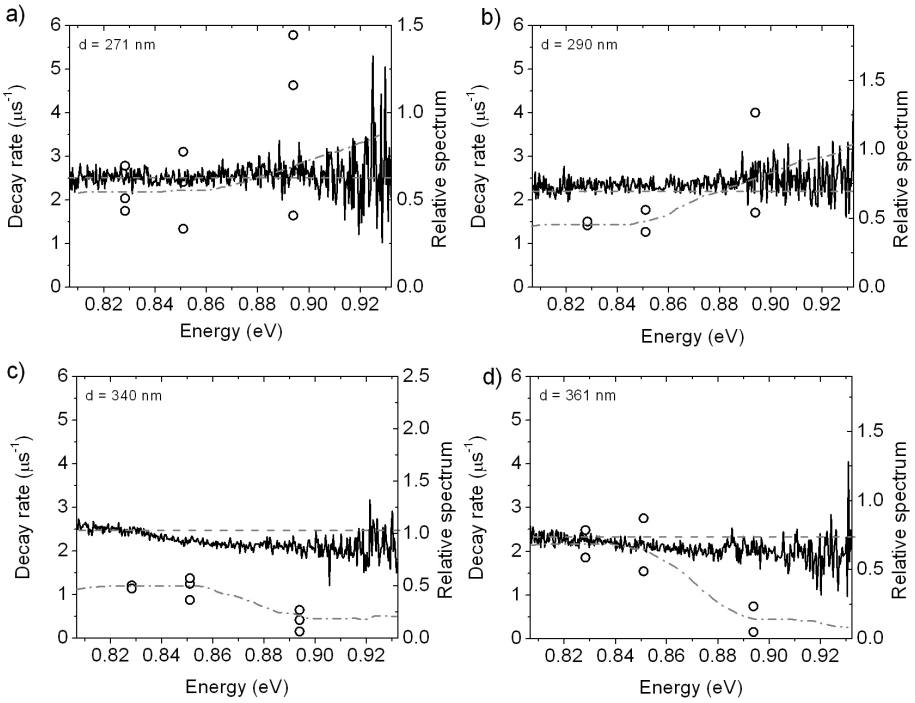

Figure 5.7.: Panel a) to d) shows both the measured total decay rate (open circles) and the relative emission spectrum (black line) for four different samples. The dash-dotted grey line is a guide to the eye.

decay rate the spectrum does not deviate significantly from a straight line (panel a)). When the decay rate is enhanced in panel b) the relative emission spectrum is higher. When inhibition of the decay is measured (panel c) and d)) a clear change to lower intensity is seen in the relative spectrum.

5.6. Discussion

The average spontaneous emission decay rate measured for quantum dots inside the band gap is 0.40 μs^{-1}. This is a factor of 4.5 inhibition compared to quantum dots in suspension with γ=1.81 μs^{-1}. The maximum inhibition of the decay rate found is a factor of 11. This is measured for quantum dots inside the band gap frequency range where γ_{tot} = 0.16 μs^{-1}. To the best of our knowledge this is the highest inhibition factor of spontaneous emission in 3D photonic crystals to date.

Such low emission rates lead to interesting complications. Our experiments are performed with an excitation repetition rate of 409 kHz, or 0.409 μs^{-1}. This rate is equal to the average rate found within the band gap frequency range. While performing time correlated single photon counting it is usually good practice to use a repetition rate of the excitation laser that is at least 5 times lower than the decay rate that needs to be measured. However, since in the near infrared frequency range the signal to noise ratio is low, it is very hard to further reduce the repetition rate, since our experiments are already performed with typically 3 10^5 dark counts per second and 4 10^3 signal counts (about 1% of the repetition rate). If the repetition rate is chosen too high, there might be a significant contribution of the signal still present when the next laser pulse arrives, especially for very slow decay. Since the background in our measurements is determined by averaging the 4.6 ns before the laser pulse, the background level is overestimated. This overestimation can affect the found decay curve and value for the decay rate. If there is still a significant contribution of the signal to this background level, a too high level will be subtracted leading to an over estimation of the slope and a higher decay rate. Therefore the values found by us can be considered upper bounds for the decay rate, but even lower rates might be present.

The photonic band gap, a frequency region with no modes at all, is a theoretical concept that only exists for infinitely large photonic crystals. Since real photonic crystals are always of finite size, the zero number of modes limit can never be reached. From calculations performed by different groups it seems that the DOS decreases exponentially with crystal size in a photonic band gap [28, 29]. The maximum factor of 11 found by us could give an indication for the distance from the surface of the photonic crystal and amount of disorder that the quantum dots experience. When considering the calculations by Ishizaki *et al.* [29] for GaAs woodpile photonic crystals a factor of 11 inhibition relates to about 7 layers of the woodpile between the emitter and the surface of the crystal. Since our structure is an inverse woodpile made of silicon it can not be directly compared to this value, but it might give an indication of the average depth of the quantum dots we are probing since the photonic strengths are comparable.

When considering the emitted intensity a modification of the spectral shape

is found when comparing quantum dots in the crystal to quantum dots in suspension. Changes in the emitted intensity do not necessarily only reflect DOS effects, but may also be caused by redistribution of the emission over different exit angles. Since our measurements were performed with a high NA objective (NA=0.7) due to the small size of the photonic crystal no information is obtained about the angle dependence of the emitted intensity. On the other hand, this high NA means that the emission is collected for many angles. Since the same trend is seen in both the decay rate measurements and the emission spectra, it is very likely that changes in the emission spectrum are directly caused by the DOS. As is shown in appendix B the quantum efficiency can still be substantial even when effects in the intensity are found, allowing both the decay rate and the intensity to be strongly modified.

Performing a saturation experiment may be an alternative way to demonstrate a band gap. It is good practice to perform spontaneous emission experiments at excitation powers where only a small fraction of the population is in the excited state. If one measures the emitted intensity as a function of the excitation power, a linear relation is found at first. When the excitation power is increased, this linear behavior levels off, giving a clear sign of saturation. For a two-level system, population inversion is never reached. For more complicated three- and four-level systems, the population can be inverted, leading to amplified spontaneous emission and laser action [30]. The excitation power level at which this saturation occurs is influenced by the photonic band gap. At saturation, the emission rate equals the excitation rate, as was demonstrated with quantum dots in cavities [31]. If the decay rate is very low due to this band gap, all the emitters inside the structure will lose their excitation energy very slowly, increasing the excited state population. This causes the emission to saturate at a lower excitation power than when measuring this same effect outside a band gap. To the best of our knowledge, this experiment has not been tried before on photonic band gap crystals.

5.7. Conclusion

We have performed spontaneous emission experiments on PbS quantum dots in 3D inverse woodpile photonic crystals, including two structures where the expected band gap overlaps with the emission frequency of the emitters. It is found that the decay rate is strongly modified by the photonic crystal. In the band gap range a maximum inhibition of a factor 11 is found compared to the decay rate in suspension. Strong enhancement of the decay rate is also seen at frequencies above the band gap. The measured spectra show a change in spectral shape that agree very well with the measured decay rate modification. The change in the emission spectra can very likely be attributed to the changes in local density of states.

References

[1] V. P. Bykov, *Spontaneous emission in a periodic structure*, Sov. Phys. -JETP **35**, 269 (1972).

[2] E. Yablonovitch, *Inhibited spontaneous emission in solid-state physics and electronics*, Phys. Rev. Lett. **58**, 2059 (1987).

[3] W. M. Robertson, G. Arjavalingam, R. D. Meade, K. D. Brommer, A. M. Rappe, and J. D. Joannopoulos, *Measurement of photonic band structure in a two-dimensional periodic dielectric array*, Phys. Rev. Lett. **68**, 2023 (1992).

[4] K. Sakoda, *Group-theoretical classification of eigenmodes in three-dimensional photonic lattices*, Phys. Rev. B **55**, 15345 (1997).

[5] W. L. Vos and H. M. van Driel, *Higher order bragg diffraction by strongly photonic fcc crystals: Onset of a photonic bandgap*, Phys. Lett. A **272**, 101 (2000).

[6] M. Megens, J. E. G. J. Wijnhoven, A. Lagendijk, and W. L. Vos, *Light sources inside photonic crystals*, Journ. Opt. Soc. Am. B **16**, 1403 (1999).

[7] S. V. Gaponenko, A. M. Kapitonov, V. N. Bogomolov, A. V. Prokofiev, A. Eychmüller, and A. L. Rogach, *Electrons and photons in mesoscopic structures: Quantum dots in a photonic crystal*, JETP Lett. **68**, 142 (1998).

[8] K. Yoshino, S. B. Lee, S. Tatsuhara, Y. Kawagishi, M. Ozaki, and A. A. Zakhidov, *Observation of inhibited spontaneous emission and stimulated emission of rhodamine 6G in polymer replica of synthetic opal*, Appl. Phys. Lett. **73**, 3506 (1999).

[9] A. Blanco, C. López, R. Mayoral, H. Míguez, F. Meseguer, A. Mifsud, and J. Herrero, *CdS photoluminescence inhibition by a photonic structure*, Appl. Phys. Lett. **73**, 1781 (1998).

[10] S. G. Romanov, T. Maka, C. M. Sotomayor-Torres, M. Müller, and R. Zentel, *Suppression of spontaneous emission in incomplete opaline photonic crystals*, J. Appl. Phys. **91**, 9426 (2002).

[11] C. Hooijer, D. Lenstra, and A. Lagendijk, *Mode density inside an omnidirectional mirror is heavily directional but not small*, Opt. Lett. **25**, 1666 (2000).

[12] S. Ogawa, M. Imada, S. Yoshimoto, M. Okano, and S. Noda, *Control of light emission by 3D photonic crystals*, Science **305**, 227 (2004).

[13] A. F. Koenderink, L. Bechger, H. P. Schriemer, A. Lagendijk, and W. L. Vos, *Broadband fivefold reduction of vacuum fluctuations probed by dyes in photonic crystals*, Phys. Rev. Lett. **88**, 143903 (2002).

[14] J. Martorell and N. M. Lawandy, *Observation of inhibited spontaneous emission in a pediodic dielectric structure*, Phys. Rev. Lett. **65**, 1877 (1990).

[15] B. Y. Tong, P. K. John, Y. Zhu, Y. S. Liu, S. K. Wong, and W. R. Ware, *Fluorescence-lifetime measurements in monodispersed suspensions of polystyrene particles*, JOSA B **10**, 356 (1993).

[16] A. F. Koenderink, L. Bechger, A. Lagendijk, and W. L. Vos, *An experimental study of strongly modified emission in inverse opal photonic crystals*, Phys. Stat. Solidi A **197**, 648 (2003).

[17] P. Lodahl, A. F. van Driel, I. S. Nikolaev, A. Irman, K. Overgaag, D. Vanmaekelbergh, and W. L. Vos, *Controlling the dynamics of spontaneous emission from quantum dots by photonic crystals*, Nature **430**, 654 (2004).

[18] D. Englund, D. Fattal, E. Waks, G. Solomon, B. Zhang, T. Nakaoka, Y. Arakawa, Y. Yamamoto, and J. Vukucic, *Controlling the spontaneous emission rate of single quantum dots in a two-dimensional photonic crystal*, Phys. Rev. Lett. **95**, 013904 (2005).

[19] A. Kress, F. Hofbauer, N. Reinelt, M. Kaniber, H. J. Krenner, R. Meyer, G. Böhm, and J. J. Finley, *Manipulation of the spontaneous emission dynamics of quantum dots in two-dimensional photonic crystals*, Phys. Rev. B **71**, 241304 (2005).

[20] M. Fujita, S. Takahashi, Y. Tanaka, T. Asano, and S. Noda, *Simultaneous inhibition and redistribution of spontaneous light emission in photonic crystals*, Science **308**, 1296 (2005).

[21] T. Lund-Hansen, S. Stobbe, B. Julsgaard, H. Thyrrestrup, T. Sünner, M. Kamp, A. Forchel, and P. Lodahl, *Experimental realization of highly efficient broadband coupling of single quantum dots to a photonic crystal waveguide*, Phys. Rev. Lett. **101**, 113903 (2008).

[22] A. F. Koenderink, M. Kafesaki, C. M. Soukoulis, and V. Sandoghdar, *Spontaneous emission rates of dipoles in photonic crystal membranes*, J. Opt. Soc. Am. B **23**, 1196 (2006).

[23] M. A. Hines and G. D. Scholes, *Colloidal PbS nanocrystals with size-tunable near-infrared emission: Observation of post-synthesis self-narrowing of the particle size distribution*, Adv. Mat. **15**, 1844 (2003).

[24] M. D. Leistikow, J. Johansen, A. J. Kettelarij, P. Lodahl, and W. L. Vos, *Size-dependent oscillator strength and quantum efficiency of CdSe quantum dots controlled via the local density of states*, Phys. Rev. B **79**, 045301 (2009).

[25] X. Fan, M. C. Lonergan, Y. Zhang, and H. Wang, *Enhanced spontaneous emission from semiconductor nanocrystals embedded in whispering gallery optical microcavities*, Phys. Rev. B **64**, 115310 (2001).

[26] J. Johansen, S. Stobbe, I. S. Nikolaev, T. Lund-Hansen, P. T. Kristensen, J. Hvam, W. L. Vos, and P. Lodahl, *Size dependence of the wavefunction of self-assembled inas quantum dots from time-resolved optical measurements*, Phys. Rev. B **77**, 073303 (2008).

[27] A. F. Koenderink, *Emission and transport of light in photonic crystals*, Ph.D. thesis, University of Amsterdam, 2003.

[28] J. S. Kole, *New methods for the numerical solution of maxwell's equations*, Ph.D. thesis, University of Groningen, 2003.

[29] K. Ishizaki, M. Okano, and S. Noda, *Numerical investigation of emission in finite-sized, three-dimensional photonic crystals with structural fluctuations*, J. Opt. Soc. Am. B **26**, 1157 (2009).

[30] A. E. Siegman, *Lasers* (University Science Books, 1986).

[31] M. Munsch, A. Mosset, A. Auffèves, S. Seidelin, J. P. Poizat, J.-M. Gérard, A. Lemaître, I. Sagnes, and P. Senellart, *Continuous-wave versus time-resolved measurements of purcell factors for quantum dots in semiconductor microcavities*, Phys. Rev. B **80**, 115312 (2009).

Chapter 6
Emission of PbS quantum dots in 2D Si photonic crystals

Ever since the seminal article by Yablonovitch [1] a wide field of research has been dedicated to the pursuit of control over the decay rate of spontaneous emission with application ranging from thresholdless lasers to solar cells [2, 3]. The ultimate control over spontaneous emission is obtained when the light emission frequency overlaps with the frequency range of a band gap in a three dimensional (3D) photonic crystal. In the complete absence of modes, the decay rate will be zero.

A two dimensional (2D) photonic crystal can not show a 3D band gap because it is only periodic in two of the three directions. However, the total solid angle over which light propagation is inhibited by photonic gaps is substantial [4]. From a calculation it is then expected that a modification of the local density of states (LDOS) is significant: indeed up to one order of magnitude is predicted in the center of hexagonally periodic pores etched in silicon [5, 6]. The reflectivity and transmission of macroporous 2D photonic crystals in silicon have been investigated extensively for hexagonal lattices and show clear stopgaps [7–9]. A big advantage of 2D photonic crystals is the relative ease of fabrication compared to 3D photonic structures.

For a 2D periodicity combined with a membrane waveguide to provide confinement in the third direction extensive measurements have been performed. It has been shown both theoretically and experimentally that the decay rate is modified by these membrane photonic crystals [10–14]. The LDOS is influenced by both the periodicity and waveguiding inside the membrane. The most commonly used emitters inside these membranes have an oriented dipole that is in the plane of the membrane, thereby selecting a subset of the LDOS that shows strong photonic features to achieve modification of the decay rate.

Surprisingly, little research activity has been dedicated to measuring emission from truly 2D photonic crystals. Emission of HgTe quantum dots from Si hexagonal macroporous structure has been investigated by ref. [15]. Less emitted light exited the photonic structure when the reflectivity was high, indicating that the photonic crystal modified the emission. However, no further study could be performed since the quantum dots were clustered, making decay properties unreliable. Si nanopillar photonic crystals have been studied by ref. [16]. Using Rhodamine-700 laser dye, a stop gap was seen. However, this emission was well within the absorption range of silicon, complicating interpretation of the results.

In this chapter, measurements of emission of PbS quantum dots from 2D silicon crystals are discussed. The structures have a centered rectangular lattice in stead

of a more common hexagonal lattice to accommodate the inverse woodpile design for the 3D structure via the fabrication process describes in chapter 4. These 2D photonic crystals are infiltrated with PbS quantum dots. No modification of the decay rate by the photonic crystal is found but redistribution of the emitted intensity of the quantum dots plays a significant role.

6.1. Samples

A more detailed discussion of the centered rectangular structures can be found in chapter 4. In this chapter the results are presented of study of emission from five samples that have identical lattice parameter a and different pore diameters d corresponding to different filling fractions of silicon to toluene. Diameters of 271, 290, 310, 340 and 361 nm are used. These diameters are determined by SEM and have a typical error of 5 %. The pores are 6 μm deep.

In fig. 6.1 a) a band structure is shown of a 2D photonic crystal with a pore diameter $d = 361$ nm. The band structure is calculated using $\epsilon = 12.1$ for the silicon backbone while the pores have $\epsilon = 2.25$ (toluene). Since the calculations are performed for a 2D structure with infinitely long pores, the bands can be separated into TE (solid lines) and TM (dashed lines) polarised contributions, where TE fields are polarised perpendicular to the pores and TM fields are polarised parallel to the pores [17]. A broad 2D band gap for TE modes is seen while no such gap exists for TM modes. In the inset the first Brillouin zone of the lattice is shown. Points of high symmetry are indicated with capital letters. Experiments are performed by measuring emission from the structure in the ΓK and ΓM' directions. Since a high-NA objective with NA = 0.7 is used, a broad range of angles are taken into account in the experiment. Inside the structure, this amounts to an angle of approximately 15 ° when using $n_{eff} = 3$.

A calculation of the 3D DOS for this particular structure is shown in fig. 6.1 b). The grey bar indicates the TE 2D band gap. The dashed line indicates a quadratic dependence of the DOS that is applicable for homogeneous media. The calculated DOS hardly deviates from this quadratic line, even in the range where there is a broad 2D TE band gap. Therefore, no appreciable modification of the spontaneous emission decay rate is expected in these 2D photonic crystals.

6.2. Results

Emission measurements on PbS quantum dots inside 2D silicon photonic crystals are presented in this section. In fig. 6.2 two emission spectra are shown when measuring on a photonic crystal with $d = 310$ nm in the ΓM' direction . The higher intensity spectrum is measured when the focus of the detection objective is on the photonic crystal (I_{PhC}). Clear peaks in the spectrum can be seen. The lower intensity spectrum is measured when the detection focus is on the silicon wafer (I_{Si}). See paragraph 4.5 for alignment details. For these spectra, we define a relative intensity as:

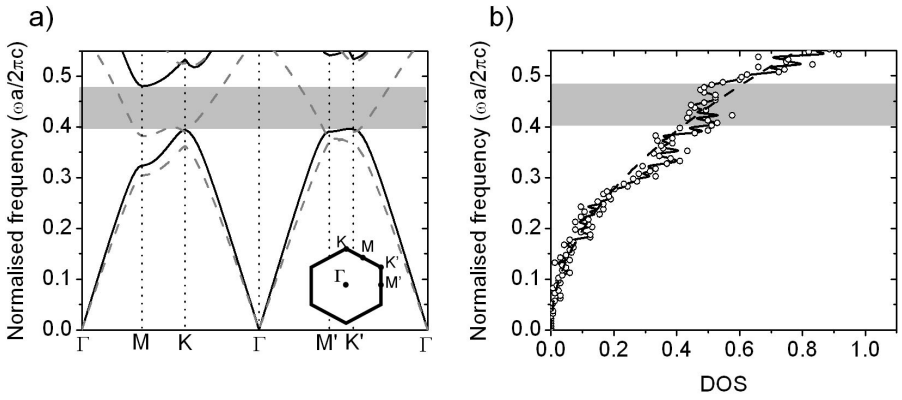

Figure 6.1.: a) Calculated photonic band structure for a 2D centered rectangular crystal with infinitely long pores. Pore diameter $d = 361$ nm, silicon dielectric constant $\epsilon = 12.1$ and toluene dielectric constant $\epsilon = 2.25$. Black solid lines represent TE polarised modes, grey dashed lines indicate TM polarised modes. Inset shows the first Brillouin zone. Captical letters indicate the points of high symmetry. b) 3D density of states (DOS) for the same crystal as in a) in units of ω^2/π^2c^3 per volume. The dashed line is a quadratic fit with $n_{eff} = 2.6$. The grey bar indicates the frequency range of the TE 2D band gap.

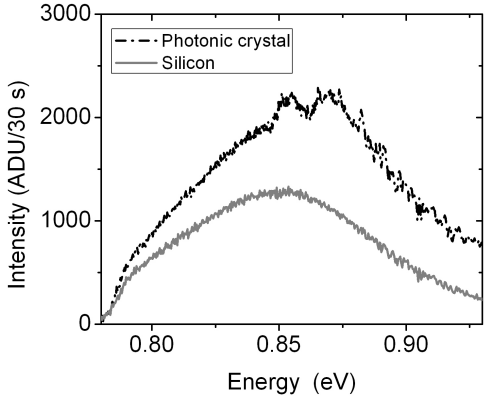

Figure 6.2.: Emission spectra of PbS quantum dots when the detection objective is focused on the photonic crystal (black dash-dotted line) and on the silicon wafer (grey solid line)

$$I_{rel} = \frac{I_{PhC} - I_{Si}}{I_{Si}} \tag{6.1}$$

In fig. 6.3 a) the relative spectra are shown for two different pore diameters. The sample with a diameter of 361 nm is measured along the ΓK direction. For the $d = 361$ nm sample the relative spectrum is constant, meaning that the shape of the quantum dot emission spectrum is not changed by the photonic crystal. Results for diameters of 271, 290 and 340 nm, not shown here, also reveal no change in the shape of the emission spectrum. However, for the sample with a diameter $d = 310$ nm, the emission spectrum is strongly modified. This sample is probed in both the ΓK and ΓM' direction. A clear difference in the emitted spectrum can be seen. For light emitted in the ΓK direction, a lower intensity is found for higher frequencies, compared to the same spectrum without photonic crystal. For light emitted in the ΓM' direction, more light is coming out at higher frequencies and very intriguing sharp peaks are observed.

In fig. 6.3 b) the measured decay rates are shown for the 2D crystals. For details on the fitting procedure see 4.6. The decay rate is measured for three different emission energies: 0.828 eV (1500 nm), 0.850 eV (1460 nm) and 0.893 eV (1390 nm) with an accuracy of 0.003 eV. Different points of the same symbol at the same frequency are measurements performed on other locations on the sample. The variation of these points gives an indication of the reproducibility of the measurement. Within this error margin, for all three samples a constant and equal decay rate is found with frequency, in agreement with the DOS calculation. This behavior differs significantly from 2D photonic crystal slabs, likely since our experiment averages over all dipole orientations, while in slab experiments only the dipole orientation with the same polarisation as the 2D band gap is present because of the choice of quantum dots [10–13].

Since the decay rate is constant, we conclude that the DOS does not contribute to the modified emission spectrum of the quantum dots inside the $d = 310$ nm sample, contrary to what was found for 3D photonic crystals (see chapter 5). The change in the spectrum is most likely caused by redistribution of light upon exiting the photonic crystal.

To investigate further the $d = 310$ nm sample, we have measured the emission for both the ΓK and ΓM' direction with a polariser to separate TE and TM polarisation. The relative spectrum is plotted in the bottom panel of fig. 6.4. For the data in this figure the relative spectrum is determined by the emission spectrum measured from the structure divided by a spectrum measured in suspension. The intensity is normalised at the low frequency side. For light in the ΓK direction, at higher frequency relatively less light is exiting the photonic crystal. For the ΓM' direction, more light exits the structure at higher frequency. It thus seems that light is redistributed from the ΓK direction to the ΓM' direction by the photonic crystal.

It is clearly seen in the figure that the peaks with centers at 0.854 and 0.868 eV only appear in the TE polarised light. In the top panel of fig. 6.4 the band structure is plotted. The peaks in the TE spectrum seem to overlap with the edge of the stopgap for TE modes in the ΓM' direction and a band crossing in

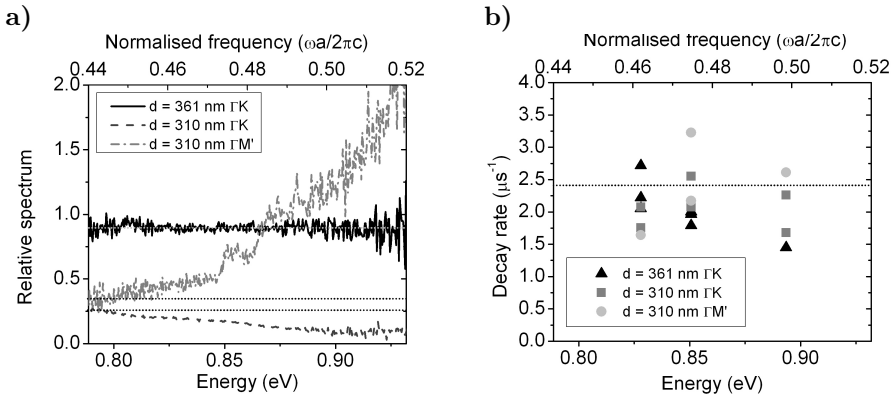

Figure 6.3.: a) The relative spectrum is shown. Lines are guides to the eye. b The decay rate is shown for the corresponding measurements in a).

the M'K' direction as indicated by the vertical dashed lines. Since we measure with a relatively large NA of 0.7 we are sensitive to more directions than only the ΓM' direction, making it possible that the bands in the M'K' direction influence our measurement. Since the peaks in the TE emission spectrum are related to band edges, they may be caused by Van Hove singularities in the two dimensional density of states for TE polarisation. Van Hove singularities are sharp maxima in the density of states, where the slope of the band diverges [18]. No such maxima are observed in the three dimensional DOS (see fig. 6.1).

6.3. Discussion

Peaks in the emission spectrum of emitters at the edge of a band gap have been reported before [19, 20] and are connected to amplified spontaneous emission. When measuring the intensity of the peaks as a function of excitation power, clear threshold behavior was found. No such threshold is present for our measurements, excluding amplified spontaneous emission.

The sample with $d = 310$ nm, for which redistribution of light is found, has a different surface than the other samples. The other samples were polished to accommodate the further process of fabricating a 3D structure. The sample with $d = 310$ nm was cleaved. Cleaving the sample gives a better surface quality than when polishing, judging from the SEM images. However, when measuring reflectivity of the samples no significant difference is found in the maximum of the reflectivity peaks between the cleaved and polished samples, while reflectivity is extremely sensitive to the surface of the probed sample. From the reflectivity measurements we conclude that the redistribution found for the cleaved samples is not caused by a better surface quality.

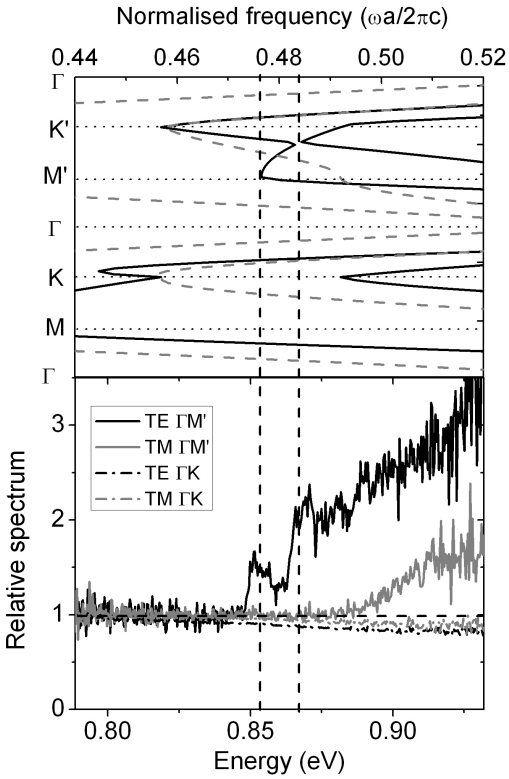

Figure 6.4.: In the top panel the 2D band structure is shown for a sample with $d =$ 310 nm. The solid black lines indicate TE polarised light, the grey dashed lines indicate the TM polarised light. In the bottom panel the relative spectrum is shown of quantum dots inside the $d = 361$ nm photonic crystal for two different directions and polarisations.

6.4. Conclusions

We have investigated emission of PbS quantum dots in a 2D silicon photonic crystal with centered rectangular symmetry. These crystals do not modify the spontaneous emission rate, in agreement with DOS calculations. However, a clear redistribution of emitted light is found, including intriguing peaks in the emission spectrum. These peaks are attributed to the edge of stopgaps in the band structure.

References

[1] E. Yablonovitch, *Inhibited spontaneous emission in solid-state physics and electronics*, Phys. Rev. Lett. **58**, 2059 (1987).

[2] H. G. Park, S. H. Kim, S. H. Kwon, Y. G. Ju, J. K. Yang, J. H. Baek, S. B. Kim, and Y. H. Lee, *Electrically driven single-cell photonic crystal lasers*, Science **305**, 148 (2005).

[3] I. Rodriguez, P. Atienzar, F. Ramiro-Manzano, F. Meseguer, A. Corma, and A. Garcia, *Photonic crystals for applications in photoelectrochemical processes photoelectrochemical solar cells with inverse opal topology*, Photonics Nanostruc. **3**, 148 (2005).

[4] T. Baba and T. Matsuzaki, *Microcavities and photonic bandgaps* (1996).

[5] D. P. Fussell, R. C. McPhedran, M. de Sterke, and A. A. Asatryan, *Three-dimensional local density of states in a finite two-dimensional photonic crystal composed of cylinders*, Phys. Rev. E **67**, 045601 (2003).

[6] Y. Zeng, X. Chen, and W. Lu, *Modified spontaneous emission from a two-dimensional photonic crystal*, Phys. Rev. E **70**, 047601 (2004).

[7] U. Grüning, V. Lehmann, S. Ottow, and K. Busch, *Macroporous silicon with a complete two-dimensional photonic band gap centered at 5 μm*, Appl. Phys. Lett. **68**, 747 (1996).

[8] J. Schilling *et al.*, *A model system for two-dimensional and three-dimensional photonic crystals: macroporous silicon*, J. Opt. A: Pure Appl. Opt. **3**, (2001).

[9] J. Schilling, A. Birner, F. Müller, R. B. Wehrspohn, R. Hillebrand, U. Gösele, K. Busch, S. John, S. W. Leonard, and H. M. van Driel, *Optical characterisation of 2D macroporous silicon photonic crystals with bandgaps around 3.5 and 1.3 μm*, Opt. Mat. **17**, 7 (2001).

[10] D. Englund, D. Fattal, E. Waks, G. Solomon, B. Zhang, T. Nakaoka, Y. Arakawa, Y. Yamamoto, and J. Vučković, *Controlling the spontaneous emission rate of single quantum dots in a two-dimensional photonic crystal*, Phys. Rev. Lett. **95**, 013904 (2005).

[11] A. Kress, F. Hofbauer, N. Reinelt, M. Kaniber, H. J. Krenner, R. Meyer, G. Böhm, and J. J. Finley, *Manipulation of the spontaneous emission dynamics of quantum dots in two-dimensional photonic crystals*, Phys. Rev. B **71**, 241304 (2005).

[12] M. Fujita, S. Takahashi, Y. Tanaka, T. Asano, and S. Noda, *Simultaneous inhibition and redistribution of spontaneous light emission in photonic crystals*, Science **308**, 1296 (2005).

[13] T. Lund-Hansen, S. Stobbe, B. Julsgaard, H. Thyrrestrup, T. Sünner, M. Kamp, A. Forchel, and P. Lodahl, *Experimental realization of highly efficient broadband coupling of single quantum dots to a photonic crystal waveguide*, Phys. Rev. Lett. **101**, 113903 (2008).

[14] A. F. Koenderink, M. Kafesaki, C. M. Soukoulis, and V. Sandoghdar, *Spontaneous emission rates of dipoles in photonic crystal membranes*, J. Opt. Soc. A. B **23**, 1196 (2006).

[15] S. Richter *et al.*, *Quantum dot emitters in two-dimensional photonic crystals of macroporous silicon*, Appl. Phys. Lett. **87**, 142107 (2005).

[16] V. V. Poborchii, T. Tada, and T. Kanayama, *Photonic-band-gap properties of two-dimensional lattices of Si nanopillars*, J. Appl. Phys. **91**, 3299 (2002).

[17] J. D. Joannopoulos, S. G. Johnson, J. N. Winn, and R. D. Meade, *Photonic crystals: molding the flow of light* (Princeton University Press, Princeton, 2008).

[18] N. W. Ashcroft and N. D. Mermin, *Solid state physics* (Brooks/Cole, Orlando, 1976).

[19] M. N. Shkunov, Z. V. Vardeny, M. C. DeLong, R. C. Polson, A. A. Zakhidov, and R. H. Baughman, *Tunable, gap-state lasing in sqitchable directions for opal photonic crystals*, Adv. Func. Mater. **12**, 21 (2002).

[20] G. R. Maskaly, M. A. Petruska, J. Nanda, I. V. Bezel, R. D. Schaller, H. Htoon, J. M. Pietryga, and V. I. Klimov, *Amplified spontaneous emission in semiconductor-nanocrystal/synthetic-opal composites: Optical-gain enhancement via a photonic crystal pseudogap*, Adv. Mater. **18**, 343 (2006).

Chapter 7
Decay of CdSe quantum dots in GaP nanowire ensembles

Changing the close surroundings of an emitter can have a strong effect on the spontaneous emission rate of an emitter. This effect is described by Fermi's Golden Rule, which states that the decay rate is determined by properties given by the emitter itself and by its environment, the local density of optical states (LDOS) that is available to couple emission to [1, 2]. This effect of the local density of states on the emission decay rate has given rise to an enormous field of research, most notably photonic crystals [3, 4]. Here interference of light with a periodic nanostructure causes strong modification of the LDOS.

In strongly scattering random materials these interference effects can lead to Anderson localization of light [5, 6]. It has been predicted that the LDOS in such random photonic materials will show spatial fluctuations due to the interference inside strongly scattering materials [7–9]. Experimentally, the effect of random strongly scattering media on spontaneous emission has only gotten attention very recently [10, 11]. In these studies light from a single emitter source is measured on the surface [10] and inside [11] a strongly scattering medium. The width of the distribution of decay rates was observed to increase with scattering strength, that is defined as $\frac{1}{kl}$ with k the wave vector of light and l the mean free path.

In this chapter measurements are presented of spontaneous emission decay rates of ensembles of CdSe quantum dots in between strongly scattering gallium phosphide nanowires. The decay is strongly modified by the radius of the nanowires. It is shown that the average modification in the decay rate can be explained by only taking into account the effect of a single scatterer. No effect of multiple scattering is found on the width of the decay rate distribution.

7.1. Experimental details

7.1.1. Sample

Gallium phosphide (GaP) nanowires were grown at Philips Research using a vapor liquid solid bottom up approach by chemical vapor deposition, molecular beam epitaxy, laser ablation and chemical beam epitaxy [12]. These wires are typically 1.5 μm long and have a radius ranging from 5 to 50 nm with a variation of typically $\pm$ 15 % per sample as determined by scanning electron microscope (SEM). An SEM picture of a typical sample is shown in fig. 7.1. The nanowires are grown randomly on a (111) interface of GaP, mostly directed vertically. Ensembles of nanowires with different radii optically behave similar to effective media with different GaP filling fractions. These ensembles of nanowires are

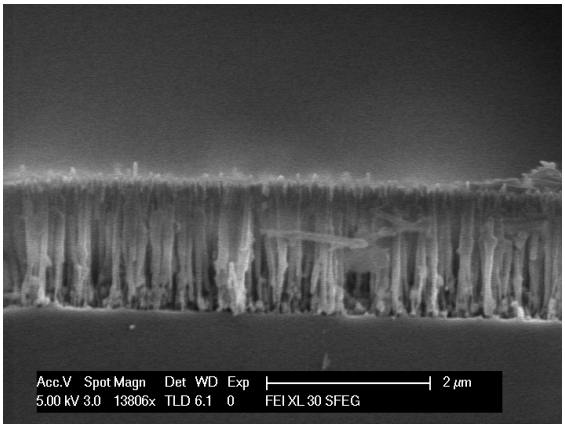

Figure 7.1.: A scanning electron micrograph of the side view of an ensemble of nanowires. The nanowires are oriented perpendicular to the surface of the GaP substrate.

strongly birefringent; the refractive index parallel to the wires is different from the refractive index perpendicular to the wires. The ordinary and extraordinary refractive indices are determined from measurements of the reflection of polarised beams from the GaP nanowire layers [13]. The mean free path of each sample has been determined by measuring the enhanced backscattering cone [14]. For two samples with the smallest radius, the samples where transparent. The mean free path was extrapolated for these samples, since no backscattering cone was present in measurements.

To dope the samples, six different ensembles of nanowires with different radii were dropcast with a suspension of commercially available CdSe quantum dots (Evident Evidot). Experiments were performed with two different batches of quantum dots with a center emission energies near 2.08 eV and 1.98 eV, which will be called CdSe1 and CdSe2 respectively. An overview of the samples is shown in table 7.1.

Table 7.1.: Nanowire properties

radius (nm)	mean free path l (μm)
15	1.7
46	1
61	0.55
76	0.29
90	0.18
108	0.16

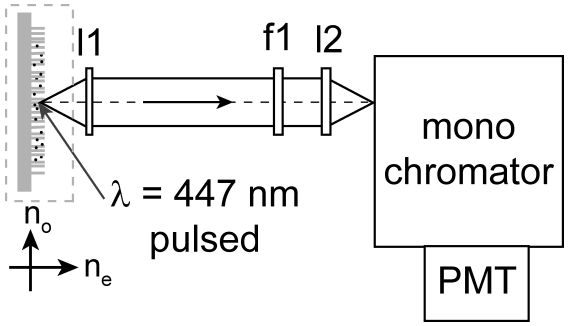

Figure 7.2.: A schematic picture of the experimental setup. Light from the laser excites the quantum dots in between the GaP nanowires inside a nitrogen purged chamber. The emitted light is detected by the photomultiplier tube after passing through a monochromator. The arrows below the sample indicate the axes of the extraordinary and ordinary refractive index for the highly birefringent nanowires.

7.1.2. Optical detection

The optical set-up used in the measurements is schematically shown in fig. 7.2. A pulsed laser (Picoquant ps diode laser) with an emission wavelength of 447 nm, a repetition rate of 20 MHz and a pulse duration of 75 ps is used to excite the quantum dots. The beam is guided into an optical fiber and focused onto the sample by an objective with a numerical aperture of 0.05, leading to a focus with a radius of 5 μm on the sample. The sample is contained in a nitrogen-purged chamber to prevent photo oxidation of the quantum dots.

The light emitted by the quantum dots is collected, collimated and focused onto the slit of the prism monochromator (Carl Leiss). The slit width is 400 μm which allows the detector to collect emitted light from a much larger area than the excitation spot. Behind the monochromator a Hamamatsu Photomultiplier tube (PMT) is positioned that is used as a photon counter. With this setup it is possible to measure spectra by scanning the spectrometer and to measure decay curves of emitters at particular emission frequencies by time correlated single photon counting (TCSPC). This technique measures the time between the arrival of an emitted photon (start) and the next laser pulse (stop) very precisely [15]. By repeating this measurement a histogram of the decay is made from which a decay rate can be determined.

Samples with different nanowire radii show the same luminescence spectra. These spectra are shown in fig. 7.3. For CdSe1 quantum dots three curves are shown, in toluene suspension, and when infiltrated into two nanowire samples with different radii. For the CdSe2 quantum dots two spectra are shown in two different nanowire samples as well. No spectral shift is observed when placing the quantum dots in between the nanowires, indicating that no chemical changes are made to the quantum dots. Time resolved measurements are performed at the

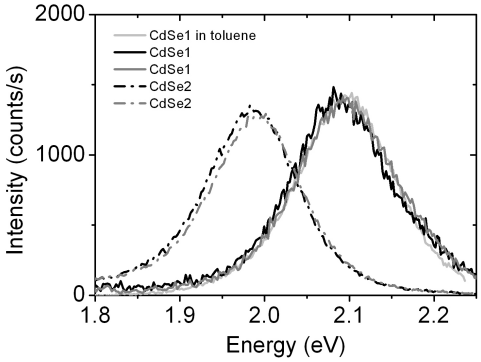

Figure 7.3.: The photoluminescence spectra for three samples and the quantum dots in toluene.

peak of the two emission curves, at 2.08 and 1.98 eV respectively with a spectral width of 0.01 eV.

To verify that the quantum dots are in the bulk of the nanowire samples and not only on the top surface of the nanowires we have studied how the emitted light escapes from the sample [16]. If the quantum dots are in the bulk of the strongly scattering nanowires it is expected that less light exits the sample at higher angles with respect to the normal to the interface. This type of profile is called Lambertian, where the emitted intensity decreases with the cosine of the angle between the detector and the normal to the surface [17]. If the quantum dots would only be deposited on the top of the nanowires the emitted intensity is expected to be constant with angle. The Lambertian behavior can clearly be seen in fig. 7.4, validating that the quantum dots are indeed in between the nanowires and not on the top surface.

We have also verified that the decay curve is not dependent on excitation power and that the emitted intensity increases linearly with excitation power. This allows us to exclude energy transfer or gain processes that might affect the observed decay rate.

7.2. Results

The decay curves have been measured on ensembles of CdSe quantum dots in between an ensemble of GaP nanowires with different average radii. Results are shown in fig. 7.5. The experimental curves are clearly different for different samples. The decay of the quantum dots is strongly modified by placing the quantum dots in between nanowires with different radii. The decay is not single exponential. This deviation from single exponential behavior is caused by the ensemble averaging inherent to the measurement. Because the decay rate is dependent on position and dipole orientation, individual emitters will have a different decay rate [18]. Summing these single exponentials in an ensemble

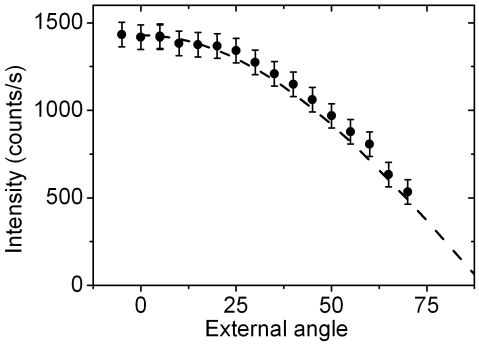

Figure 7.4.: The escape function is shown of the emission of CdSe1 quantum dots from a sample containing nanowires (circles). The dashed line shows a cosine function.

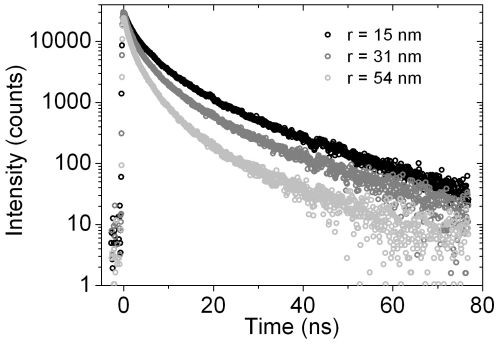

Figure 7.5.: Decay curves of emission of CdSe1 quantum dots in three samples of GaP nanowires with different average radius r of the nanowires.

measurements leads to a non-exponential decay.

To model the decay curve the data are fitted with a distribution of decay rates as explained in ref. [19]. A function of the following form is used to model the decay curve:

$$f(t) = \int_0^\infty \sigma(\gamma_{tot}) \exp(-\gamma_{tot} t) \mathrm{d}\gamma_{\mathrm{tot}} \tag{7.1}$$

where the normalised distribution in decay rates is chosen to be lognormal

$$\sigma(\gamma) = A \exp\Big[- \Big(\frac{ln(\gamma) - ln(\gamma_{mf})}{w} \Big)^2 \Big] \tag{7.2}$$

The normalisation factor A equals $A = [\gamma_{mf} w \sqrt{\pi} \exp(w^2/4)]^{-1}$. The two relevant adjustable parameters that can be extracted from the model are the most frequent decay rate γ_{mf} which is the peak of the lognormal distribution and $\Delta\gamma = 2\gamma_{mf} \sinh(w)$ which is the $\frac{1}{e}$ width of the lognormal distribution.

A typical fit for two different radii of nanowires is shown in fig. 7.6. The residuals for most curves are equally distributed around 0 as shown for the $r = 23$ nm sample. In general a goodness of fit χ^2_{red} around 1.6 is found, indicating a reasonably good fit. An exception is the sample with average radius $r = 38$ nm where the lognormal distribution of decay rates does not fit as good, confirmed by a χ^2_{red} near 4. Here, the least squares fitting routine preferentially fits the high intensity part of the curve while the long time tail is not well fit by this curve. We will discuss below a possible reason why this behaves anomalously.

7.3. Discussion

7.3.1. Effect of changing the radius of the nanowires

In fig. 7.7 the most frequent decay rate from our experiment is plotted versus the sample radius for the two different sizes of quantum dots CdSe1 and CdSe2. A clear increase in most frequent decay rate is observed with increasing nanowire radius. It is striking that both the quantum dot types CdSe1 and CdSe2 show not only the same trend but also the same absolute values of the most frequent decay rate. The latter observation is a coincidence since these quantum dots have a different size and should not necessarily have the same decay rate [20].

In the simplest interpretation our measurements correspond to a situation where a CdSe quantum dot is attached to one single GaP nanowire. The quantum dot will always be connected to a nanowire or the substrate in the experiment since the solvent is evaporated. Even if there is only one nanowire, a different LDOS is expected depending on the dipole orientation and the radius of the nanowire [21]. Therefore we have calculated the LDOS of an emitter connected to an infinitely long nanowire. We have modeled the GaP with $\epsilon = 11.26$. The LDOS is normalised to one in vacuum. We have used the same cylindrical conventions for directions as Klimov and Ducloy [21] as shown in fig. 7.8. Depending on the dipole orientation, strongly different decay rates are found, as shown in fig. 7.7. For emitters with a dipole moment pointing radially outward from the

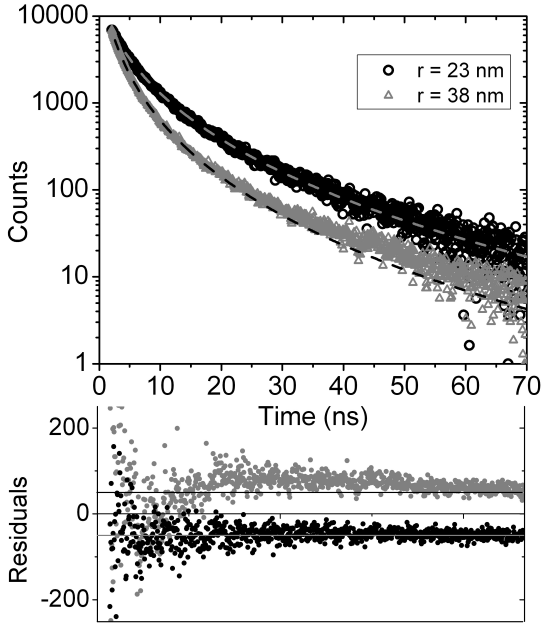

Figure 7.6.: The decay curve is shown for quantum dots in samples with two different average radii of the nanowires. The dashed lines indicate the lognormal models with $\gamma_{mf} = 0.198$ and $\Delta\gamma = 0.666$ for $r = 29$ nm and $\gamma_{mf} = 0.476$ and $\Delta\gamma = 2.01$ for $r = 38$. In the bottom panel the residuals are shown. The residuals are offset by -50 and +50 for clarity.

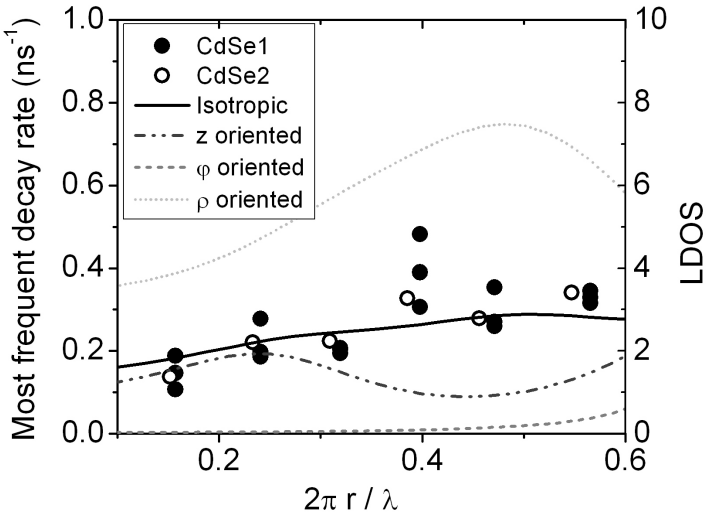

Figure 7.7.: On the left axis the most frequent decay rate for CdSe1 and CdSe2 quantum dots is plotted versus the average radius of the nanowires normalised to the wavelength. On the right axis the calculated LDOS is shown for an emitter with different dipole orientations versus the normalised radius of the nanowire. The black solid line shows the isotropic LDOS, the LDOS averaged over all dipole orientations.

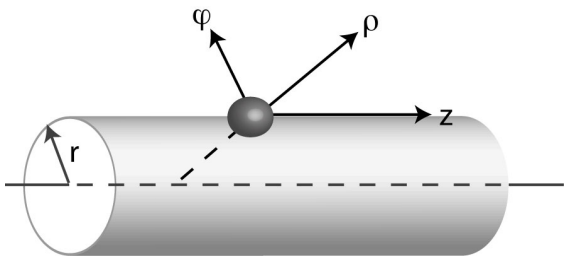

Figure 7.8.: Conventions used for the calculation of the LDOS on the surface of a nanowire.

nanowire a strongly increased LDOS is found, peaking at an LDOS of 8 times that in vacuum. Emitters with a dipole parallel to the nanowire have an LDOS that varies between 1 and 2 times the vacuum value. The lowest decay rate is found for emitters with a dipole moment oriented in the ϕ direction. Here the LDOS can be as low as 0.03 times the LDOS in vacuum. Since we perform experiments on ensembles of quantum dots that each have a random dipole orientation, it is reasonable to assume that the most frequent decay rate shows the same trend as the isotropic LDOS, which is the average of the three orientations. See appendix C for more details. Since the light exiting the sample is diffuse in nature, there is no longer a relation between the emission direction and the detection angle, making sure that the emission pattern does not affect the ensemble. Indeed the isotropic LDOS follows our data points very well.

7.3.2. Width of the distribution

It has been predicted that when the degree of multiple scattering increases and the mean free path becomes smaller, the spatial variations in the local density of states will increase [22]. These variations have recently been linked to C_0 correlations [8]. With our ensemble of emitters in between the GaP nanowires we probe the spatial distribution of the local density of states directly, where we probe a certain subset of the local density of states since the quantum dots have to be attached to either a nanowire or the substrate. It is expected that the distribution in radiative decay rates increases with the inverse of the mean free path for an infinite medium with Gaussian white noise [22]. This Gaussian white noise is an assumption where the scatterers are modeled by point scatterers. Since the nanowires are larger than the wavelength, this approximation is not valid for nanowires.

Mirlin [22] has predicted that the probability distribution $P(\rho)$ of the LDOS in a 3D multiple scattering sample has the following shape:

$$P(\rho) \sim \exp(-constant\ l\ \ |\ ln^3 \rho\ |) \tag{7.3}$$

where l is the mean free path of the sample and ρ is the normalized LDOS. Therefore, the stronger the sample scatters light, the smaller the mean free path

is, hence the narrower is this distribution. The shape of this distribution is very similar to the lognormal distribution that has been used to fit the decay curves. In fact the distribution 7.3 fits the decay curves just as well as the lognormal distribution. We have still used the lognormal distribution because the first and second moments of the lognormal distribution are known analytically while this is not the case for the distribution suggested by Mirlin. The distribution calculated by Mirlin is again for white Gaussian noise typical of point scatterers. Since the distribution in local density of states is known to strongly depend on the size and shape of the scatterers [23] the distribution found in our experiment on nanowires may have a different shape.

In the paper by Van Tiggelen en Skipetrov [8] it is stated that for Gaussian white noise the following linear relation should hold between the variance of the LDOS distribution and the photonic strength given by the inverse mean free path:

$$\frac{Var[\rho(r)]}{\langle\rho(r)\rangle^2} \approx \frac{\pi}{kl} \tag{7.4}$$

In fig. 7.9 we have plotted the normalised variance of the decay rate distribution $\frac{var(\sigma)}{<\gamma>^2}$ versus $\frac{\pi}{kl}$. This normalised variance is equal to $(\exp(\frac{w^2}{2}) - 1)$ for the lognormal distribution of decay rates. It is seen that the normalised variance remains constant, independent of scattering strength. Therefore, no effect of the mean free path is apparent on the normalised variance of the decay rate distribution, in contrast to the linear relation as expected for point scatterers[8]. It was shown in reference [11] that for spherical scatterers the normalised variance is linear with $\frac{1}{kl}$ but with a slope that is 20 times smaller than π. The difference between the experiment of reference [11] and our experiment is that Birowosuto *et al.* obtained an unweighted distribution of emission rates for single nanosphere emitters. In contrast, our modeling of decay curves with a (lognormal) distribution is weighted with the decay rate, as explained by reference [19] and seen in equation 7.2. Indeed, Birowosuto *et al.* also observed non exponential decay, whose lognormal width was much broader than the multiple scattering width, consistent with our results.

An alternative hypothesis for the width of the decay rate distribution is that the ensemble of quantum dots is distributed randomly in orientation and position on the surface of each wire. Therefore we have calculated the distribution of decay rates for quantum dots attached to one infinitely long nanowire. More details can be found in appendix C. The 2D dipole plane of CdSe quantum dots [24, 25] is taken into account to calculate this distribution. The normalised variance as a function of radius r is plotted in fig. 7.9. The normalised variance expected from the variation in LDOS is of order 0.075. This variance is much smaller than would naively be expected from the variation of γ with orientation (see fig. 7.7). The reason is that the quantum dot 2D dipole moment strongly limits the extreme values of the distribution (see appendix C). At any rate this variance is much smaller than the value of 1.25 found in experiment.

The calculations in appendix C also shed light on why in particular the sample with $r = 38$ nm is not modeled very well by the lognormal distribution of

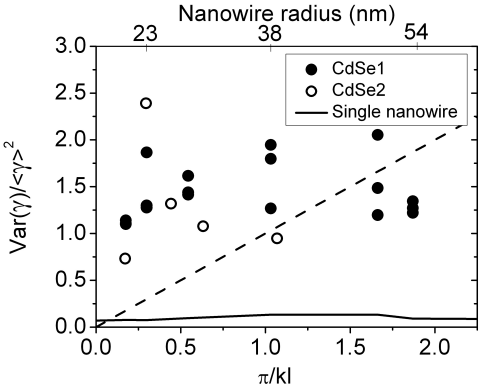

Figure 7.9.: The normalised variance versus $\frac{\pi}{kl}$. The dashed line indicates the expected relation (equation 7.4). The solid line shows the normalised variance expected for emitters on a single nanowire as a function of nanowire radius. Note that the radius axis is not linear.

decay rates. The calculated distribution is strongly asymmetrical, making the lognormal less likely to be a good model.

The fact that the samples are birefringent only contributes marginally to the distribution of decay rates that is measured, to a maximum of about 10 % for the samples studied. More details can be found in appendix D. Therefore, the birefringence can not explain the increase in normalised varience.

Moreover, a small variation in radiative decay rates can be expected because of a distribution in radii of the nanowires in each sample. Since the standard deviation of the radius per sample is approximately 15 % and there are no strong resonances in the LDOS near a nanowire, this variation in radius can not cause a large increase in the normalised variance.

Next to the distribution in radiative decay rates there might also be a variation of nonradiative decay rates present in our experiment, which broadens the resulting distribution. It is expected that this variation in nonradiative rate is not dependent on radius or mean free path, in accordance with our data. However, a low quantum efficiency of the dots would be very surprising, also in view of earlier experiments of such dots in inverse opal photonic crystals, where the efficiency remained elevated [18].

7.4. Conclusions

We have measured the time resolved emission of CdSe quantum dots from inside ensembles of strongly scattering gallium phosphide nanowires. The decay rate is modified substantially by the nanowire surroundings. The observed change in most frequent decay rate is attributed to the effect of a single nanowire scatterer on the emission of the quantum dots. The normalised variance of the distribution does not change with scattering strength, at variance with the prediction

of multiple light scattering theory. We have examined hypotheses concerning the distribution caused by different dipole orientations near a single nanowire, birefringence and size distribution, but we have not yet found a hypothesis that explains the width of the distribution.

References

[1] R. Sprik, B. A. van Tiggelen, and A. Lagendijk, *Optical emission in periodic dielectrics*, Europhys. Lett. **35**, 265 (1996).

[2] L. Novotny and B. Hecht, *Principles of nano-optics* (Cambridge University Press, Cambridge, 2006).

[3] E. Yablonovitch, *Inhibited spontaneous emission in solid-state physics and electronics*, Phys. Rev. Lett. **58**, 2059 (1987).

[4] P. Lodahl, A. F. van Driel, I. S. Nikolaev, A. Irman, K. Overgaag, D. Vanmaekelbergh, and W. L. Vos, *Controlling the dynamics of spontaneous emission from quantum dots by photonic crystals*, Nature **430**, 654 (2004).

[5] P. W. Anderson, *Absence of diffusion in certain random lattices*, Phys. Rev. **109**, 1492 (1958).

[6] D. S. Wiersma, P. Bartolini, A. Lagendijk, and R. Righini, *Anderson localization of light*, Nature **390**, 671 (1997).

[7] A. D. Mirlin, *Statistics of energy levels and eigenfunctions in disordered systems*, Phys. Rep. **326**, 259 (2000).

[8] B. A. Van Tiggelen and S. E. Skipetrov, *Fluctuations of local denisty of states and c_0 speckle correlations are equal*, Phys. Rev. E **73**, 045601 (2006).

[9] L. S. Froufe-Pérez, R. Carminati, and J. J. Sáenz, *Fluorescence decay rate statistics of a single molecule in a disordered cluster of nanoparticles*, Phys. Rev. A **76**, 013835 (2007).

[10] P. V. Ruijgrok, R. Wüest, A. A. Rebane, A. Renn, and V. Sandoghdar, *Spontaneous emission of a nanoscopic emitter in a strongly scattering disordered medium*, Opt. Expr. **18**, 6360 (2010).

[11] M. D. Birowosuto, S. E. Skipetrov, W. L. Vos, and A. P. Mosk, *Observation of spatial fluctuations of the local density of states in random media*, Phys. Rev. Lett. **105**, 013904 (2010).

[12] O. L. Muskens, S. L. Diedenhofen, M. H. M. Van Weert, M. T. Borgström, E. P. A. M. Bakkers, and J. Gómez Rivas, *Epitaxial growth of aligned semiconductor nanowire metamaterials for photonic applications*, Adv. Funct. Mater. **18**, 1039 (2008).

[13] O. L. Muskens, M. T. Borgström, E. P. A. M. Bakkers, and J. Gómez Rivas, *Giant optical birefringence in ensembles of semiconductor nanowires*, Appl. Phys. Lett. **89**, 233117 (2006).

[14] O. L. Muskens, S. L. Diedenhofen, B. C. Kaas, R. E. Algra, E. P. A. M. Bakkers, J. Gómez Rivas, and A. Lagendijk, *Large photonic strength of highly tunable resonant nanowire materials*, Nano Lett. **9**, 930 (2009).

[15] V. O. O'Connor and D. Philips, *Time correlated single photon counting* (1984).

[16] I. Nikolaev, P. Lodahl, and W. Vos, *Quantitative analysis of directional spontaneous emission spectra from light sources in photonic crystals*, Phys. Rev. A **71**, 053813 (2005).

[17] M. Born and E. Wolf, *Principles of optics* (Cambridge University Press, 1999).

[18] I. S. Nikolaev, P. Lodahl, A. F. van Driel, A. F. Koenderink, and W. L.

Vos, *Strongly nonexponential time-resolved fluorescence of quantum-dot ensembles in three-dimensional photonic crystals*, Phys. Rev. B **75**, 115302 (2007).

[19] A. F. van Driel, I. S. Nikolaev, P. Vergeer, P. Lodahl, D. Vanmaekelbergh, and W. L. Vos, *Statistical analysis of time-resolved emission from ensembles of semiconductor quantum dots: Interpretation of exponential decay models*, Phys. Rev. B. **75**, 035329 (2007).

[20] M. D. Leistikow, J. Johansen, A. J. Kettelarij, P. Lodahl, and W. L. Vos, *Size-dependent oscillator strength and quantum efficiency of CdSe quantum dots controlled via the local density of states*, Phys. Rev. B **79**, 045301 (2009).

[21] V. V. Klimov and M. Ducloy, *Spontaneous emission rate of an excited atom placed near a nanofiber*, Phys. Rev. A **69**, 013812 (2004).

[22] A. D. Mirlin, *Distribution of local density of states in disordered metallic samples: Logarithmically normal asymptotics*, Phys. Rev. B **53**, 1186 (1996).

[23] S. E. Skipetrov and R. Maynard, *Nonuniversal correlations in multiple scattering*, Phys. Rev. B. **62**, 886 (2000).

[24] S. A. Empedocles, R. Neuhauser, and M. G. Bawendi, *Three-dimensional orientation measurements of symmetric single chromophores using polarization microscopy*, Nature **399**, 126 (1999).

[25] A. L. Efros, *Luminescence polarization of cdse microcrystals*, Phys. Rev. B. **46**, 7448 (1992).

Chapter 8
Summary and outlook

In this thesis experimental results are presented that show that we can control the process of spontaneous emission by placing the emitter close to a nanostructure. We have investigated spontaneous emission near interfaces, in 2D and 3D photonic crystals and near random arrays of nanowires.

We have shown that the analytically known local density of states close to a silver mirror can be used as a tool to determine the emission properties of emitters. Using the position dependence of the LDOS, we found that the quantum efficiency of the technologically important CdSe quantum dot is close to 80 %. The non-radiative rate is strongly size dependent. Larger quantum dots typically have a lower non-radiative contribution to their decay. The transition dipole moment is hardly size dependent and was found on the order of 0.7, much lower than expected from calculations.

The dipole orientation dependence of the local density of states plays a significant role close to the experimentally very easily accessible interface between glass and air. More than a factor of two difference is found in LDOS for dipoles oriented parallel and perpendicular 10 nanometer from the interface. When investigating ensembles of emitters that have a random dipole orientation, a multi-exponential decay curve is measured. When the interface close to the emitters is removed a single exponential decay is found. By only taking into account the difference in LDOS between parallel and perpendicularly oriented dipoles the decay curve can be modeled very precisely without any adjustable parameters.

The ultimate control over spontaneous emission can be achieved in a photonic crystal where the photonic band gap overlaps in frequency with the emission spectrum of the emitter. Theoretically the LDOS is zero inside an infinite photonic crystal, leaving the emitter forever in its excited state. We have systematically studied the decay of PbS quantum dots at different emission energies in four crystals with different filling fraction. We have showed that in a real and finite Si 3D inverse woodpile photonic crystal the decay is strongly inhibited up to 11 times inside the frequency range of the photonic band gap. This figure is even more impressive when considering that the quantum dots have a distribution of positions and orientations and the experiments were performed at room temperature. Therefore future experiments on single sources and at low temperatures will undoubtedly yield much greater inhibitions.

Although inhibition up to 11 times is very exciting, it is not proof of the existence of a band gap, a region with truly zero density of states. Since experiments will always be performed on finite photonic crystals, the density of states will not be zero. However, in a photonic band gap frequency region the LDOS should scale exponentially with the crystal size. Future experiments will examine the role of crystal size on the decay rate of emitters inside such a crystal. Inhibition

of spontaneous emission does not only change the decay curve of the emitter, but can also influence the excitation rate as discussed in appendix B. Signs of a photonic band gap might also be experimentally accessible by measuring saturation of the emitted intensity as a function of excitation power. This type of measurement has not been explored to the best of our knowledge. Our analysis was performed for two level systems that do not show lasing. If a different type of emitter is used that does show lasing, the lack of spontaneous emission inside the band gap of a photonic crystal leads to the long-heralded thresholdless laser.

Two dimensional photonic crystals are more easily fabricated than their 3D counterpart but can still interact strongly with light. By placing PbS quantum dots inside 2D centered rectangular macroporous silicon photonic crystals we show that the light is strongly redirected inside the photonic crystal. No modification of the decay rate is seen, as expected from density of states calculations. The observed peaks in the emitted intensity are attributed to the edge of stopgaps in the band structure, indicating that these effects might be caused by interaction with 2D Van Hove singularities. At Van Hove singularities fractional decay is expected to be observed. To convincingly show this fractional decay experiments have to be performed with single emitters. This is not feasible with the current experimental scheme due to the low signal to noise ratio in the near infrared wavelength range. Both improving the detector to have a lower noise count rate and changing the emitter to a type that has a higher decay rate might make these experiments attainable in the future.

Finally CdSe quantum dots are placed inside strongly scattering ensembles of gallium phosphide nanowires to investigate the effect of disorder on the decay dynamics. We find that increasing the radius of the nanowires increases the most frequent decay rate found in the experiment. This increase can be explained by modeling the local density of states modification by a single nanowire on the emitter. No effect of the mean free path on the relative width of the distribution of decay rates is seen. The influence of the mean free path is most likely averaged out because of the ensemble average in our measurements. Future experiments should focus on measuring single emitters inside strongly scattering structures.

Appendix A
Inhomogeneous versus homogeneous linewidth of PbS quantum dots by fluorescence line narrowing

The measured spectral linewidth in the emission of quantum dots has two contributions: A homogeneous and an inhomogeneous part [1]. The homogeneous linewidth is the typical linewidth of a single emitter while inhomogeneous broadening is for instance caused by the fact that the measurement is performed over an ensemble of quantum dots with slightly different size. Since the size of the quantum dot determines the emission energy a distribution in sizes leads to an inhomogeneously broadened spectrum.

Knowledge of the homogeneous linewidth is important for interpretation of decay curve measurements. The decay rate of an emitter depends on the local density of states. In an experiment, the local density of states is averaged over the homogeneous linewidth of the emitter. Features in the local density of states on a scale comparable to the homogeneous linewidth are therefore difficult to detect.

For widely used quantum dots like CdSe it is well known that most of the spectral linewidth is caused by inhomogeneous broadening of the ensemble since the homogeneous linewidth of a single quantum dot is much narrower [2]. For PbS quantum dots single quantum dot emission has been measured [3], however, this measurement was performed for relatively small quantum dots that emit near 800 nm where a Si detector can be used. For the near infrared emitting quantum dots we use in the telecom range around 1500 nm, the noise levels of detectors are an order of magnitude larger than for the visible range making the investigation of single emitters extremely hard. Thus the contributions of the homogeneous and imhomogeneous broadening are presently not known.

In this appendix fluorescence line narrowing of the PbS emission of ensembles of quantum dots around 0.84 eV (1475 nm) is presented. By scanning the energy of the excitation light through the emission spectrum, the linewidth decreases by a factor of two, showing that the homogeneous linewidth is maximum 44 meV.

A.1. Experimental

A sketch of the experimental set-up is shown in fig. A.1. A supercontinuum white light source (Fianium) is used to excite the quantum dots. The white light

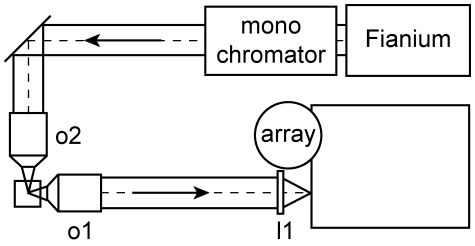

Figure A.1.: Schematic of the experimental setup to measure near infrared emission.

is sent through a grating monochromator to select a certain bandwidth of light. The spectral width is approximately 0.015 eV (5 nm) FWHM. By rotating the grating, a different center energy between 0.6 to 3.1 eV (400 to 2100 nm) can be chosen as excitation light. The excitation light is focused inside the suspension of quantum dots using an objective with NA=0.05 (o2). The detection objective (o1) with NA=0.7 is placed under an angle of 90 ° with respect to the excitation objective to prevent direct reflection of excitation light into the detector. Since the excitation light has the same wavelength as the emission light, it is not possible to block the excitation light with a filter. The amount of scattered excitation light even under the 90 ° angle is substantial. The emission light is passed through a grating monochromator and imaged onto an liquid nitrogen cooled InGaAs diode array. For the measurement a suspension of quantum dots is used with a concentration of $4{\cdot}10^{-6}$ M PbS-1500 quantum dots (Evident) in toluene.

A.2. Results

The measured emission spectra are shown in fig. A.2. The excitation band seems much broader than 0.015 eV because the detector is strongly saturated at the excitation energy, giving overflow to the surrounding pixels. An energy band of 0.033 eV has been blocked in the emission spectra. It is clearly seen that the emission spectrum narrows when the quantum dots are excited at lower energy. The emission spectrum excited at 1.167 eV is a reference spectrum where the excitation energy does not overlap with the emission spectrum. There the center energy is 0.845 eV with a full width at half maximum (FWHM) linewidth of 0.086 eV.

To analyse the data the emission spectra were modeled with a Gaussian. This is shown in fig. A.2 with the black curves. The result of this fit is shown in fig. A.3. Here both the center emission energy and the FWHM are shown as a function of excitation energy. With decreasing excitation energy, the emission peak shifts linearly to lower energy from 0.872 to 0.811 eV. A decreasing emission energy is expected for inhomogeneously broadened emitters, since the quantum dots emitting at the blue edge of the emission peak are no longer excited. The

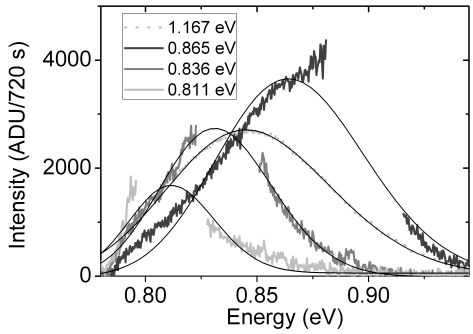

Figure A.2.: The emission spectra of PbS quantum dots are shown when excited at different energies. The solid black lines show a Gaussian model of the data.

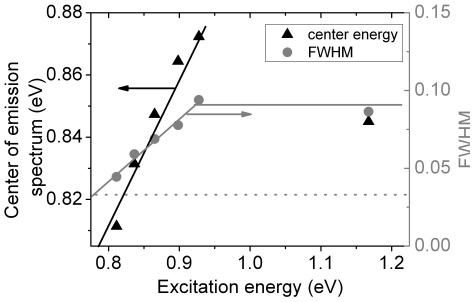

Figure A.3.: The result of the Gaussian fits are shown. In the left ordinate the center energy is plotted, on the right axis the FWHM is shown. The dashed line indicates the width of the excitation band in the measurement.

FWHM decreases linearly from 0.086 eV to 0.044 eV with decreasing excitation energy. Since the broadened excitation line from the white light source influences the measured spectrum over an energy range larger than 0.033 eV the actual linewidth could be smaller. Thus our measurements give an upper bound. A unexpected result in fig. A.3 is that the peak of emission is higher when the excitation energy is at the blue edge of the emission than when looking at the reference spectrum excited with an energy far away from the emission spectrum. We do not currently have an explanation for this shift.

A.3. Conclusion

We have performed a fluorescence line narrowing experiment on PbS quantum dots in suspension. We measure that the linewidth decreases from 0.086 to 0.044 eV when scanning the excitation wavelength over the emission spectrum. From

this we conclude that the homogeneous linewidth of PbS quantum dots emitting around 0.84 eV is at most 0.044 eV, indicating that about half of the linewidth is caused by homogeneous broadening.

References

[1] A. E. Siegman, *Lasers* (University Science Books, 1986).
[2] S. A. Empedocles, D. J. Norris, and M. G. Bawendi, *Photoluminescence spectroscopy of single cdse nanocrystallite quantum dots*, Phys. Rev. Lett. **77**, 3873 (1996).
[3] J. J. Peterson and T. D. Krauss, *Fluorescence spectroscopy of single lead sulfide quantum dots*, Nano Lett. **6**, 510 (2006).

Appendix B
Can (L)DOS change the emitted intensity?

The decay rate that is measured in experiments is the total decay rate γ_{tot} which consists of a radiative and a non-radiative part:

$$\gamma_{tot} = \gamma_{rad} + \gamma_{nrad} \tag{B.1}$$

In the radiative process energy is lost through emission of a photon. Energy can also be lost non-radiatively, for example by generating phonons. The quantum efficiency (QE) η of an emitter, given by

$$\eta = \frac{\gamma_{rad}}{\gamma_{tot}} \tag{B.2}$$

gives the fraction of excitation energy that is transferred to spontaneous emission. Depending on the value of the QE the (local) density of states will have a different effect on the emission [1–3].

If the QE is 100 % all the absorbed energy is converted in light and $\gamma_{tot} = \gamma_{rad}$. Since the local density of states only affects the radiative decay rate, modification of the measured total decay rate will be proportional to the LDOS change.

If the QE is very low, say 1 %, $\gamma_{tot} \approx \gamma_{nrad}$. In this situation modifying the density of states hardly affects the measured total decay rate.

In literature a change in the emitted spectrum of emitters in a photonic crystal is often attributed to a modified local density of states [4–7], even for very low contrast photonic structures. However, there are different processes that influence the emitted intensity beside the (L)DOS. Changes in the emission spectrum do not necessarily have to be caused by the (L)DOS of the photonic crystal. In this appendix it is explained which processes influence the emitted intensity, and what the role of the quantum efficiency is on the emitted intensity.

B.1. From excitation photon to emitted photon

In fig. B.1 the processes that are involved with converting excitation to emission photons in a photonic structure are shown. The emission process is modeled as a quasi two-level process, where the excitation energy is higher than the emission energy. The relaxation to the emission upper level from the excitation upper level is assumed to be a very fast process. For quantum dots this model is applicable, since this decay is much faster than the spontaneous decay rate. Generally the non-radiative decay from excitation to emission upper level has picosecond timescales while the emission process is typically on 500 ns timescales.

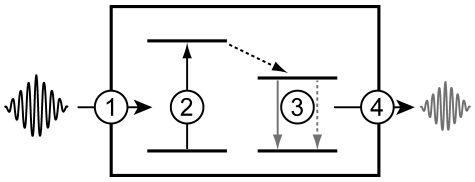

Figure B.1.: Schematic diagram of the excitation and emission process.

Starting from the excitation photon on the left, there are 4 aspects that influence the number of emitted photons. First the excitation photon needs to enter the photonic crystal (indicated by the square). This process is influenced by the photonic crystal if the photonic crystal has spectral features near the excitation energy. Since in our experiments the quantum dots are excited with the same laser line, this step will not influence the measured emission spectra.

Secondly the excitation photons have to be absorbed by an emitter. The a chance that the excitation photon is absorbed depends on several experimental conditions like the absorbtion cross section, the concentration and the level of saturation of the emitters.

In the third step the excitation energy is lost from the emission upper level by either emitting a photon (radiative decay) or by another loss process (non-radiative decay). The radiative process is proportional to the local density of states and depends of frequency, position, and dipole orientation of the emitter with respect to the photonic structure.

Finally the emitted photon needs to exit the photonic crystal to be detected. There will be a far field distribution of the emission, that might be influenced by two different contributions. The first contribution is the emission pattern of each individual dipole. The doughnut shaped emission pattern of a dipole in vacuum is strongly influenced by higher refractive index media in the near field of the emitter. Even for a simple interface, this emission pattern is strongly modified (see, e.g., chapter 3). For a photonic crystal environment the dipole pattern will be more complicated [8]. The other contribution to the distribution of emission comes from multiple scattering. When the photon does not exit the structure ballistically but is multiply scattered before it leaves the structure, the redistribution is known to be affected by the band structure of the photonic crystal [9].

B.2. What happens to the emitted intensity?

The absorption and emission process (step 2 and 3 in fig. B.1) of spontaneous emission can be described by using rate equations to describe the population of the emission excited state level N_2

$$\frac{dN_2}{dt} = P - \gamma_{tot} N_2 \tag{B.3}$$

We consider a quasi two-level system that is pumped at a constant rate P. In

steady state, the time derivative is zero and $N_2 = P/\gamma_{tot}$. The number of emitted photons per unit time is equal to $I = \eta\gamma_{tot}N_2 = \eta P = P\gamma_{rad}/\gamma_{tot}$.

When η=1 the emitted intensity is not dependent on the radiative rate and therefore LDOS, because I = P. Since every excitation quantum is converted to an emitted photon the emitted number of photons is only dependent on the number of excitation quanta.

When η is very low $\gamma_{tot} \approx \gamma_{nrad}$. This results in the situation where the emitted intensity is directly proportional to the radiative decay rate γ_{rad} and therefore (L)DOS.

B.3. (L)DOS modification

The radiative decay rate is directly proportional to the LDOS, as is described by Fermi's Golden Rule. The LDOS is dependent on frequency ω, the position $\mathbf{r}$ of the emitter and the orientation of its dipole moment $\hat{d}$. As a consequence the quantum efficiency η will also in general be dependent on ω, $\mathbf{r}$ and $\hat{d}$. By modifying the LDOS, η is changed. This change is discussed in this section.

The quantum efficiency of a certain emitter for a particular value of the (L)DOS is often known and will be called η_{hom}. It is assumed here that this value holds for (L)DOS is 1 (but the analysis in general still holds if this value is not equal to unity). Here, the radiative decay rate will be set proportional to DOS(ω) in stead of LDOS for convenience: $\gamma_{rad}(\omega) = A\ DOS(\omega)$. The nonradiative decay rate is assumed to be independent of frequency and constant.

$$\eta(\omega) = \frac{A\ DOS(\omega)}{A\ DOS(\omega) + \gamma_{nrad}} \tag{B.4}$$

When $\gamma_{nrad} = 0$, η is again equal to unity independent of frequency. A can be determined for $\eta_{hom} < 1$, since for DOS = 1, $\eta = \eta_{hom}$.

$$A = \frac{\gamma_{nrad}\eta_{hom}}{1 - \eta_{hom}} \tag{B.5}$$

$$\eta(\omega) = \frac{\frac{\gamma_{nrad}\eta_{hom}}{1-\eta_{hom}} DOS(\omega)}{\frac{\gamma_{nrad}\eta_{hom}}{1-\eta_{hom}} DOS(\omega) + \gamma_{nrad}} = \frac{\eta_{hom} DOS(\omega)}{\eta_{hom} DOS(\omega) - \eta_{hom} + 1} \tag{B.6}$$

It should be emphasized that for these equations to hold, a constant excitation rate P is assumed. This only holds for situations where the total decay rate is larger than the absorption rate per emitter. When this is not the case, the emitters will saturate, no longer absorbing excitation quanta. When DOS=0 and η=1 this situation automatically occurs. Hence saturation measurements are a particularly sensitive probe in the vicinity of a photonic band gap.

The above analysis only holds for emitters where the homogeneous line width is much narrower than any spectral features in the (L)DOS. This is generally the case for quantum dots inside photonic crystals.

When η is not unity but still non negligible the situation can now be calculated when the DOS is known as a function of frequency. The next section will show a few examples.

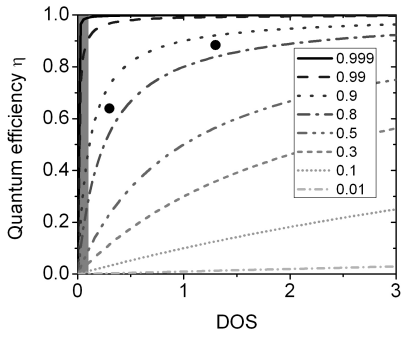

Figure B.2.: The quantum efficiency is plotted as a function of DOS for different values of η_{hom}.

B.4. Examples for different values of η_{hom}

In fig. B.2 the quantum efficiency η is plotted as a function of DOS (equation B.6). The emitted intensity is proportional to η for a constant pump rate P. If the DOS is too low, equation B.6 no longer holds since the pump rate is no longer constant. This region is indicated with the grey bar, using an upper level of DOS=0.1 which is more or less arbitrarily chosen. In reality the boundary of DOS may depend on η_{hom}, since time scales for radiative and non-radiative decay can be different.

When the homogeneous quantum efficiency $\eta_{hom} = 0.999$, modification of the DOS hardly changes η. However even for large quantum efficiency the quantum efficiency and emitted intensity can be strongly modified by the DOS. This is a surprising result in view of the prior expectations from ref. [2]. For very low quantum efficiency (for instance $\eta = 0.1$) the quantum efficiency is almost linear with DOS.

Two data points are added in fig. B.2 that are taken from the emission spectrum of a 3D photonic crystal (see fig. 5.6 c). We observed values for the average intensity at the low frequency side where the DOS is 1.3 and in the band gap, where the DOS value for the lower intensity was estimated to be 0.3, or $\frac{1}{5}$ of the higher level DOS, as shown. These measurements imply that the quantum efficiency of our quantum dots is between 80 and 90 %, which is nicely high.

In fig. B.3 the measured total decay rate is shown as a function of DOS. The decay rate measurements that show inhibition in the band gap are left out since we do not know the DOS for these measurements. Clearly the total decay rate is linear with DOS. The line is a linear fit to the data, giving a quantum efficiency of approximately 54 $\pm$ 30 %. The error margin is determined from the standard error of the linear fit.

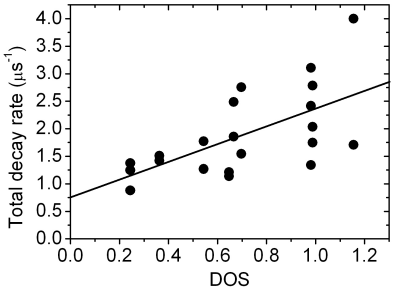

Figure B.3.: The total decay rate vs the DOS is shown. The line is a linear fit of the data, giving $\gamma_{rad} = 0.9 \pm 0.5 \mu s^{-1}$ and $\gamma_{nrad} = 0.8 \pm 0.4 \mu s^{-1}$

B.5. Conclusion

For situations where the quantum efficiency is not unity or very small, the emitted intensity is calculated. Even for $\eta_{hom} = 0.99$ an effect of a low DOS can be seen on the emitted intensity. We have not taken into account redistribution of light in our analysis. We derive that the QE of our PbS quantum dots to be about 80 %, much higher than specified by the manufacturer.

References

[1] A. F. Koenderink, *Emission and transport of light in photonic crystals*, Ph.D. thesis, University of Amsterdam, 2003.

[2] A. F. Koenderink, L. Bechger, H. P. Schriemer, A. Lagendijk, and W. L. Vos, *Broadband fivefold reduction of vacuum fluctuations probed by dyes in photonic crystals*, Phys. Rev. Lett. **88**, 143903 (2002).

[3] A. F. Koenderink, L. Bechger, A. Lagendijk, and W. L. Vos, *An experimental study of strongly modified emission in inverse opal photonic crystals*, Phys. Stat. Solidi A **197**, 648 (2003).

[4] S. V. Gaponenko, A. M. Kapitonov, V. N. Bogomolov, A. V. Prokofiev, A. Eychmüller, and A. L. Rogach, *Electrons and photons in mesoscopic structures: Quantum dots in a photonic crystal*, JETP Lett. **68**, 142 (1998).

[5] K. Yoshino, S. B. Lee, S. Tatsuhara, Y. Kawagishi, M. Ozaki, and A. A. Zakhidov, *Observation of inhibited spontaneous emission and stimulated emission of rhodamine 6G in polymer replica of synthetic opal*, Appl. Phys. Lett. **73**, 3506 (1999).

[6] A. Blanco, C. López, R. Mayoral, H. Míguez, F. Meseguer, A. Mifsud, and J. Herrero, *CdS photoluminescence inhibition by a photonic structure*, Appl. Phys. Lett. **73**, 1781 (1998).

[7] S. G. Romanov, T. Maka, C. M. Sotomayor-Torres, M. Müller, and R. Zentel, *Suppression of spontaneous emission in incomplete opaline photonic crystals*, J. Appl. Phys. **91**, 9426 (2002).

[8] D. N. Chigrin, *Radiation pattern of a classical dipole in a photonic crystal: Photon focusing*, Phys. Rev. E **70**, 056611 (2004).

[9] A. F. Koenderink and W. L. Vos, *Light exiting from real photonic band gap crystals is diffuse and strongly directional*, Phys. Rev. Lett. **91**, 213902 (2003).

Appendix C
Comparing ab initio distributions and the lognormal model

In chapter 3 it is discussed that it is possible to calculate the decay curve and decay rate distribution of an ensemble of emitters from *ab initio* in a well defined environment. Very often in experiments a non-exponential decay curve is found. This decay curve is then modeled with an analytical distribution of decay rates, like a lognormal [1] or a gamma [2] distribution. Both functions have the benefit of excluding unphysical negative decay rates. Another choice is the bi-exponential model. However, when all four parameters are adjustable in this fit it is difficult to get reliable results [3]. It remains an open question which values derived from a model are representative of the measurement, especially in the case of non-symmetric distributions such as a lognormal or a gamma distribution.

In this appendix an *ab initio* distribution of decay rates is calculated for an ensemble of CdSe quantum dots near a nanowire and compared with a lognormal model that is used in both chapter 2 and 7 of this thesis. It is shown that the most frequent decay rate γ_{mf} of the lognormal distribution is a good indicator for the mean value of the underlying distribution.

C.1. Decay rate distribution near a nanowire for CdSe quantum dots

In chapter 7 the decay is discussed of emitters near an infinitely long wire that is thin with respect to the wavelength of light. The local density of states (LDOS) near such a wire can be calculated following reference [4]. Since the minimum, the median and the maximum decay rate are known, it is possible to calculate the distribution of radiative decay rates [5]. However, since CdSe quantum dots have a 2D dipole plane or bright plane [6, 7] this has to be taken into account when calculating the distribution of decay rates. The LDOS will be averaged over the bright plane of the quantum dot. Taking into account this averaging, the distribution is now calculated using the same Monte Carlo algorithm discussed in chapter 3. Since for our batch of CdSe quantum dots the quantum efficiency is 80 %(see chapter 2 and [8]) it is possible to calculate the expected total decay rate and expected decay curve.

C.2. Modeling the calculated decay curves with a lognormal distribution of decay rates

To model the calculated decay curve the calculation is fitted with a distribution of decay rates. A function of the following form is used to model the decay curve:

$$f(t) = \int_0^\infty \sigma(\gamma_{tot}) \exp(-\gamma_{tot} t) \mathrm{d}\gamma_{\mathrm{tot}} \tag{C.1}$$

where the normalised distribution of decay rates is chosen to be lognormal

$$\sigma(\gamma) = A \exp\Big[- \Big(\frac{ln(\gamma) - ln(\gamma_{mf})}{w} \Big)^2 \Big] \tag{C.2}$$

The normalisation factor A equals $A = [\gamma_{mf} w \sqrt{\pi} \exp(w^2/4)]^{-1}$. The two relevant independent adjustable parameters that can be extracted from the model are the most frequent decay rate γ_{mf} which is the peak of the lognormal distribution and w. The mean of the distribution is given by $\gamma_\mu = \gamma_{mf} \exp(\frac{3w^2}{4})$ and the normalised variance is given by $\frac{<\gamma^2> - <\gamma>^2}{<\gamma>^2} = \exp(\frac{w^2}{2}) - 1$.

C.3. Results

In fig. C.1 the calculated decay curves are shown for an ensemble of quantum dots with random bright plane orientations near a nanowire for two different radii of nanowire. The dynamic range was chosed as the experimentally accessible range, typically about 3 decades of signal (solid line). The calculated curve is modeled with a lognormal distribution of decay rates (dotted line). For the $r = 23$ nm nanowire the agreement is good. For the $r = 38$ nm nanowire the agreement is less good, especially for longer times.

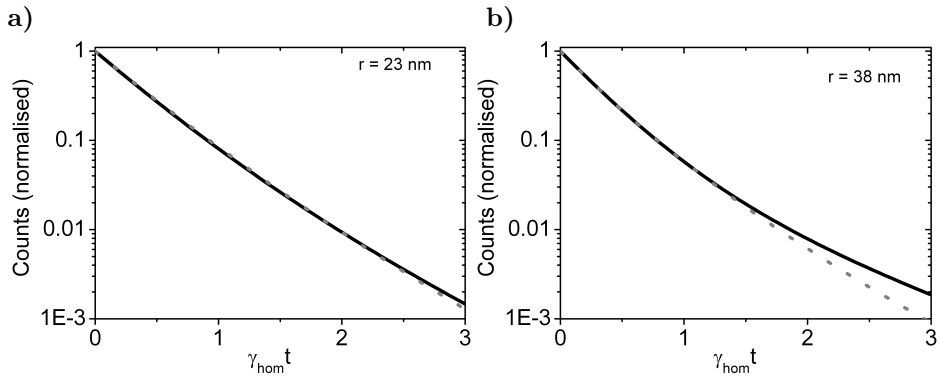

Figure C.1.: The calculated decay curve (solid black line) and a lognormal fit (dotted grey line) for a nanowire of radius $r = 23$ nm and $r = 38$ nm.

In fig. C.2 the calculated distribution of decay rates from the *ab initio* model is plotted. The distribution found for $r = 23$ nm is clearly more symmetrical than the distribution for a nanowire of $r = 38$ nm. The solid lines indicate the lognormal distribution that was extracted from the model of the decay curve in fig. C.1. For $r = 23$ nm the fitted lognormal distribution matches the *ab initio* distribution quite well. However, the contribution of low decay rates is underestimated, while the high decay rate contribution is overestimated. For $r = 38$ nm the *ab initio* distribution and the lognormal distribution do not agree well in shape. Again the low decay rate contribution is underestimated by the lognormal while the high decay rate contribution is overestimated. The arrows in the plot indicate the mean decay rate $< \gamma >$ of the *ab initio* distribution, and the most frequent decay rate γ_{mf} and mean decay rate γ_μ of the lognormal distribution. For both the radii the mean of the *ab initio* distribution agrees better with the most frequent decay rate than with the mean decay rate of the lognormal fit.

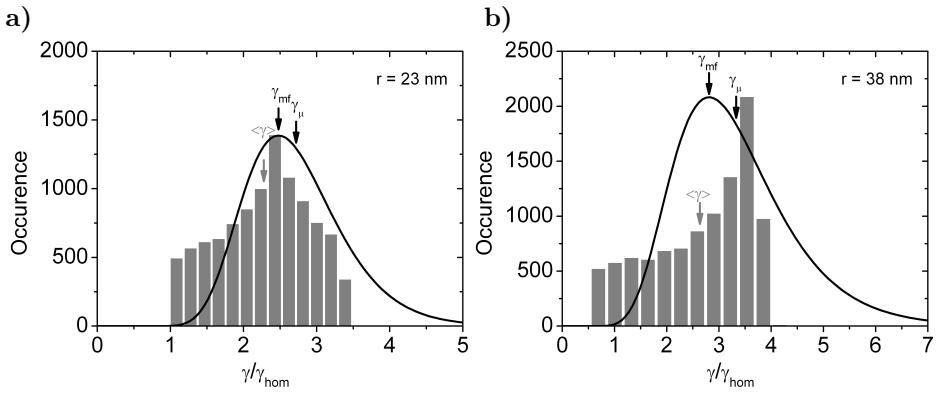

Figure C.2.: The distributions of decay rates are shown with the grey bars for emission near a nanowire with $r = 23$ and 38 nm. The fitted lognormal distribution is shown with the black line. The arrows indicate the mean of the calculated *ab initio* distribution $< \gamma >$, and the most frequent decay rate γ_{mf} and the mean decay rate γ_μ found in the fit.

In fig. C.3 the results for the mean and normalised variance are summarised for different nanowire radii. In fig. C.3 a) the mean decay rate of the *ab initio* distribution $< \gamma >$ is plotted together with the most frequent decay rate γ_{mf} and mean decay rate γ_μ of the lognormal distribution. The mean decay rate of the *ab initio* distribution shows the same trend as the most frequent decay rate of the lognormal distribution, and the value is only slightly overestimated. Especially for the more asymmetric distributions found for radii of 38 and 45 nm, the mean of the lognormal distribution deviates from the mean of the *ab initio* distribution. In fig. C.3 b) the normalised variances for the*ab initio* distribution and for the lognormal distribution are plotted. The trend in the *ab initio* distribution is

followed well by the lognormal distribution, although the absolute value is slightly underestimated.

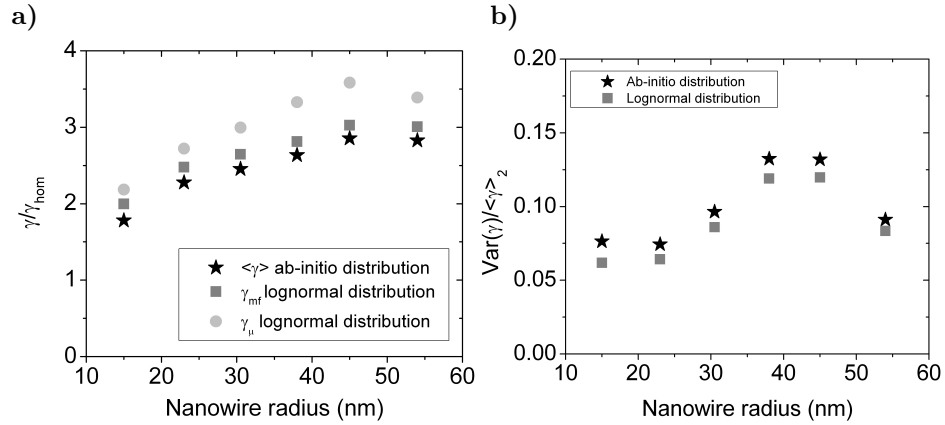

Figure C.3.: a) The mean of the *ab initio* distribution $< \gamma >$, and the most frequent decay rate γ_{mf} and the mean decay rate γ_{μ} of the fitted lognormal distribution for different nanowire radii. b) The normalised variance of the *ab initio* distribution and the lognormal distribution.

C.4. Conclusion

We have seen in case of quantum dots near nanowires that for different distributions the most frequent decay rate γ_{mf} and the normalised variance of a lognormal model are good indicators for the mean and normalised variance of the underlying distributions, even though these distributions have a different shape than lognormal. This validates our choice for the most frequent decay rate γ_{mf} as important parameter to determine the quantum efficiency and dipole moment in chapter 2.

References

[1] A. F. van Driel, I. S. Nikolaev, P. Vergeer, P. Lodahl, D. Vanmaekelbergh, and W. L. Vos, *Statistical analysis of time-resolved emission from ensembles of semiconductor quantum dots: Interpretation of exponential decay models*, Phys. Rev. B. **75**, 035329 (2007).

[2] R. A. L. Vallée, N. Tomczak, L. Kuipers, G. J. Vancso, and N. F. van Hulst, *Single molecule lifetime fluctuations reveal segmental dynamics in polymers*, Phys. Rev. Lett. **91**, 038301 (2003).

[3] J. R. Lakowicz, *Principles of fluorescence spectroscopy* (Kluwer Academic, 1999).

[4] V. V. Klimov and M. Ducloy, *Spontaneous emission rate of an excited atom placed near a nanofiber*, Phys. Rev. A **69**, 013812 (2004).

[5] W. L. Vos, A. F. Koenderink, and I. S. Nikolaev, *Orientation-dependent spontaneous emission rates of a two-level quantum emitter in any nanophotonic environment*, Phys. Rev. A **80**, 053802 (2009).

[6] A. L. Efros, *Luminescence polarization of cdse microcrystals*, Phys. Rev. B. **46**, 7448 (1992).

[7] S. A. Empedocles, R. Neuhauser, and M. G. Bawendi, *Three-dimensional orientation measurements of symmetric single chromophores using polarization microscopy*, **399**, 126 (1999).

[8] M. D. Leistikow, J. Johansen, A. J. Kettelarij, P. Lodahl, and W. L. Vos, *Size-dependent oscillator strength and quantum efficiency of CdSe quantum dots controlled via the local density of states*, Phys. Rev. B **79**, 045301 (2009).

Appendix D
Emission of light in birefringent uniaxial media

This appendix explains how the decay rate of an emitter is affected in a homogeneous, birefringent uniaxial material. Therefore we calculate the local density of states (LDOS) when the refractive index depends on angle. Naively one would expect the decay rate to be proportional to the refractive index in a certain direction. However, since there is an angle integration in the derivation for LDOS, the effect of an angle dependent refractive index will be integrated over angle, reducing the influence of the birefringence on the LDOS. We will find that the effect of birefringence on the decay rate of an emitter is less than 10 %, even for very strong birefringence.

The radiative local density of states is given by the following equation [1]:

$$N(\vec{r},\omega,\hat{e}_d) = \frac{1}{2\pi\epsilon(\vec{r})}\sum_p \int_0^\infty d\vec{k}\delta(\omega-\omega_{\vec{k},p})|\hat{e}_d\cdot\vec{\Lambda}_{k,r}(\vec{r})|^2 \tag{D.1}$$

where

$$\sum_p \int_0^\infty d\vec{k} = 2\int_0^{2\pi} d\phi \int_0^\pi d\theta \sin\theta \int_0^\infty dk\ k^2 \tag{D.2}$$

is a sum over modes $\vec{k}$ and polarisation p, and where $\hat{e}_d$ is the transition dipole moment orientation, $\vec{\Lambda}$ is the electromagnetic mode function and $\omega_{\vec{k},p}$ are the eigenfunctions of the mode. Here, θ is the angle between the emitting dipole and the electromagnetic field.

D.1. Homogeneous medium

In a homogeneous medium without birefringence there is no dependence on place or angle between electric field and dipole moment, and $k = n\omega/c$ which simplifies the integral for the local density of states to

$$N(\omega) = \frac{1}{n^2(2\pi)^3}4\pi\int_0^\infty d\theta\sin\theta\cos\theta^2\frac{n^3}{c^3}\int_0^\infty d\omega_k\delta(\omega-\omega_k)\omega_k^2 \tag{D.3}$$

$$= \frac{n}{2c^3\pi^2}\frac{2}{3}\int_0^\infty d\omega_k\delta(\omega-\omega_k)\omega_k^2 \tag{D.4}$$

$$= \frac{n\omega^2}{3c^3\pi^2} \tag{D.5}$$

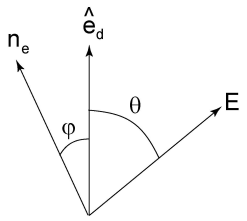

Figure D.1.: Angle definitions

D.2. Birefringent medium

In a birefringent medium the refractive index is angle dependent. For uniaxial media with two directions with an ordinary refractive index and one direction with extraordinary refractive index the following relation holds:

$$n(\alpha) = n_e \cos^2 \alpha + n_o \sin^2 \alpha \tag{D.6}$$

where n_e and n_o are the extraordinary and ordinary refractive indices. In a system where the angle α is a sum of θ and ϕ (see fig. D.1) where θ is again the angle between the dipole and the E field and ϕ is the angle between the dipole and the direction of the extraordinary refractive index, the following expression for the local density of states is found:

$$N(\omega, \phi) = \frac{1}{2\pi^2 c^3} \int_0^\infty d\theta \sin\theta \cos\theta^2 n(\theta + \phi) \int_0^\infty d\omega_k \delta(\omega - \omega_k) \omega_k^2 \tag{D.7}$$

$$= \frac{1}{2\pi^2 c^3} (n_o(\frac{1}{3} + \frac{1}{15}\cos(2\phi)) + n_e(\frac{1}{3} - \frac{1}{15}\cos(2\phi)))\omega^2 \tag{D.8}$$

D.3. Example

The local density of states depends on angle ϕ of the dipole axis with respect to the axis of the extraordinary refractive index. In figure D.2 the expected local density of states is plotted as a function of angle ϕ. We have used values for the ordinary and extraordinary refractive index that are found for ensembles of gallium phosphide nanowires [2]. These are the same sample on which emission experiments are performed as discussed in chapter 7. These nanowire ensembles show strong form birefringence.

The difference in LDOS for different orientations of the dipole with respect to the extraordinary refractive index axis is less than 10 %. For comparison, the difference in refractive indices for calcite, a birefringent natural crystal, is 0.17 which is much smaller than the difference in refractive index for the ensembles of nanowires. Therefore, in naturally birefringent crystals, the effect of the birefringence on spontaneous emission will be even smaller.

This derivation holds specifically for emitters with an axial transition dipole moment. If in stead an emitter is used that has a bright plane with two possible

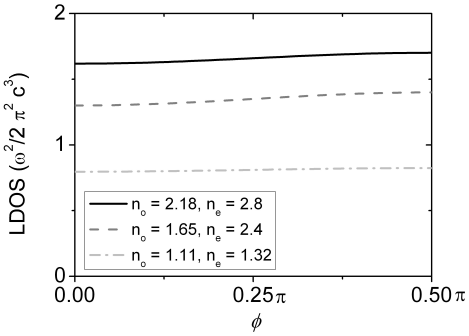

Figure D.2.: Plot of LDOS versus angle ϕ is shown for three different values of the ordinary and extraordinary refractive index.

directions of the dipole like for instance CdSe quantum dots [3, 4], the effect will be even smaller since the decay rate will be averaged over a plane.

In this appendix we assume that the medium in which the emitter is placed can be described as a homogeneous medium. In chapter 7 it is clearly shown that ensembles of nanowires do not form a homogeneous medium on the scale of the emitter. This derivation can therefore not strictly be applied to ensembles of nanowires.

D.4. Conclusion

The local density of states in uniaxial homogeneous media has been calculated. For a medium with a birefringence comparable to ensembles of nanowires, the expected difference in LDOS as a function of dipole orientation is less than 10 %.

References

[1] R. Sprik, B. A. van Tiggelen, and A. Lagendijk, *Optical emission in periodic dielectrics*, Europhys. Lett. **35**, 265 (1996).

[2] O. L. Muskens, M. T. Borgström, E. P. A. M. Bakkers, and J. Gómez Rivas, *Giant optical birefringence in ensembles of semiconductor nanowires*, Appl. Phys. Lett. **89**, 233117 (2006).

[3] S. A. Empedocles, R. Neuhauser, and M. G. Bawendi, *Three-dimensional orientation measurements of symmetric single chromophores using polarization microscopy*, **399**, 126 (1999).

[4] A. L. Efros, *Luminescence polarization of cdse microcrystals*, Phys. Rev. B. **46**, 7448 (1992).

Nederlandse samenvatting

Licht is zo'n belangrijk fenomeen in ons dagelijks leven dat we zelden nadenken hoe dit ontstaat. Vrijwel al het licht om ons heen wordt gemaakt in atomen en moleculen. Zo'n atoom of molecuul heeft een bepaalde grondtoestand met een minimale lage energie. Door bijvoorbeeld dit atoom of molecuul op te warmen, ontstaat een overschot aan energie en kan het atoom of molecuul naar een toestand met hogere energie. Bij terugval naar de grondtoestand kan er licht worden uitgezonden. Het uitzenden van licht gebeurd in pakketjes, die fotonen worden genoemd. Dit is schematisch weergegeven in het figuur 3 links. De meest voorkomende manier waarop dit gebeurt heet spontane emissie. Naast spontane emissie heb je ook gestimuleerde emissie. Hiermee wordt laserlicht gegenereerd. In ons onderzoek ligt de focus op de spontane emissie, dat nu verder zal worden toegelicht. Het atoom of molecuul dat het licht uitzendt wordt voor het gemak verder de lichtbron genoemd.

Spontane emissie

Bij spontane emissie zendt de lichtbron een foton uit in een willekeurige richting na een willekeurige tijd. Het bijzondere is dat dit proces niet alleen wordt bepaald door de lichtbron zelf, maar ook wordt beïnvloed door de omgeving van de lichtbron. Overal om ons heen fluctueert het elektromagnetische veld. Zelfs in een vacuüm bestaan deze fluctuaties. Gemiddeld in tijd is het elektromagnetische veld nul, maar er zijn de hele tijd fluctuaties rond nul. De lichtbron wisselwerkt met dit fluctuerende elektromagnetische veld, zodat een foton uitgezonden wordt. Dat betekent ook dat je voor een bepaald foton niet van te voren kunt bepalen hoe lang het zal duren voordat de lichtbron dit foton uit zal zenden. Want dat hangt af van het fluctuerende elektromagnetische veld waarover je van te voren niets kunt zeggen. Waar je wel iets over kunt zeggen is de gemiddelde tijd die het duurt als je het uitzenden van het foton heel vaak herhaalt.

Dit is precies wat wij doen in experimenten. Door miljarden keren te meten hoe lang het iedere keer duurt voordat het foton wordt uitgezonden is het mogelijk een histogram te maken van het emissieproces. Een voorbeeld van een histogram is afgebeeld in figuur 3 rechts. Uit zo'n histogram of vervalcurve is het mogelijk conclusies te trekken over bijvoorbeeld de karakteristieke of gemiddelde tijd die het duurt voordat een foton wordt uitgezonden. Dit wordt ook wel de levensduur van de lichtbron genoemd. Deze levensduur is afhankelijk van de fluctuaties van het elektromagnetische veld. Het bijzondere is nu dat die fluctuaties kunnen worden beïnvloed door structuren heel dicht bij de lichtbron te plaatsen. De maat voor de omgevingsinvloed heet de lokale toestandsdichtheid.

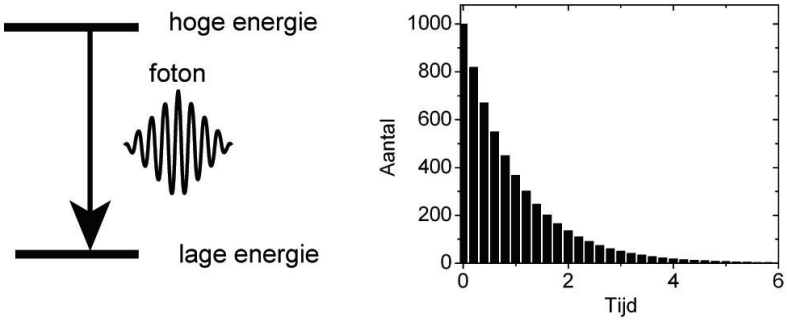

Figuur 3.: In de figuur links is schematisch te zien dat bij een verschil in energie een foton kan worden uitgezonden. De rechter figuur toont een histogram van aankomsttijden van fotonen bij spontane emissie.

De lokale toestandsdichtheid

Er zijn verschillende manieren om de lokale toestandsdichtheid te veranderen. Een kernbegrip daarbij is interferentie. Licht is een golf van elektromagnetische straling. Bij een golf hoort een bepaalde golflengte. Golven hebben de eigenschap dat ze interferentie kunnen vertonen. Als de pieken van de twee golven op hetzelfde moment op dezelfde plaats zijn zullen die elkaar versterken omdat ze optellen. Maar als een piek en een dal samenvallen dan is de opgetelde golf juist volledig uitgedoofd. Bij het versterken heet de interferentie constructief, bij uitdoven destructief. Dit effect is bijvoorbeeld verantwoordelijk voor de kleur van zeepbellen. Een zeepbel bestaat uit een heel dun vliesje water. Het licht van buiten de zeepbel reflecteert zowel van de voorkant als de achterkant van het vlies. Voor sommige golflengtes past de afstand tussen de voor- en achterkant precies op de golflengte. Daardoor ontstaat voor die kleur constructieve interferentie en zie je die kleur. Terwijl juist voor andere kleuren destructieve interferentie ontstaat en die kleur niet meer zichtbaar is.

Ook de fluctuaties in het elektromagnetisch veld die zorgen voor de lokale toestandsdichtheid zijn gevoelig voor interferentie verschijnselen. Daarom kan een voorwerp in de omgeving van een lichtbron dat zorgt voor reflectie of verstrooiing van het licht ook interferentie veroorzaken en de lokale toestandsdichtheid beïnvloeden. En dat is precies het type experimenten dat wij hebben uitgevoerd. Door een lichtbron op speciale plekken te plaatsen in de buurt van objecten die zorgen voor reflectie van het licht zijn de fluctuaties in het elektromagnetisch veld te varieren. Daarmee is ook de levensduur van een lichtbron aan te passen. Om preciezer te zijn: de toestandsdichtheid wordt beïnvloed door de plaats van de lichtbron ten opzichte van een object, de golflengte van het uitgezonden licht en de trillingsrichting van het uitgezonden foton van de lichtbron.

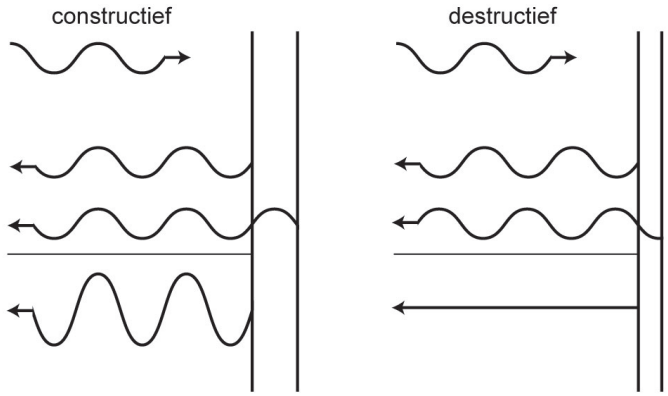

Figuur 4.: De inkomende golf van links wordt aan twee oppervlakken gereflecteerd. Links is de afstand tussen de twee oppervlakken zo dat de toppen en dalen van de twee gereflecteerde golven overeenkomen en ontstaat constructieve interferentie. Rechts valt een dal van de ene golf juist samen met een piek van de andere golf. Hierdoor ontstaat destructieve interferentie en blijft er geen golf over.

In dit proefschrift

In hoofdstuk 2 van dit proefschrift worden experimenten beschreven waarbij lichtbronnen vlakbij een vlakke zilverspiegel zijn geplaatst. Om preciezer te zijn, dichterbij de spiegel dan de golflengte van het licht. Nu is de golflengte van bijvoorbeeld groen licht 500 nanometer, oftewel 0,0005 millimeter dus het positioneren van de lichtbronnen moet met uiterste precisie gebeuren. Op bepaalde afstanden van de spiegel is de toestandsdichtheid verhoogd door constructieve interferentie, terwijl op andere plaatsen het licht dat wordt uitgezonden door de lichtbron juist destructief interfereert. Voor een vlakke spiegel is dit relatief makkelijk te berekenen. Daarom kan je een spiegel gebruiken om belangrijke gegevens over de lichtbronnen te verkrijgen omdat de toestandsdichtheid bekend is.

In hoofdstuk 3 wordt een lichtbron heel dicht bij een overgang van lucht naar glas geplaats. Ook dit is een spiegel voor het uitgezonden licht. Nu wordt niet de afstand van de lichtbron tot de spiegel gevarieerd, maar wordt gekeken naar het effect van de trillingsrichting van het licht. In onze experimenten meten we aan heel veel lichtbronnen tegelijk. Iedere lichtbron heeft een iets andere trillingsrichting. Daardoor ziet iedere bron een iets andere toestandsdichtheid en krijgt daarom ook een iets andere levensduur. Als je al die histogrammen tijdens een meting optelt krijg je een specifieke vervalcurve. Wij laten voor het eerst zien dat je die specifieke vorm van de vervalcurve kunt voorspellen.

Een heel bijzondere structuur om de toestandsdichtheid te beïnvloeden is een

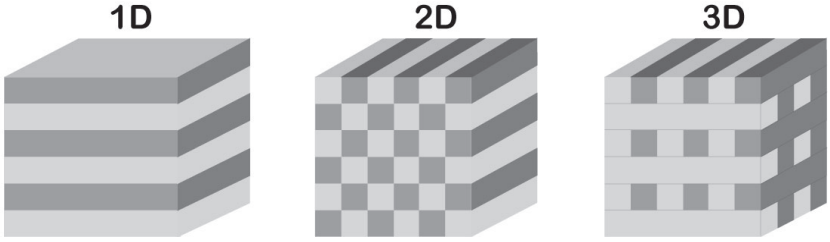

Figuur 5.: Een 1D fotonisch kristal heeft een zich herhalende structuur in 1 richting, maar blijft in de andere richtingen constant. Een 2D kristal in het midden heeft ook een periodieke structuur in een tweede richting. In een 3D kristal verandert het patroon in alle drie de richtingen.

fotonisch kristal. Dit is een periodiek herhalende structuur waarbij de periode van de orde van golflengte van licht is. Deze structuren moeten extreem precies zijn op een kleinere schaal dan de lichtgolflengte. Daarom worden deze structuren gefabriceerd in een speciale *clean room*, een extreem stofvrije ruimte, omdat stof desastreuze gevolgen zou hebben. In figuur 5 staan voorbeelden van een fotonisch kristal met een herhalende structuur in 1, 2 en 3 dimensies. Zo'n structuur kan je zien als allemaal kleine spiegels, die het interferentie effect zoals bijvoorbeeld in een zeepvlies optreedt sterker maken. In een 3D kristal is het mogelijk niet alleen in 1 richting interferentie te krijgen maar in alle 3 de richtingen. Hierdoor wordt in fotonische kristallen de toestandsdichtheid extreem beïnvloed. Het is zelfs mogelijk om volledige destructieve interferentie te veroorzaken, zodat er helemaal géén fluctuaties meer optreden. Binnenin een fotonisch kristal is het stiller dan in een vacuüm! Dit betekent dat als een lichtbron in zo'n fotonisch kristal in een hogere energie toestand zit, het niet naar de grond toestand vervalt via spontane emissie. De levensduur wordt oneindig lang. Dit golflengte gebied waar volledige destructieve interferentie optreedt wordt een fotonische bandkloof genoemd.

In hoofdstuk 5 worden experimenten beschreven waarbij lichtbronnen in een fotonisch kristal met een bandkloof worden gestopt. Inderdaad vinden we dat binnenin deze bandkloof de levensduur aanzienlijk langer wordt. De lichtbron houdt zijn energie tot 11 keer langer vast omdat er veel minder fluctuaties van het elektromagnetisch veld aanwezig zijn die zorgen dat de lichtbron vervalt. Voor andere fotonische kristallen waarbij de lichtbron niet binnen de bandkloof uitzendt wordt de levensduur juist korter, omdat hier de interferentie constructief is en er meer fluctuaties aanwezig zijn.

In hoofdstuk 6 is onderzocht of het ook mogelijk is om de levensduur te veranderen in fotonische kristallen waarbij maar in 2 van de 3 richtingen een periodieke structuur is aangebracht. Deze structuren zijn namelijk aanzienlijk makkelijker te fabriceren. In deze structuren blijken de interferentieverschijnselen niet sterk

genoeg om de levensduur te veranderen. Wel is gevonden dat het licht een andere kant wordt opgestuurd binnen het kristal. Aan een kant komt meer licht naar buiten, aan de andere kant juist minder.

In hoofdstuk 7 tenslotte is weer een heel andere nano structuur gebruikt. De lichtbronnen zijn hier geplaatst tussen heel dunne draden. De straal van de draden is veel kleiner dan de golflengte van het licht. De draden zijn willekeurig geplaatst ten opzichte van elkaar. Dit zorgt ervoor dat licht tussen deze draden zo vaak wordt verstrooid dat het de weg kwijt raakt en een dronkemanswandeling door de laag maakt. Hierbij wordt het licht diffuus. Over de invloed van diffusie op de toestandsdichtheid is nog niet veel bekend. We hebben gevonden dat de levensduur van lichtbronnen tussen nanodraden vooral wordt beïnvloed door de straal van de nanodraden. Effecten van de meervoudige verstrooiing van het licht hebben wij niet gevonden hoewel deze effecten wel voorspeld worden in de literatuur. Mogelijk kunnen wij deze effecten niet zien omdat we naar heel veel lichtbronnen tegelijk kijken, zodat het effect wordt uitgemiddeld.

In het onderzoek in dit proefschrift hebben we aangetoond dat de spontane emissie van lichtbronnen kan worden beheerst door de omgeving van de lichtbron te veranderen. Zowel het effect van de plaats van de lichtbron ten opzichte van de nanostructuur, de golflengte van het licht en de trillingsrichting van het licht zijn onderzocht.

Dankwoord

Ondanks dat alleen mijn eigen naam op de voorkant van dit proefschrift staat, hebben een heleboel mensen in vier jaar tijd bijgedragen om de inhoud van dit boekje mogelijk te maken.

Allereerst wil ik mijn promotor Willem Vos bedanken. Zijn enthousiasme voor de wetenschap en oog voor detail dwingt je om goed over de dingen na te denken. Zowel werk van anderen als eigen resultaat wordt kritisch bekeken. Daarnaast wil ik hem bedanken voor de flexibiliteit tijdens het afronden van dit proefschrift. Het heeft zeker geholpen om de deadline te halen.

Ad Lagendijk, hoewel niet mijn promotor, heeft altijd veel interesse getoond in mijn resultaten. Als ik iets wilde bespreken stond zijn deur altijd open. Ook zijn lessen wetenschapscommunicatie hebben (hopelijk) bijgedragen aan de leesbaarheid van dit werk. De open en kritische groepscultuur is voor een belangrijk deel zijn verdienste.

Een voordeel van werken in Enschede is dat Allard Mosk in de buurt zit voor advies. Daar heb ik dankbaar gebruik van gemaakt. Ook Allard maakt altijd tijd om te helpen waar hij kan. Heel hartelijk dank hiervoor.

I would like to thank professors Jean-Jacques Greffet, Klaus Boller, Gert 't Hooft and Ad Lagendijk for carefully reading the manuscript of my thesis.

Hoofdstuk 2 van dit proefschrift is voortgekomen na een flinke worsteling met onwillige quantum dots en samples. Hulp van Steven Kettelarij, bijgestaan door Hans Zeijlemakers en Chris Rétif van het Nanocenter, is daarbij onontbeerlijk gebleken. I would like to thank Jeppe Johansen and Peter Lodahl from DTU in Denmark for their contributions. I am still amazed at the impeccable timing of Jeppe on when to plan this one week of measuring. It was great fun to have a partner in the lab. Verder wil ik graag Ad Lagendijk en Pedro de Vries bedanken voor hun hulp bij berekeningen.

De "silicium"hoofdstukken in dit proefschrift zijn het resultaat van jaren werk in de groep. Mijn metingen aan deze ontzettend mooie fotonische kristallen waren niet mogelijk geweest zonder het harde werk van Léon Woldering, Willem Tjerkstra en Hannie van den Broek aan de fabricage. Simon Huisman and Rajesh Nair have worked very hard to finish the reflectivity measurements in time, for which I am very grateful. Zonder de NIR opstelling, ontwikkeld door Bart Husken, was ik ook niet ver gekomen.

Het hoofdstuk over de nanowires is ontstaan uit een vrijdagmiddag experiment samen met Otto Muskens, met nanowires afkomstig van Silke Diedenhofen uit de groep van Jaime Gomez Rivas bij Philips.

Tijdens mijn promotie heb ik het genoegen gehad om Niels Zijlstra te begeleiden tijdens zijn AMOLF metingen. Ondanks tegenvallende resultaten bleef hij er lol in houden. Later werd ik de 'echte' begeleider van Simon Huisman, zonder wiens keiharde werk ik mijn deadline vermoedelijk nooit had gehaald. Heel erg bedankt voor deze inzet.

Dankwoord

De verhuizing van het lab van AMOLF naar Twente kwam voor mij op het slechts denkbare moment, zowel privé als qua metingen. De verhuizing is voorspoedig verlopen dankzij de hulp van Cock Harteveld, Iwert Meinders en Rob Troost. Heel veel dank hiervoor. Ook wil ik graag FOM en AMOLF bedanken voor de financiële steun bij het extra huishouden in Enschede en het vele heen en weer reizen. Albert Polman, Bart van Leijen en Ed Kruller wil ik bedanken voor het regelen van het mooie kantoor in het nieuwe AMOLF, waar ik aan mijn proefschrift mocht schrijven.

Ik wil graag alle groepsleden van de Photonic Bandgaps en Photon Scattering groepen op AMOLF en de COPS groep in Twente bedanken voor de goeie discussies tijdens besprekingen en gezelligheid op andere momenten. Ook de overige Nanophotonics groepen op AMOLF bedankt voor de zeer leerzame discussies tijdens het colloquium. Extra dank gaat uit naar Femius Koenderink voor het beantwoorden van al die vragen over berekeningen en fotonische kristallen. Tijdens werk is een beetje afleiding hard nodig. Experimentele fysica kan naast bijzonder interessant ook een extreem frustrerende bezigheid zijn. Koffiepauzes met collega's zijn daarvoor onontbeerlijk. Hartelijk dank aan al die collega's op AMOLF en in Twente voor de gezelligheid. In het bijzonder wil ik mijn kamergenoten van het eerste uur op de gezelligste kamer van AMOLF Bart en Ramy bedanken voor hun luisterend oor en juist de vele gesprekken over andere dingen dan natuurkunde. Daarnaast ook Alex bedankt, de gezamenlijke uurtjes 'opbouwende kritiek' in de trein hebben mij goed gedaan.

Op deze plaats wil ik graag al die familieleden en vrienden bedanken voor het altijd tonen van interesse in mijn werk, ook al was mijn uitleg niet even duidelijk. Mike, bedankt voor het altijd meedenken en paraat staan als dat nodig is. Speciale dank gaat uit naar mijn lieve vriendinnetjes. Dorien, Merel, Mariska, Marleen en Stephanie, we kennen elkaar inmiddels zo lang dat ik jullie beschouw als familie. Bedankt voor de vele leuke gedeelde momenten. Petrie, bedankt voor de vele gezellige thee bezoekjes. Sanneke en Janneke, naast de toffe uitjes ook heel erg bedankt dat jullie mijn paranimfen willen zijn. We gaan er wat moois van maken.

In het bijzonder wil ik hier mijn ouders en schoonouders bedanken voor hun niet aflatende steun en oprechte interesse. Mijn ouders hebben mij altijd gesteund in mijn plannen en me geholpen waar dat kon. Pap en mam, ik ben jullie daar heel dankbaar voor. Na 10 jaar worden schoonouders ook een beetje ouders. Vonne en Joost, heel erg bedankt voor alles.

Zonder Wouter was dit proefschrift ondenkbaar geweest. Bedankt dat je er altijd bent. Om me op te halen als ik een lekke band heb, als ik moet ventileren, als ik opeens naar Enschede moet verhuizen. Ik kan mijn leven niet voorstellen zonder je. En het mooist denkbare kadootje, dat hebben we eigenlijk al gekregen! Bente, bij iedere schop werd ik herinnerd aan onze deadline, hoewel lifeline eigenlijk toepasselijker is. Je gevoel voor timing is nu al indrukwekkend. Ik ben heel benieuwd naar je volgende stappen.